PRECONDITIONING, FORMATION, AND IMPACT OF MAUD RISE AND WEDDELL SEA POLYNYAS IN A HIGH-RESOLUTION EARTH SYSTEM MODEL

A Thesis

by

PRAJVALA KISHORE KURTAKOTI

Submitted to the Office of Graduate and Professional Studies of
Texas A&M University
in partial fulfillment of the requirements for the degree of

DOCTOR OF PHILOSOPHY

Chair of Committee,	Achim Stössel
Committee Members,	Ping Chang
	Alejandro Orsi
	R. Lee Panetta
Head of Department,	Shari Yvon Lewis

May 2019

Major Subject: Oceanography

ABSTRACT*

Open ocean polynyas (OOPs) in the Southern Ocean are ice-free areas within the winter ice pack that are associated with deep convection, potentially contributing to the formation of Antarctic Bottom Water (AABW). To enhance the credibility of Earth System Models (ESMs), their ability to simulate OOPs realistically is thus crucial. Here we investigate OOPs that emerge intermittently in a high-resolution (HR) pre-industrial simulation with the Energy Exascale Earth System Model (E3SMv0), an offspring of the Community Earth System Model (CESM). While low-resolution (LR) simulations with E3SMv0 show no signs of OOP formation, the preindustrial E3SMv0-HR simulation produces both small Maud Rise polynyas (MRPs) as well as large Weddell Sea polynyas (WSPs). The former is associated with a prominent seamount in the eastern Weddell Sea, and their preconditioning and formation is the focus of the first part of this dissertation.

The second part of my dissertation is on the generation of WSPs in the same preindustrial E3SMv0-HR simulation. While the formation of MRPs requires HR to simulate the detailed flow around Maud Rise, a realistic simulation of WSPs requires the ability of a model to produce MRPs. Furthermore, WSP formation will not occur without a prolonged build-up of a heat reservoir at depth, and a prolonged period of less negative wind stress curl in association with the core of the southern hemisphere westerlies being located at an anomalously northward position.

The third part of my dissertation discusses the potential effects of AABW anomalies due to WSPs on the Atlantic Meridional Overturning Circulation (AMOC). Earlier studies indicate these anomalies propagate relatively fast along the deep western boundary in the form of internal

* Partly published in AMS Journal of Climate (Kurtakoti et al., 2018)

boundary waves. Since the simulation contains 2 major WSP events that prevail over several years, their impact on AABW anomalies along the deep western boundary can readily be traced. However, they do not seem to affect the outflow of North Atlantic Deep Water (NADW) to the extent of a noticeable impact on the strength of the AMOC. It is hypothesized that this is because of the eddy-resolving capability of E3SMv0-HR, and HR in general leading to a more confined deep western boundary current.

DEDICATION

To my mom who taught me to believe in myself and my dad who makes me laugh.

ACKNOWLEDGEMENTS

I would like to start by thanking my advisor Dr. Achim Stössel for his continuous support of my PhD study and related research, as well as for his patience, motivation, and immense knowledge. I am grateful to have an advisor who genuinely cares for my well-being while encouraging me to figure out my own path. I have deeply benefitted from hundreds of research meetings where you have both challenged and encouraged me with your honest yet unambiguous outlook and your dry sense of humor. I would also like to thank you for helping me improve my academic writing style through rigorous feedback.

I would also like to thank my unofficial co-advisor Dr. Milena Veneziani for playing a pivotal role in my academic and career development through her research expertise and insightful questions. You have been nothing but supportive of me since the first time you interviewed me for an internship at LANL. In a field that is primarily dominated by men, it is crucial for women in the workplace to have strong female role models and mentors which you have clearly demonstrated. Your kindness and humility are qualities that I will always remember. I would like to thank Wilbert Weijer for his incredible feedback on my manuscripts. I would also like to thank Matt Maltrud for his support and all the numerous scientists at LANL who have inspired me to keep pushing myself to become a better researcher.

I would like to thank my committee members Dr. Alejandro Orsi, Dr. Lee Panetta and Dr. Ping Chang for their guidance and useful comments throughout the course of my PhD. I am also going to miss the long discussions in the hallway with Dr. Ping Chang which has always been very insightful.

I would like to sincerely thank my parents Premalatha and Kishore Kurtakoti for supporting and encouraging me to pursue my dreams whatever they may be. They always stood by me with unwavering love and hope.

I would like to thank my best friend and unofficial partner Tarun Verma. I'd like to think of myself as a strong independent woman who is nevertheless constantly energized through your unconditional love! I derive strength from your support and I'm grateful I never have to ask for it. I love our little family and our adorable cats. Thanks also to my best friend Pooja for your constant friendship and love. I'd also like to thank all my friends who have become family including Veronica, Maya, Noura, Wei-Ching, Karina, Eric, Nisha, Biren, Manisha, Preeti, Mimli, Elizabeth, Joe, Xiao, Lixin, Jongsun, Jiaxu, Maya for everything ranging from game nights, potlucks, deserts, Mexican food, movie nights, jams, birthday parties, moving, and most importantly for showing me that there is more to life than just research. My friends have become my family and I am very grateful for them. I'd also like to thank all the TAMU and LANL administrative staff for helping me with mountains of paperwork and for making my time at Texas A&M University a great experience.

CONTRIBUTORS AND FUNDING SOURCES

I would like to thank and acknowledge the support of the U.S. Department of Energy (DOE)'s Office of Science (BER) through the E3SM project and the Center for Space and Earth Science (CSES) at the Los Alamos National Laboratory through a 2-yr graduate student project and for providing me access to the data analyzed in this dissertation. I would also like to thank the Department of Oceanography at Texas A&M University for supporting my graduate study through Scholarships and Teaching Assistantships. I also thank Milena Veneziani and Wilbert Weijer for their support from the CSES project at LANL. I am also thankful for Mat Maltrud and Elizabeth Hunke's support in providing guidance on the POP and CICE model fields whenever necessary.

NOMENCLATURE

AABW	Antarctic Bottom Water
ACC	Antarctic Circumpolar Current
AMIP	Atmospheric Model Intercomparison Project
AMOC	Atlantic Meridional Overturning Circulation
ASW	Antarctic Surface Water
CAM5-SE	Community Atmosphere Model version 5 with Spectral Element
CDW	Circumpolar Deep Water
CESM	Community Earth System Model
CICE4	Community Ice Code version 4
CLM4.5	Community Land Model version 4.5
CMIP5	Coupled Model Intercomparison Project 5
DWB	Deep Western Boundary
ESM	Earth System Model
E3SMv0	Energy Exascale Earth System Model version 0
E3SMv0-HR	Energy Exascale Earth System Model High Resolution simulation
E3SMv0-LR	Energy Exascale Earth System Model Low Resolution simulation
EMB	Embayment
GCM	General Circulation Model
GEBCO	General Bathymetric Chart of the Oceans
GFDL	Geophysical Fluid Dynamics Laboratory

HR	High Resolution
JASO	July-August-September-October
LR	Low Resolution
MLD	Mixed Layer Depth
MRP	Maud Rise polynya
MRP-I	MRP initiation
MRP-P	MRP preceding
MRP-N	No MRP
NADW	North Atlantic Deep Water
OHC	Ocean Heat Content
OOP	Open Ocean Polynyas
POP2	Parallel Ocean Program version 2
SAM	Southern Annular Mode
SOSE	Southern Ocean State Estimate
WSC	Wind Stress Curl
WDW	Weddell Deep Water
WSBW	Weddell Sea Bottom Water
WSDW	Weddell Sea Deep Water
WSP	Weddell Sea polynya

TABLE OF CONTENTS

LIST OF FIGURES

LIST OF TABLES

1. INTRODUCTION*

Polynyas are large ice-free areas along a coast or in the midst of the winter sea ice pack, and are found both in the north and south polar oceans (Morales Maqueda 2004). Coastal polynyas, also called latent heat polynyas, form when katabatic winds blowing off Antarctica push newly formed sea ice away from the coast, thereby continuously creating an area of ice-free ocean that is subject to extreme heat loss to the atmosphere. Open ocean polynyas, also called sensible heat polynyas, form far from the coast amidst the winter sea ice pack. They are generally observed in conjunction with deep convective overturning events in the ocean that lead to direct interaction between mid-depth and surface ocean waters, and are also characterized by a strong positive ocean to atmosphere heat flux. In this study, we focus on open ocean polynyas that occur in the Weddell Sea. We use the term "Weddell Sea Polynya" (WSP) to describe a large open ocean polynya in the central Weddell Sea and the term "Maud Rise Polynya" (MRP) to describe a small open ocean polynya that occurs over and around the Maud Rise seamount in the eastern Weddell Sea (Gordon 1978; Martinson, Killworth, and Gordon 1981; Gordon and Huber 1990). MRPs have been observed as recently as in the austral winter of 2017 (Fig. 1a).

1.1 Weddell Sea water masses and Open Ocean Polynyas

Physical processes in the Weddell Sea are important for the global ocean overturning circulation through their potential impact on the formation of Antarctic Bottom Water (AABW) (Deacon 1963). It is therefore useful to describe the general circulation and define the different water masses in the Weddell Sea referenced throughout this dissertation. The Weddell Gyre is a zonally elongated cyclonic gyre with a double cell circulation pattern that extends eastward to 30°E and is bound by the Antarctic coast in the south, the Antarctic Peninsula in the west, and the

* Partly published in AMS Journal of Climate (Kurtakoti et al., 2018)

Scotia Ridge in the north (Carmack and Foster 1975; Orsi, Nowlin JR, and Whitworth 1993; Schröder and Fahrbach 1999; Fahrbach et al. 2011). A westward return flow is located at 6°E between 62°S and 67°S and another westward return flow is located at 65°S between 35°E and 40°E (Schröder and Fahrbach 1999).

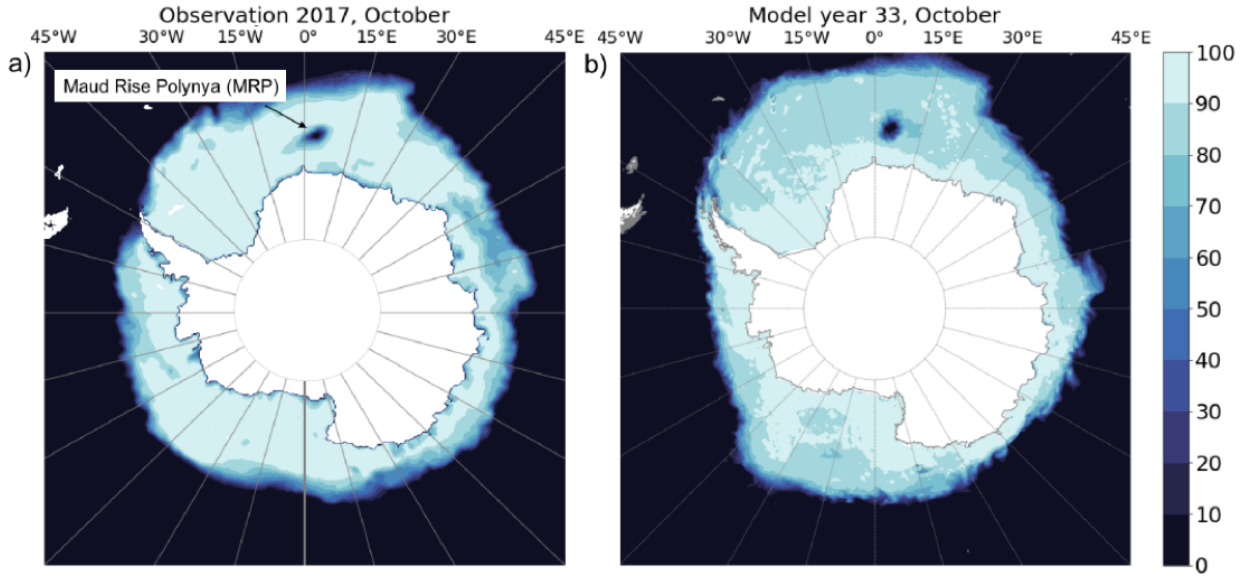

Figure 1: (a) Satellite derived (Maslanik and Stroeve 1999) and (b) simulated sea ice concentration during the month of October (observation year 2017; model year 33, respectively) over the Southern Ocean. The dark blue region surrounded by sea ice is the Maud Rise Polynya (MRP). The location of the seamount peak is at 2.5°E, 65°S.

A characteristic water mass of the Weddell Sea is the Weddell Deep Water (Gordon and Huber 1990) or Warm Deep Water (WDW) (Fahrbach et al. 2011). It fills most of the subsurface Weddell Sea from 200 to 1500 m and exhibits a temperature maximum at about 500 m, with a characteristic potential temperature between 0 and 0.8°C and salinity between 34.64 and 34.72 psu (Foster and Carmack 1976; Gordon 1982; Gordon and Huber 1990). This water mass is fed by the Circumpolar Deep Water (CDW), which diverges from the Antarctic Circumpolar Current (ACC), flows south and then westward into the central Weddell Sea following the eastern limb of the Weddell Gyre, subsequently impinging on Maud Rise (Foster and Carmack 1976). Below the

WDW lie two other water masses: the Weddell Sea Deep Water (WSDW) with a characteristic potential temperature between -0.6 and 0°C and salinity between 34.63 and 34.7 psu, and the Weddell Sea Bottom Water (WSBW), which is denser than WSDW mainly due to potential temperatures lower than -0.6°C. WSBW constitutes an important component of AABW (Orsi, Nowlin JR, and Whitworth 1993). Another water mass that fills the upper 100-150 m in the eastern Weddell Sea is the Antarctic Surface Water (ASW) (Martinson 1990).

During the austral winters of 1974-1976, a large and persistent open ocean polynya was detected in the Weddell Sea by the first operational satellite passive microwave radiometer (Zwally et al. 1983). This WSP at its biggest had an ice-free area of about 250,000 km^2 (Gordon, Visbeck, and Comiso 2007), roughly the size of the United Kingdom. Prior to the WSP of 1974-1976, MRPs were observed during part of 1973 (June, October) and 1974 (June, July, and August). The Maud Rise seamount has a diameter of about 200 km and extends from the surrounding deep ocean floor at 5000 m depth up to a depth of 1700 m at 2.5°E, 65°S. In the winters of 1974-75, the MRP extended westward into the central Weddell Sea, thus initiating a WSP. Deep water cooling by more than 0.4°C was observed in the WSP, implying deep convection that introduced cold and fresh surface winter water into WDW and WSDW in the 200-2700 m depth range (Martinson, Killworth, and Gordon 1981). In particular, Gordon (1981) found that the WSDW became significantly fresher and colder in the post-polynya years (1976-1978) when compared to the pre-polynya year (1973). This requires full-scale open-ocean deep convection and a significant transfer of heat from the ocean into the atmosphere.

Early idealized model studies investigated possible processes responsible for this deep convection. Martinson et al. (1981), for example, concluded that convection was initiated by static instabilities, induced by surface cooling and continuous sea-ice formation with associated brine

rejection. More recent studies based on numerical simulations with sea-ice–ocean models revealed a more complex dynamical picture. Using a low-resolution (1° horizontal resolution) version of such model together with interannual atmospheric forcing, Hirabara et al. (2012) were able to simulate an open ocean polynya in the eastern Weddell Sea (Hirabara et al. 2012). They found that common factors essential for a MRP to form are: (1) increased potential instability, (2) high surface salinity and (3) a cyclonic wind stress anomaly near Maud Rise. They suggested that air-sea interactions should be simulated using fully coupled atmosphere–ice–ocean general circulation models (GCMs) to reproduce the open ocean polynya formation processes more realistically. Such comprehensive models are nowadays mostly referred to as Earth System Models (ESMs).

Cheon et al. (2015) simulated a WSP using a low-resolution version of the GFDL sea-ice–ocean model forced by atmospheric reanalysis winds. They found that an anomalously strong negative wind stress curl over the Weddell Sea intensifies the cyclonic Weddell Gyre causing the warm and salty WDW to upwell, thereby triggering a WSP. Cheon et al. (2014) attributed the transition to a more negative wind stress curl to the recovery of the Southern Annular Mode (SAM) index from a prolonged negative phase to more positive values. Furthermore, a prolonged negative phase of SAM and a strong La-Niña were found to induce drier and colder surface conditions, and thus more sea ice formation and brine rejection, both of which increase the sea surface salinity, potentially triggering deep convection (Gordon, Visbeck, and Comiso 2007).

To summarize, three main processes have been identified to precondition and sustain convection in the WSP region: (1) heat content of the WDW, which provides a heat reservoir at depth (Lindsay et al. 2008; Martin, Park, and Latif 2013; Cheon et al. 2015); (2) strong negative wind stress curl over the Weddell Sea, which enhances the cyclonic Weddell gyre causing

upwelling of WDW (Cheon et al. 2015); and (3) increase in surface salinity, which destabilizes the upper ocean and increases the upward flux of WDW (Gordon 2014; de Lavergne et al. 2014).

The low-resolution model studies described above focused on WSPs since they could not fully resolve the circulation and bathymetry around the Maud Rise seamount. Yet, MRPs are observed as precursors to the WSPs in the 1970's. Therefore, separate model studies, more or less idealized but all at resolutions higher than 15 km, have set about investigating MRP formation processes somewhat independently from those responsible for WSPs.

1.2 Overview of Maud Rise Polynyas

Holland (2001) used an idealized model to show that oceanic eddies shedding at Maud Rise provide the necessary upward heat flux from the WDW to the upper mixed layer to form MRPs. The study demonstrated that cyclonic eddies can lead to a reduction of ice concentration at the northern flank of Maud Rise due to the associated ice-ocean stress leading to ice divergence (Holland 2001). Other studies (Ou 1991; Alverson and Owens 1996; Beckmann et al. 2001) focused on the impact that a Taylor column forming over Maud Rise may have on localized convection around Maud Rise.

The Taylor Proudman theorem states that in a homogeneous fluid under the condition of slow, steady, and inviscid flow, the horizontal component of velocity cannot vary with depth (Proudman 1916; Taylor 1923). In the ideal settings of a laboratory, a Taylor column appears as a stagnant cylinder recirculating over an obstacle in a rotating flow. This means that variations in bottom topography can influence oceanic flows even at the surface depending on the height of the Taylor column and on the ambient stratification. In the eastern Weddell Sea, where Maud Rise lies, the stratification is very weak, the oceanic flows are characterized by small Rossby numbers, and the flow is nearly frictionless (Alverson and Owens 1996). Under these specific conditions,

the Maud Rise region can theoretically support a weak Taylor column (Hogg 1973; Chapman and Haidvogel 1992). The Maud Rise seamount rises from the surrounding sea floor by more than half of the surrounding water depth. Its "scaled bump height" (defined as the ratio of the seamount height to the surrounding ocean depth) (Meredith et al. 2015) is well capable of influencing oceanic flow above it. Alverson and Owens (1996) looked at the effect of flow impinging on a Gaussian seamount in a stratified domain, and found that it created a Taylor cap. A Taylor cap is similar to a Taylor column except that it does not necessarily form a column but instead shows a doming of water properties over the seamount, thus forming an envelope where fluid remains trapped. Prior to the formation of a steady state Taylor cap, anticyclonic and cyclonic eddies are generated as water columns are squeezed upstream and stretched downstream of the seamount. These eddies co-rotate about the seamount, until the cyclonic eddy is shed downstream while the anticyclonic eddy remains trapped over the seamount. If the Taylor cap is tall enough to reach the surface mixed layer (or, alternatively, if the mixed layer is deep enough to tap into the Taylor cap underneath), full water column convection can be triggered. The surface mixed layer is much colder (and fresher) than the water trapped in the Taylor cap due to its exposure to the cold atmosphere. Convection over the seamount is significantly enhanced when the seamount is more pronounced (steeper flanks) and/or when stratification over the seamount is weaker (Alverson and Owens 1996). Based on real-world parameters of bathymetry, stratification, and impinging currents around Maud Rise, this region is predestined for Taylor columns or caps to form and to prevail over extended periods of time (Meredith et al. 2015).

Only in recent years have advances in high-performance computing platforms allowed coupled climate models to perform centennial time-scale simulations with a high, ocean eddy-resolving resolution (0.1º or higher). A recent such study by Dufour et al. (2017) shows that the

GDFL high-resolution climate model configuration with pre-industrial CO_2 conditions is indeed able to produce WSPs. The WSPs in these simulations were preceded by MRPs. The study focused on the model processes and parameterizations that control the stratification in the central Weddell Sea, their impact on the accumulation of the subsurface heat reservoir (WDW), and thus on the preconditioning of WSPs (Dufour et al. 2017).

The most recently observed MRP is clearly visible in the monthly mean ice concentration for October 2017 (Fig.1a). As explained in Kurtakoti et al. (2018), the formation of MRPs in Earth System Models (ESMs) requires a detailed representation of the bathymetry, in this case in form of a steep and high enough Maud Rise seamount (and Astrid Ridge to the east of Maud Rise) for tall enough Taylor columns to form to affect the mixed layer and circulation around Maud Rise (e.g., Meredith et al., 2015). The associated dynamics lead to a doming of isopycnals over Maud Rise, a ring or crescent of anomalously warm and salty Weddell Deep Water around Maud Rise, a halo of lower sea-ice concentration and of positive ice-drift vorticity along the north-western flank of Maud Rise, as well as an anti-cyclonic outer circulation, and a cyclonic inner circulation around Maud Rise, all of which are supported by observational and theoretical studies of MRPs (Gordon and Huber 1990; Bersch et al. 1992; Alverson and Owens 1996; Muench et al. 2001; Holland 2001; de Steur, Holland, Muench, and Mcphee 2007).

1.3 Overview of Weddell Sea Polynyas and their impact on deep water masses

In the late 70's, two observational cruises were carried out in the Weddell Sea after Gordon (1978) detected a deep-penetrating cold core cyclonic eddy in February 1977 extending down to 4000m within the Weddell Gyre. Within the eddy, the water was relatively cold and fresh, with no stratification indicating penetration of bottom water to the surface (Carmack 1986). Gordon (1978) hypothesized it to be a winter convective pattern that survived into the summer. Gordon et al.

(1981) developed an idealized convective model for the WSP in which the sequence of a preconditioned area in the ocean, surface cooling, and sea ice formation can lead to static instability that can further lead to deep convection. In early winter, once convection was triggered, the warm and salty WDW helped maintain the WSP by melting the sea ice or prohibiting its formation in the winter. From the monthly winter sea ice concentration around the WSP of the 1970's it can be inferred that sea ice forms around an area of warm surface water (Martinson, Killworth, and Gordon 1981).

The preconditioning and formation of WSPs have been studied extensively since they were first detected in satellite passive-microwave images in the mid 1970s (Carsey 1980; Martinson, Killworth, and Gordon 1981; Gordon 1982; Zwally et al. 1983). It seems that almost 40 years down the road we are now able to simulate the sequence of features that lead up to WSPs in global ESMs. The importance of being able to capture the processes that trigger WSPs in ESMs lies in the fact that the associated mode of large-scale open-ocean convection gives rise to a large extra amount of AABW formation (Martinson 1990), which potentially affects the Atlantic meridional overturning circulation (AMOC) by modifying the flow of North Atlantic Deep Water (NADW) across 30ºS (Stössel and Kim 2001; Swingedouw et al. 2009; Hirabara et al. 2012; Martin, Park, and Latif 2013; Patara and Böning 2014; Zanowski, Hallberg, and Sarmiento 2015).

Here we investigate the reasons for the intermittent occurrence of MRPs and WSPs in a 131 year-long preindustrial simulation with the high-resolution (HR) Exascale Energy Earth System Model (E3SMv0-HR). All of the simulated WSPs in E3SMv0-HR are preceded by MRPs, suggesting that MRPs are a prerequisite for the occurrence of WSPs. This is in line with what has been observed in the 1970s. Gordon and Huber (1991), for example, argue that convection associated with MRPs renders the regional mixed layer salinity high enough for it to trigger WSPs

upon spreading westward with the background flow of the Weddell gyre. They further claim that this goes along with a more cyclonic wind stress curl that spins up the Weddell gyre, which in turn leads to a shallower pycnocline that favors open-ocean convection.

While forced ice-ocean general circulation models (GCMs) or coupled ESMs with low resolution (LR) ocean components would not be able to resolve the circulation around Maud Rise with sufficient detail to produce realistic Taylor columns/caps, most LR ocean models nevertheless simulate WSPs, either permanently (de Lavergne et al. 2014; Stössel et al. 2015) or intermittently (Hirabara et al. 2012; Martin, Park, and Latif 2013; Cheon et al. 2014). During pre-industrial times when the precipitation-rich westerlies were located more equatorward and drier conditions than today prevailed over the Weddell Sea, WSPs could potentially occur fairly regularly at inter-decadal intervals. In some studies it has been argued that WSPs have not been seen since the 1970s because of the southward shift of the westerlies in association with the anthropogenic increase of atmospheric CO_2 (Toggweiler and Russell 2008; Gordon 2014). Based on an analysis of a subset of LR-ESM simulations out of the suite of the 5th IPCC assessment report's Coupled Model Intercomparison Project 5 (CMIP5), de Lavergne et al. (2014) argue that this transition is best captured in so-called "convecting models", i.e. ESMs that feature WSPs during preindustrial conditions.

Several recent modeling studies have quantified the different effects of convective events in the Weddell Sea on the ocean, atmosphere and sea ice. *Cabré et al.*, 2017 using a 1000 year-long run of a low resolution coupled ocean-atmosphere Geophysical Fluid Dynamics Laboratory (GFDL) model showed that WSPs are associated with an increase in SST in the southern hemisphere. *Zhang et al.*, 2019 show that the absence of WSPs since the late 1970s can explain the recent observed trends between 1979-2012 in sea ice and SST in the Southern Ocean. *Martin*

et al., 2015 showed that WSPs can have an effect on the strength of the AMOC, primarily through the advance/retreat of AABW in the deep ocean also known as the Bipolar Ocean Seesaw effect. It is defined as the seesaw effect wherein the increase in the formation of deep water in the polar oceans of one hemisphere is followed by a decrease in the formation of deep water in the polar oceans of the opposite hemisphere, i.e., an increase in AABW formation will be affiliated with a decrease in the NADW formation. These deep water anomalies propagate at both fast (interannual to decadal) and slow (decadal to centennial) timescales (Zanowski and Hallberg 2017). Large scale oceanic waves propagate the deep water anomalies rapidly while advection works on much longer timescales (Zanowski and Hallberg 2017; Swingedouw et al. 2009).

1.4 Research Motivation and Questions

The E3SMv0-HR simulation provides a unique opportunity to study the impact of small scale processes that need high spatial resolution on the large scale ocean and atmospheric circulation in the Weddell Sea. The small scale processes that play an important role in the Weddell Sea include coherent baroclinic eddies over Maud Rise, Taylor caps over tall bathymetric features in the eastern Weddell Sea and realistic open ocean convection in the Weddell Sea.

In analyzing the preconditioning and formation mechanisms of MRPs and WSPs in the E3SMv0-HR simulation, this dissertation primarily addresses the following questions:

a) Does the resolution of bathymetry affect Taylor cap formation over the Maud Rise-Astrid Ridge complex? (Chapter 3)
b) Is the convection over Maud Rise dependent on the presence of a Taylor cap over Maud Rise? (Chapter 3)

c) What are the mechanisms explaining the westward spreading/propagation of the convective events over the Maud Rise-Astrid Ridge complex (MRP) into the central Weddell Sea (WSP)? (Chapter 4)

d) Why don't all MRPs develop into WSPs? (Chapter 4)

This dissertation is organized as follows: the E3SM model, the E3SMv0-HR simulation, its evaluation against observations as well as the analysis strategy are described in Chapter 2. Chapter 3 describes the preconditioning and formation mechanisms of MRPs; this part of my dissertation has been published (Kurtakoti et al. 2018). Chapter 4 focusses on the generation and impact of WSPs in the same fully-coupled preindustrial ESM simulation, while Chapter 5 discusses the potential effects of AABW anomalies due to WSPs on the AMOC. Finally, Chapter 6 summarizes the main findings of this dissertation, and provides an outlook for future research on this topic.

2. MODEL DESCRIPTION, EVALUATION, AND ANALYSIS STRATEGY*

E3SMv0-HR is a high-resolution fully-coupled ESM based on the Community Earth System Model (CESM) (Hurrell et al. 2013). The atmosphere component is the Community Atmosphere Model version 5 with the Spectral Element dynamical core (CAM5-SE) (Dennis et al. 2011), the land component is the Community Land Model version 4.5 (CLM4.5) (Lawrence et al. 2011), the ocean component consists of the Parallel Ocean Program version 2 (POP2) model (Smith et al. 2010), and the sea-ice component is the Community Ice Code version 4 (CICE4) model (Hunke and Lipscomb 2008). The atmosphere and land model components have a nominal 0.25° horizontal resolution. The ocean and sea-ice models feature a tri-polar grid with a nominal 0.1° horizontal resolution and 42 vertical levels (vertical resolution varies between 10 m at the surface and 250 m near the bottom). This configuration is similar to that of the high-resolution model simulation described in Small et al. (2014), except that the latter is forced with present-day atmosphere conditions (Small et al. 2014) while E3SMv0-HR is forced with fixed pre-industrial atmospheric CO_2 levels. Parameterizations in the ocean component of E3SMv0-HR include the K-profile boundary layer scheme (Large, Mcwilliams, and Doney 1994) to represent unresolved vertical mixing in the upper ocean, and a biharmonic scheme for subgrid-scale horizontal mixing of momentum and tracers, while parameterizations for tidal mixing, dense water overflows, and (sub)mesoscale eddy transport of tracers have been deactivated. It should be emphasized here that E3SMv0-HR was a computationally expensive, multi-institutionally designed experiment. Its specific configuration thus reflects this multiple stake-holders' community effort.

The simulation was run for 131 years; its POP/CICE components were initialized from a short forced simulation (which started from rest/climatology), and its CAM/CLM components

* Partly published in AMS Journal of Climate (Kurtakoti et al., 2018)

were initialized from a standard Atmospheric Model Intercomparison Project (AMIP) run. In addition to E3SMv0-HR, we refer to a similarly configured simulation with pre-industrial conditions, but with a standard 1° horizontal resolution in all model components (ocean, sea-ice, atmosphere and land components), hereafter referred to as E3SMv0-LR.

The E3SMv0-HR simulation and its main results are described in McClean et al. 2019, which is an initialization study using an ensemble of high-resolution fully-coupled transient simulations that have been initialized from different states of E3SMv0-HR and from different states of a forced POP/CICE simulation. The paper shows that the top of the atmosphere energy budget in E3SMv0-HR comes into balance after simulation year 70, oscillating about a mean value of 0.26 W/m^2 (within ±0.5 W/m^2) until the end of the run. The globally averaged ocean heat content follows a similar trend, with heat mostly being stored in the upper 700 m during the first 70-80 years, while later being redistributed at intermediate and deeper depths, and reaching near-equilibrium at all depths in the last 30 years of the simulation. The AMOC stabilized after about 50 years. In terms of sea ice, the simulation reproduces the Arctic ice area in winter well, but underestimates the northern hemisphere ice extent in summer, especially for pre-industrial conditions, thus leading to an overall underrepresentation of Arctic sea-ice volume.

On the other hand, the seasonal cycle of Antarctic sea-ice extent and volume are generally well represented. Spatial maps of monthly climatology of sea ice thickness and sea ice concentration (contours) are shown in Fig. 2, together with satellite-derived ice extent. The impact of the open ocean polynyas on mean sea-ice thickness can clearly be seen during winter (July-October). Sea-ice thickness is lower over the Maud Rise and Astrid Ridge complex than in the central Weddell Sea, indicating that MRPs occur more frequently than WSPs.

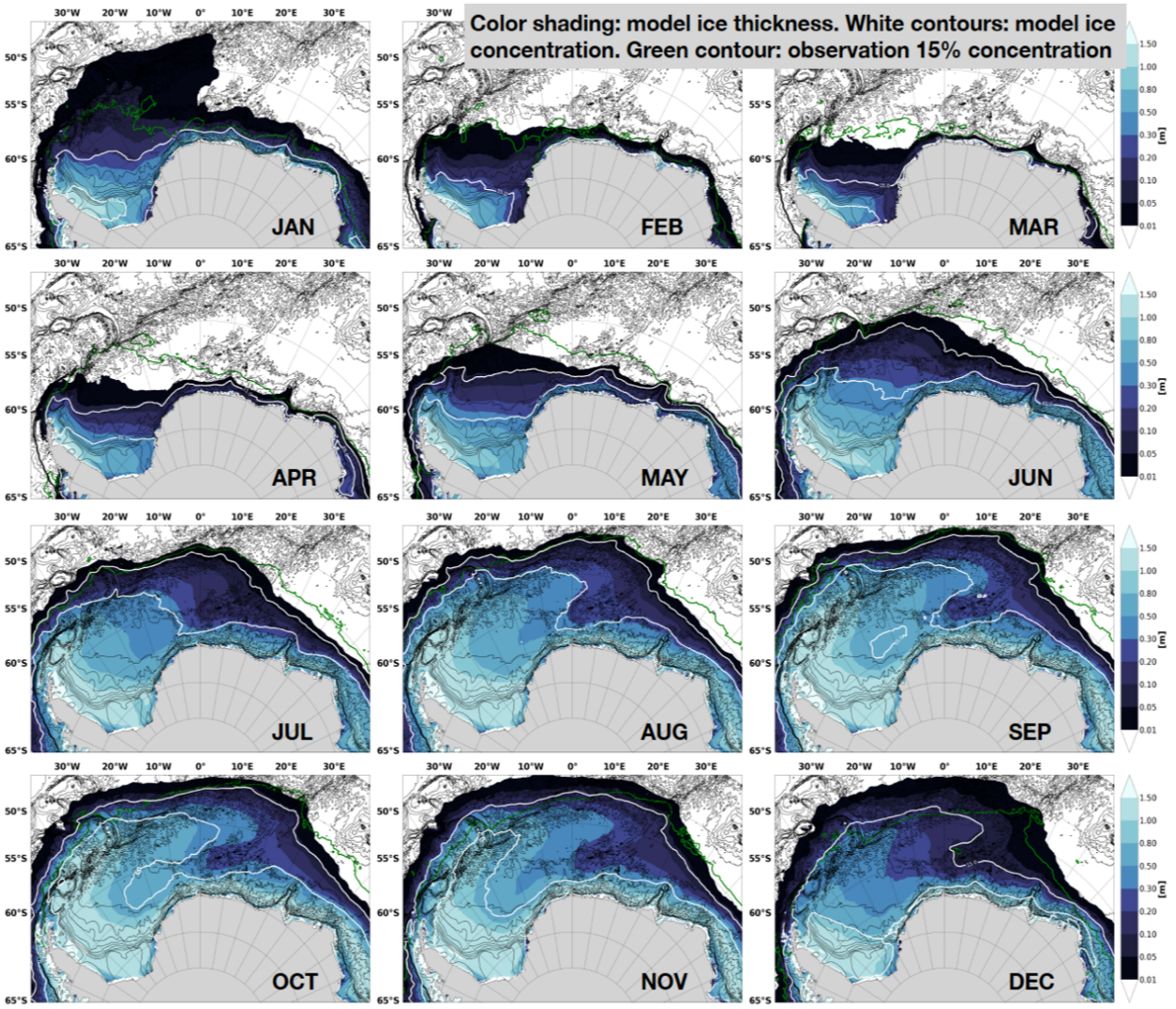

Figure 2: Simulated monthly climatology of sea ice thickness (color shading) and concentration (white contour lines) over the Weddell Sea. The climatologies are calculated over years 20-127. The yellow contour is the 15% sea ice concentration line (ice extent) observed (satellite passive microwave) climatology over years 1978-2018. The white contour lines each represent 15% and 65% model sea ice concentration. The black contours represent the bathymetry.

Evidence for coastal polynyas, in particular along the Ronne ice shelf in the western Weddell Sea, exist all year round as indicated by lower ice thickness. Since coastal polynyas are often short-lived and may disappear within a few days (Markus, Kottmeier, and Fahrbach 1998), they emerge in monthly averages only as lower ice thickness. The coastal polynyas are seen clearly in the high frequency daily data of the simulation saved during three years. The coastal polynyas

remain open for days-weeks and thus the monthly sea ice average does not represent their presence well. Coastal polynyas are highly sensitive to the wind forcing (Stössel, Zhang, and Vihma 2011) and resolution of the model.

An evaluation of the model net transport of the Antarctic Circumpolar Current across the Drake Passage is useful since a main focus of our study is the Weddell Sea. While previous estimates of net transport across the Drake Passage have been ~134 Sv (Cunningham et al. 2004; Mazloff, Heimbach, and Wunsch 2010), newer estimates suggest that it can be as high as 173 Sv (Donohue et al. 2016). In E3SMv0-HR, the mean transport through the Drake Passage over the first 40 years is 136 Sv, with the remainder of the simulation averaging out to 123 Sv (Fig. 3). Small et al. (2014) show the Drake Passage transport being lower in their HR CESM simulation compared to a corresponding LR CESM simulation (Small et al. 2014), which is apparently related to the difference in the position and strength of the Southern Hemisphere westerlies in their two coupled simulations. E3SMv0-HR showing a lower ACC strength than their HR CESM simulation is likely due to the fact that the E3SMv0-HR is run under preindustrial conditions when the southern hemisphere westerlies were weaker and located more equatorward (Toggweiler and Russell 2008).

The Weddell gyre is known for its double cell structure (Timmermann 2002; Fahrbach et al. 2011). The circulation pattern of the eastern Weddell gyre is particularly important for this study since it affects the stratification of the upper ocean, upstream of the Maud Rise – Astrid Ridge complex. The northern boundary of the central and eastern Weddell Gyre is determined by the southern edge of the ACC while their southern boundary is determined by the Antarctic coastline.

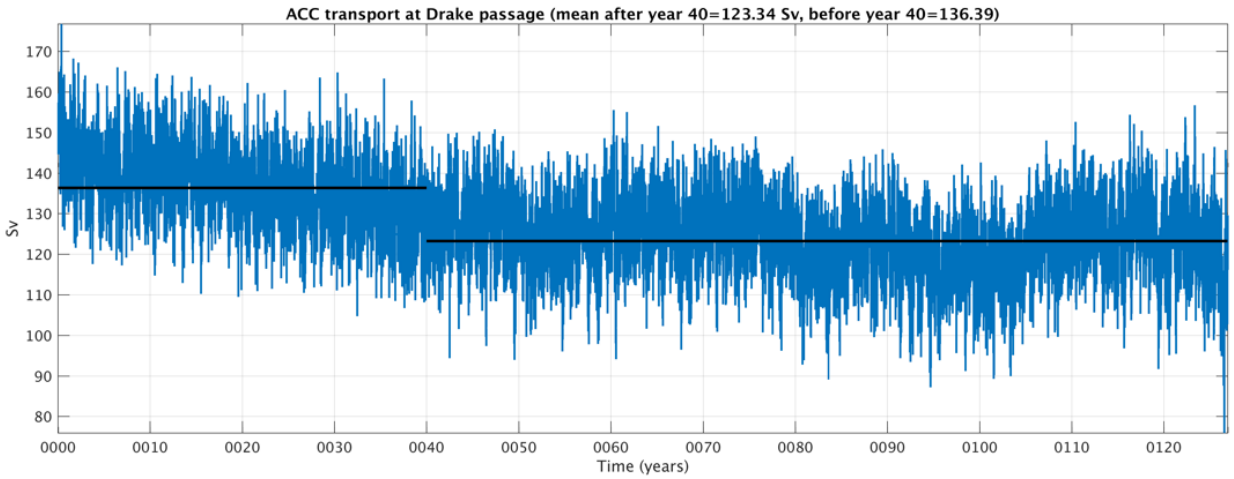

Figure 3: Monthly-mean transport of the ACC across the Drake Passage in the E3SMv0-HR simulation.

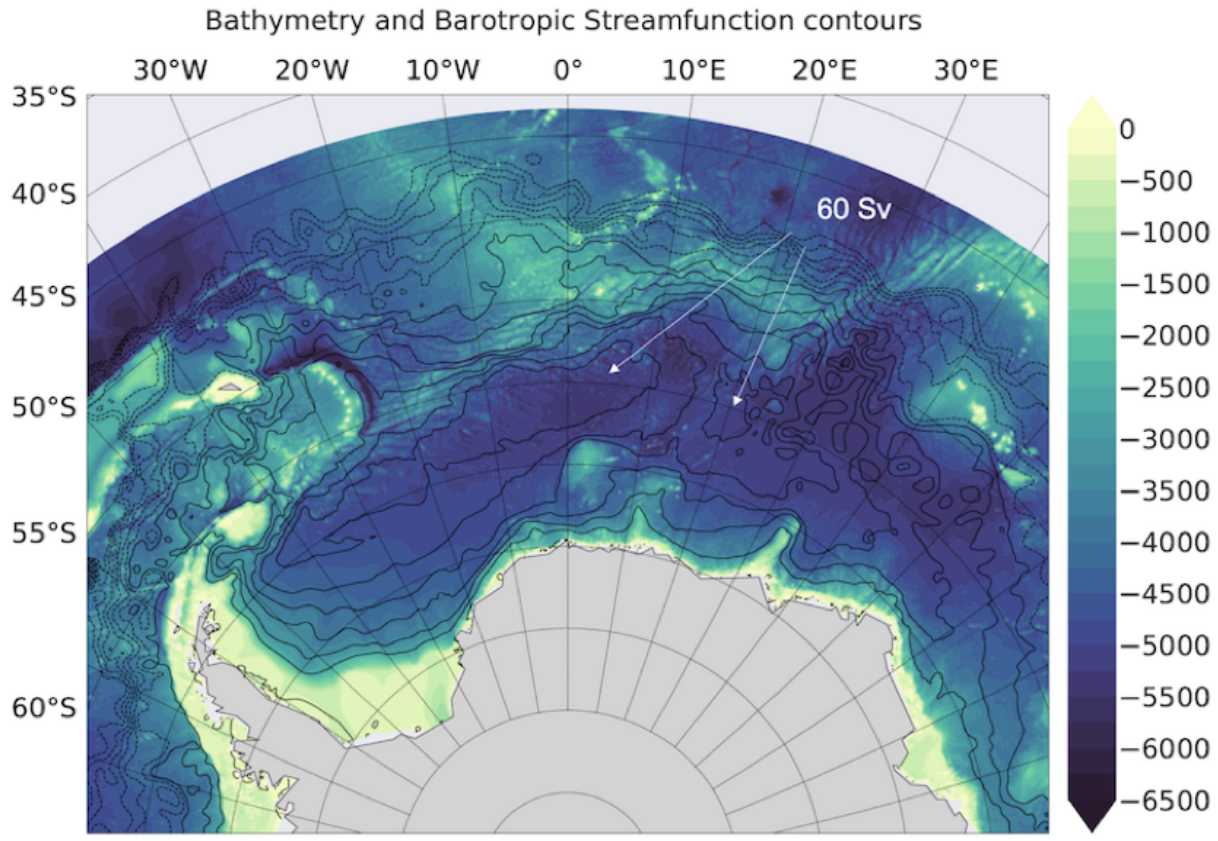

Figure 4: Bathymetry of Weddell Sea and surroundings (colorbar: depths (m)) in E3SMv0-HR with contours of the barotropic volume transport stream function climatology showing the Weddell Gyre circulation. The contours (increments every 10 Sv) indicate the zonal and meridional extent of the cyclonic double cell Weddell Gyre.

To the west, the meridional boundary of the central Weddell Gyre is determined by the Antarctic peninsula. To the east, the meridional boundary of the central Weddell Gyre is just east of the Greenwich Meridian, and that of the eastern Weddell gyre cell is ~30°E (Orsi, Nowlin JR, and Whitworth 1993). The structure of the eastern Weddell gyre is mainly determined by the wind field, ocean stratification and subtle bathymetric features (Schröder and Fahrbach 1999). According to observations, the eastern Weddell gyre transitions from flowing eastward to westward at ~65°S and between 35°E-40°E (Schröder and Fahrbach 1999). At that point, the southern limb of the eastern Weddell gyre turns and flows westward towards Maud Rise (~3°E, 65°S). Fig. 4 shows the Weddell gyre by means of the barotropic volume transport stream function averaged over year 50-127 of the E3SMv0-HR simulation. It compares well with observations, clearly revealing the characteristic double cell structure, and the intricate pattern in the eastern cell (Fahrbach et al. 2011). While LR simulations are able to reproduce the double cell structure, they do not capture the intricate noisiness of the eastern cell (Timmermann 2002).

Meridional cross sections of temperature and salinity along the 0° and 35°E lines for the September month climatology (with climatologies computed over years 50-127) are used to visualize the simulated double cell structure of the Weddell gyre (Figs. 5 and 6). These cross sections are compared to observations based on hydrographic data collected from 1989–1996 (Schröder and Fahrbach 1999; their Figs. 4 and 5). The meridional cross section along the Greenwich meridian (Fig. 5) shows the cold and relatively fresh water below ~2000 m depth doming upward between 57°S-63°S, similarly to the observations. This water mass fills the bottom of the basin up to ~69°S in the south and ~55°S in the north. At intermediate depths of 200 - 2000 m, a warm and salty water mass apparently circulates the dome of colder and fresher water. This

water mass is the WDW at the southern rim of the gyre, and the CDW transitioning into WDW at the northern rim of the gyre (Orsi, Nowlin JR, and Whitworth 1993; Fahrbach et al. 2011).

The meridional cross section along 35°E (Fig. 6) reflects the eastern cell of the Weddell gyre. The observations for this region end at 65°S, so we can only compare the structure north of 65°S. There is no strong doming of the cold and fresh bottom water mass as seen along the Greenwich meridian (Fig. 5). The isotherms primarily rise toward the continental slope with a weak dome between 64°S-66°S. The main difference between Figs. 5 and 6 is in the temperature and salinity values between 200–2000 m, in that this subsurface water mass is significantly warmer and saltier along 35°E than along the 0° longitude. Along both longitudes, the simulation reproduces the observed temperature and salinity structure reasonably well.

Figs. 7 and 8 show comparisons between simulated and Southern Ocean State Estimate (SOSE) salinity and temperature at the surface and 500 m depth, for the climatological months of February (Fig. 7) and September (Fig. 8). The SOSE reanalysis data is generated from an ocean model that assimilates observations during 2005-2006 (Mazloff, Heimbach, and Wunsch 2010). While similarities can readily be identified, one should note that the E3SMv0-HR simulation has been run under preindustrial conditions, while SOSE represents in essence present-day conditions. Both in February and in September, the surface salinities of both products are comparable, but the surface temperatures are not. The surface temperature in the E3SMv0-HR simulation is much warmer in February, and slightly warmer in August. The latter could be attributed to the presence of large open ocean polynyas and a more dynamic sea-ice cover in the model. The subsurface ocean at 500 m depth in the eastern Weddell Sea is warmer and saltier in E3SMv0-HR than in SOSE, which indicates a more vigorous infusion of CDW into the Weddell gyre in the former, consistent with a 30% weaker gyre transport in SOSE (about 40 Sv) compared to E3SMv0-HR

(about 60 Sv; Fig. 4). On the other hand, the subsurface ocean in the central Weddell Sea is much cooler in E3SMv0-HR than in SOSE, consistent with a more pronounced doming of colder and fresher WSDW in a stronger gyre (see Fig. 5).

The emergence of open ocean polynyas in the Southern Ocean encouraged us to investigate the possible reasons for their occurrence. Animations of monthly sea ice concentration over the entire length of the E3SMv0-HR simulation indicate that open ocean polynyas form intermittently throughout the simulation, exhibiting geographical extents, timing (July through October) and locations (in the central and eastern Weddell Sea) that are very similar to satellite observations, available since 1973. Only two periods, years 55-62 and 105-115 show a large ice-free embayment in the central Weddell Sea in winter. Such have not been observed since the beginning of the satellite record. In contrast to E3SMv0-HR, no open ocean polynyas form in E3SMv0-LR, and neither in any LR CESM simulation performed in the past.

The first long lasting (i.e. occurring for more than one winter season) MRP forms in the austral winter (July-August-September-October or JASO) of simulation year 24, re-emerging sporadically and sometimes for several years in a row thereafter. The first MRP occurs east of Maud Rise (at ~15°E), slowly expanding westward over Maud Rise and slightly beyond during years 25 and 26, and finally becoming a small WSP in year 27. This pattern is seen before every initiation of a WSP and of an embayment, suggesting that MRPs are a precursor for WSPs, similarly to what was observed in the 1970's.

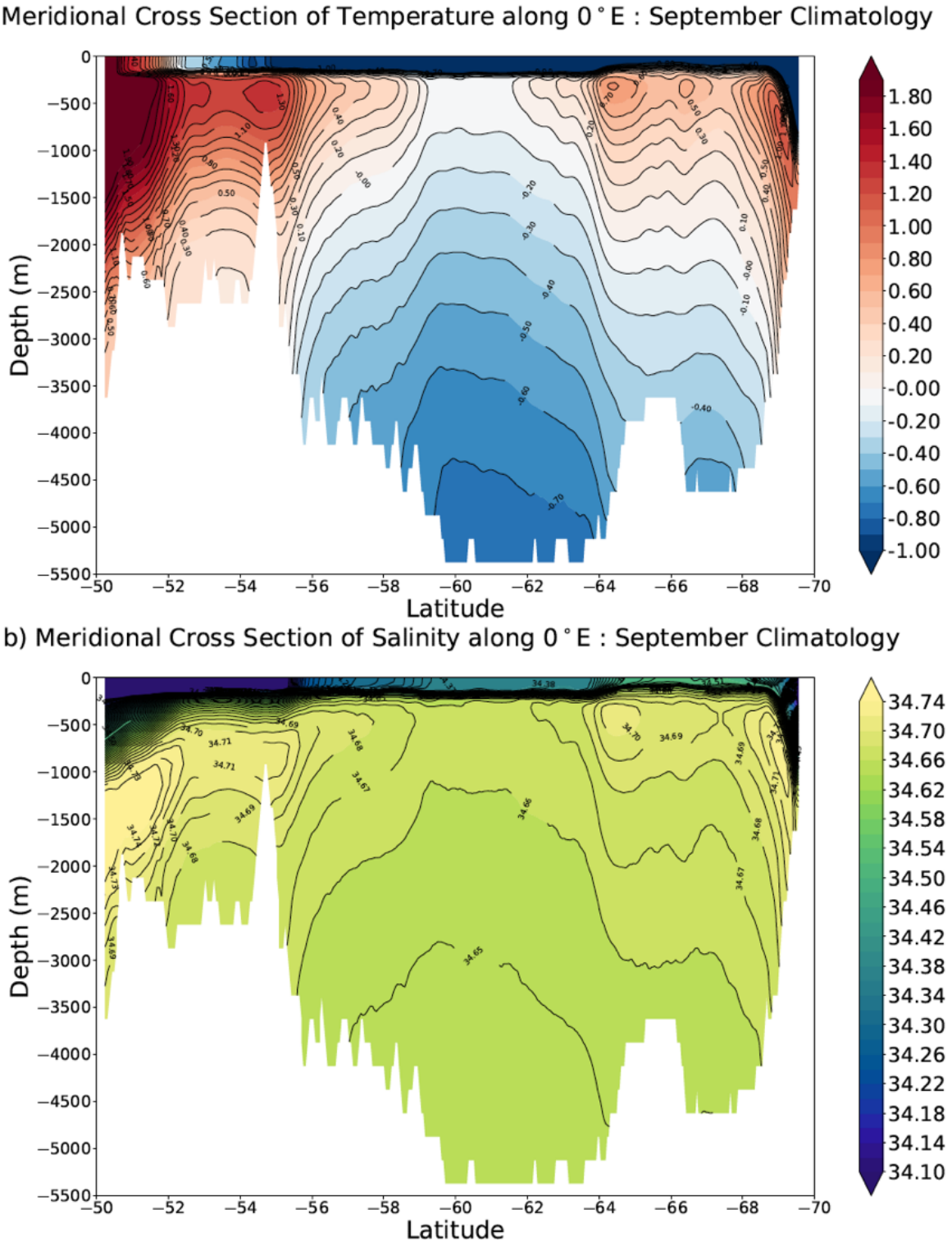

Figure 5: September climatology of simulated a) temperature and b) salinity in the central Weddell Sea along 0°.

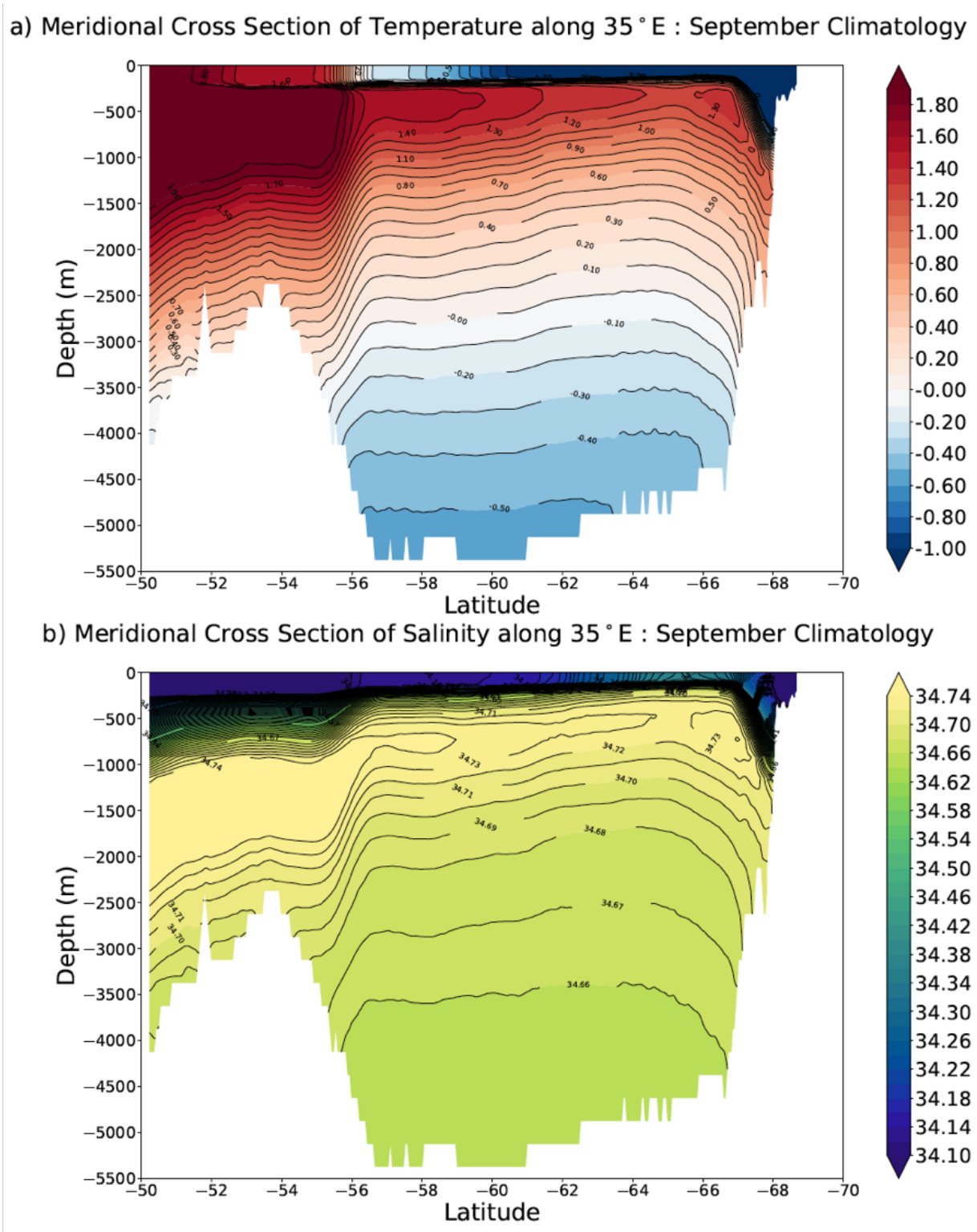

Figure 6: Sections along 35°E; otherwise as Fig.5.

In Chapter 3, we focus on six MRP initiation events, i.e. polynya events that start from a condition of no MRP. Since MRPs seem to originate east of Maud Rise, we extend our definition of MRPs to *long lasting open ocean polynyas occurring within the wider region between Astrid Ridge and Maud Rise* (see bathymetry in Figs. 4 and 9). Astrid Ridge is another prominent bathymetric feature that lies 480 km east of Maud Rise and extends northward from the Antarctic coast to 65°S (Fig. 2 in *Bergh*, 1987). The most prominent peak on the ridge is located at 12.5°E, 65.5°S, extending from the seafloor to 2500 m below the sea surface, and is part of Queen Maud Land region of Antarctica. Each sequence of the newly defined MRPs starts in JASO of simulation years 24, 31, 47, 64, 69, and 101, respectively, from here on referred to as "MRP initiation", or MRP-I years. These MRPs then continue to occur for a few years after their respective MRP-I year, but we exclude those subsequent years from the analysis of the polynya-state in order to avoid any preconditioning effects on the stratification due to the presence of the polynya itself.

To illustrate the mean polynya extent for each MRP-I year, Fig. 10 presents the JASO average of sea ice concentration around Maud Rise and shows the presence of a large quasi ice-free area with mean sea-ice concentration lower than 15% and mean sea-ice thickness lower than 0.1 m. In order to investigate the potential MRP formation mechanisms, we then study the transition from MRP-off to MRP-on conditions by analyzing a composite that consists of the years immediately preceding each MRP-I event (years 23, 30, 46, 63, 68, and 101). We refer to these years as "MRP preceding", or MRP-P years. Finally, years that show no sign of MRP or WSP formation, are from here on referred to as "no MRP", or MRP-N years. In addition to comparing mean fields over the composites described above, we also consider anomaly fields with the purpose of better characterizing anomalous properties when transitioning from MRP-P to MRP-I and MRP-N years. The anomalies are computed with respect to a mean monthly climatology, in turn calculated over

years 20-127, i.e. excluding the first 20 years of the simulation when the strongest adjustments take place. Since we are in essence looking at inter-annual variability around Maud Rise, we do not expect the continuing climate drift of the model (up until year 50) to affect our conclusions.

In Chapter 4, we focus on the formation of WSPs and their transformation from MRPs. We study four independent WSP events that begin as MRPs over the Maud Rise - Astrid Ridge complex and spread westward into the Weddell Sea over consecutive years, thereby developing into full-scale WSPs. In some years, the WSPs grow into larger "embayments" (EMBs), meaning that open water is not totally enclosed by sea ice. These are still included in our analyses and are considered as WSP since they form west of Maud Rise. Four of the six MRP-I events studied in chapter 3 turn into WSPs. The four years when MRPs transition into WSPs, we refer to as "MRP+WSP" years. The years with MRP events that do not develop into WSPs are referred to as "MRP-only" years.

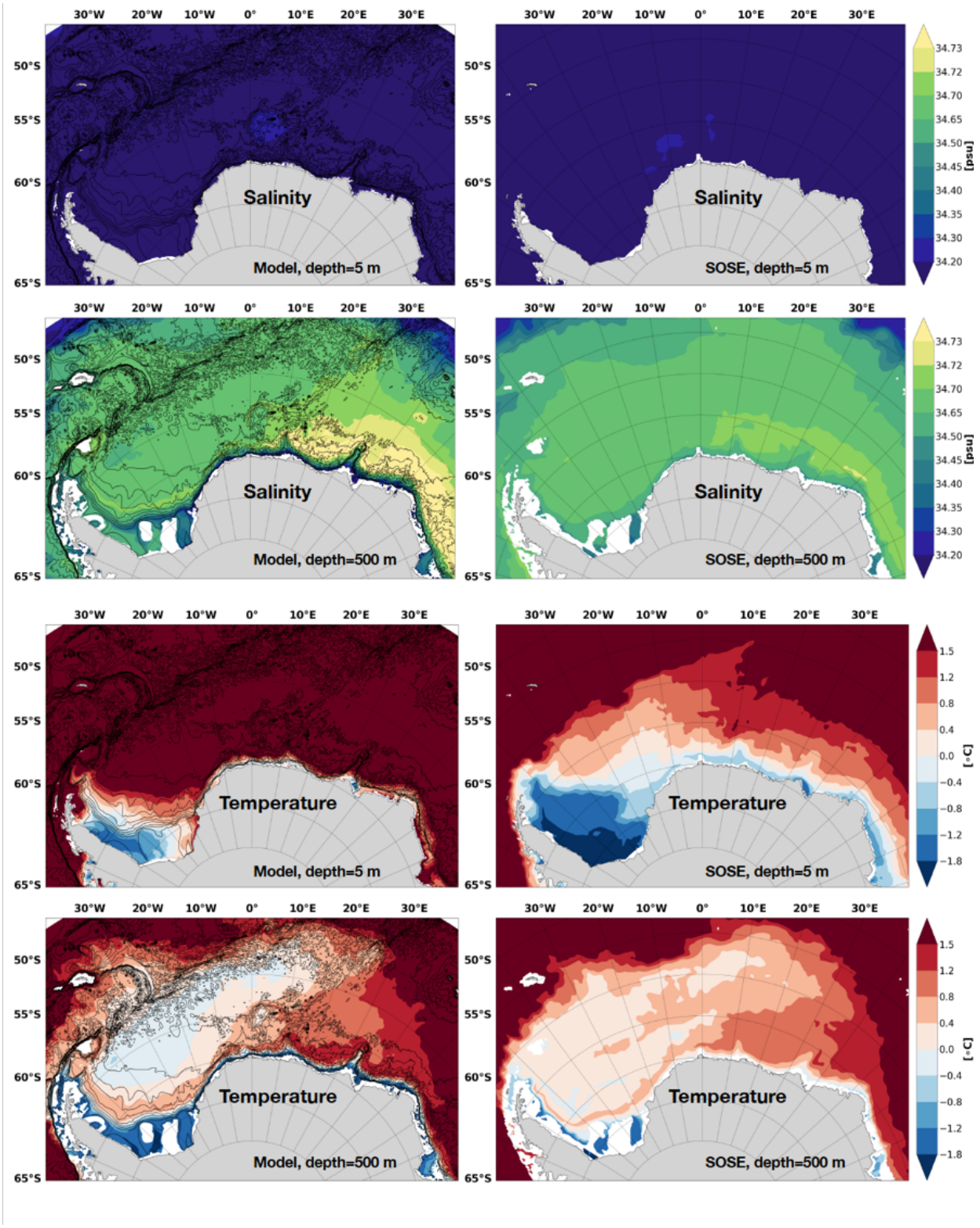

Figure 7: Comparison of SOSE data (right panels) and E3SMv0-HR simulation climatology of temperature and salinity for the month of February at 5m (respective upper panels) and 500m depths (respective lower panels). Notice nonlinear color scale.

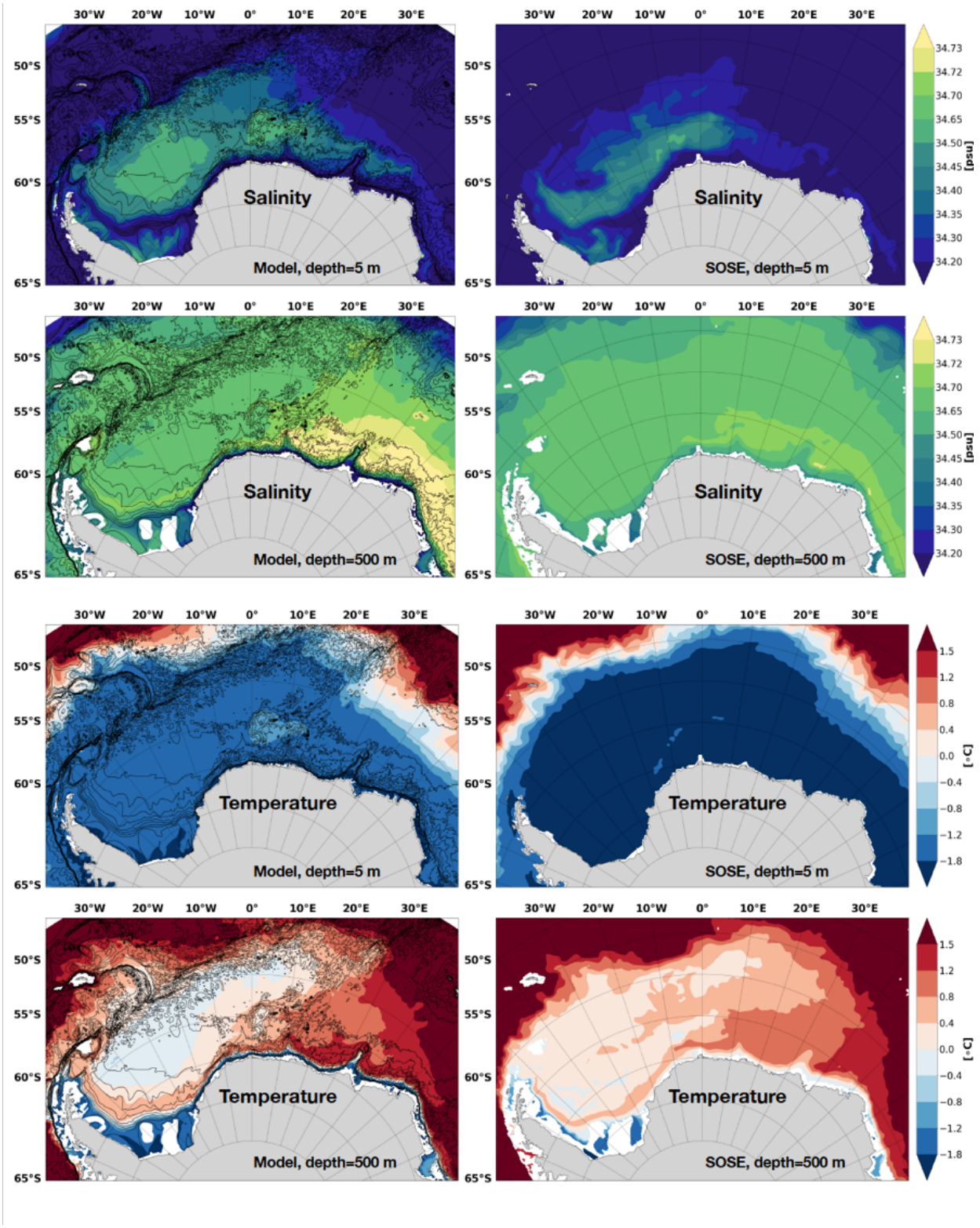

Figure 8: Same as Fig.7, but for September.

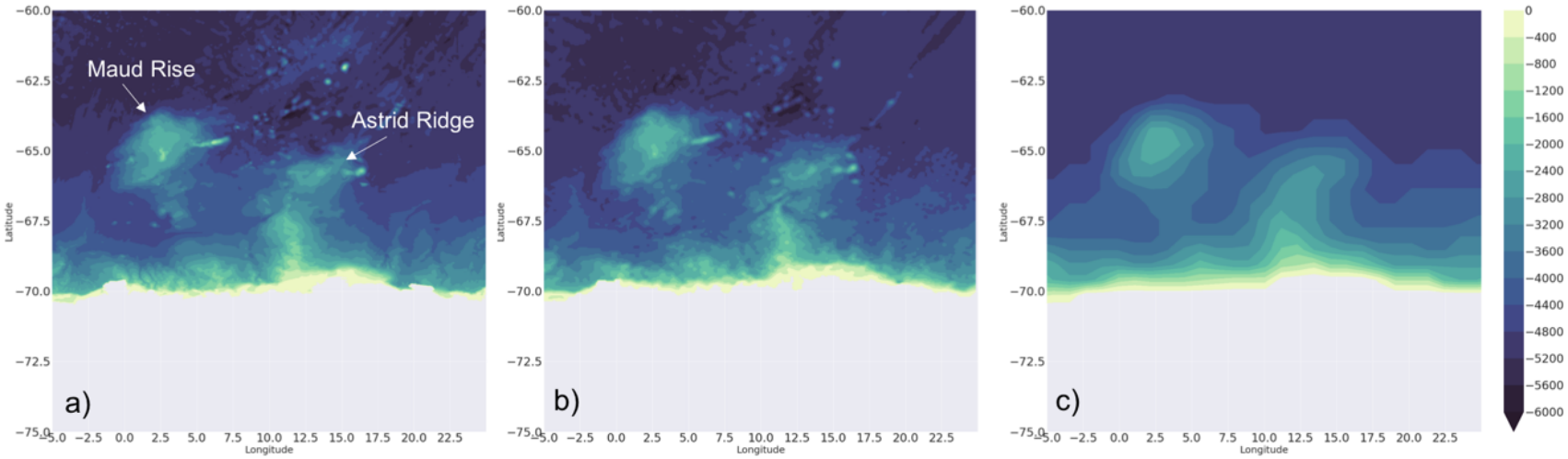

Figure 9: Bathymetry around Maud Rise and Astrid Ridge in (a) the GEBCO observations, (b) E3SMv0-HR simulation, and (c) E3SMv0-LR simulation.

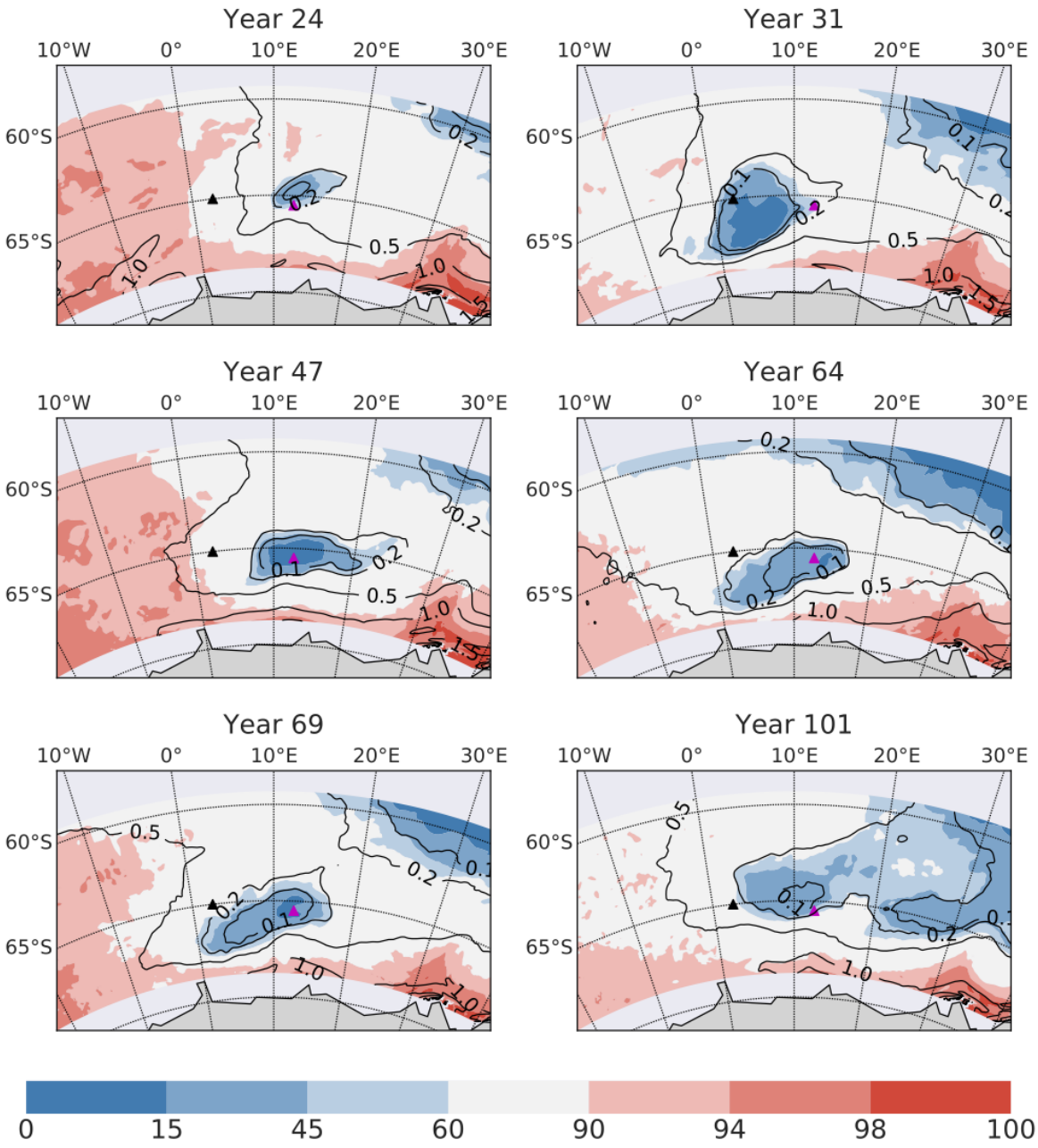

Figure 10: Annual winter (July-August-September-October) average of sea ice concentration around Maud Rise and Astrid Ridge of the six MRP-I years in the E3SMv0-HR simulation. The contours represent sea-ice thickness in meters. The shaded dark blue region is the MRP. The peaks of Maud Rise and Astrid Ridge are indicated by a black and pink triangle, respectively. Notice the nonlinear color scale.

Description	Term used	Years
Maud Rise Polynya: OOP over Maud Rise -Astrid Ridge complex (0°-15°E, ~65°S)	MRP	N/A
Year of transition from no polynya to onset of MRPs	MRP-I years	Years 23, 30, 46, 63, 68, 100
The last no polynya year preceding MRP-I year	MRP-P years	Years 22, 29, 45, 62, 67, 99
Weddell Sea polynya: large OOP in central Weddell Sea west of Maud Rise	WSP	N/A
Years of MRP that evolve into WSP	MRP+WSP years	Years 24-27, 47-62, 69-80, 100-123
Years of MRPs that do not develop into WSPs	MRP-only years	Years 31-39, 64-66
Years with no OOPs	No polynya years including MRP-N years	Years 20-23, 40-46, 67-68; 81-100

Table 1: Terminologies used for the different types of open ocean polynyas in the Weddell Sea.

3. PRECONDITIONING AND FORMATION OF MAUD RISE POLYNYAS IN A HIGH-RESOLUTION EARTH SYSTEM MODEL *

The discussion of the results of this part of my dissertation is organized as follows: Section 3.1 describes the evolution of the simulated MRPs over Maud Rise and Astrid Ridge; Section 3.2 discusses the importance of an isolated Taylor column over Maud Rise and Astrid Ridge as a necessary pre-condition for deep convection; Sections 3.3 and 3.4 present two possible mechanisms that trigger the convection, the intensification of the large scale Weddell gyre circulation and the formation of anomalously high salinity waters in the upper ocean near Maud Rise; finally, Section 3.5 describes the impact of a sequence of consecutive MRPs on deep water masses that lie below the WDW.

3.1 Evolution of MRPs in E3SMv0-HR

The time-space evolution of the simulated polynya events is illustrated in Fig. 11, through a Hovmöller diagram of JASO mean maximum mixed-layer depth (Fig. 11a; maximum value computed over monthly periods) and JASO mean sea ice concentration (Fig. 11b) averaged over the latitudinal band 64°S-68°S and spanning the entire E3SMv0-HR simulation period. The vertical pink line represents the peak of Maud Rise (2.5°E) and the white vertical line represents the peak of Astrid ridge (12.5°E). Deep mixed layers coincide with low sea ice concentration. Open ocean polynyas thus reflect deep convective events. Fig. 11b reveals consecutive MRPs occurring over Maud Rise and between the seamount and Astrid Ridge after each MRP-I event (MRP-I years are indicated by red dashed lines in Fig. 11). We also note WSPs and large embayments occurring west of Maud Rise, with the embayments characterized by massive convective events extending to 40°W and beyond during two distinct time periods, years 55-62

* Partly published in AMS Journal of Climate (Kurtakoti et al., 2018)

and 105-115. Prior to WSPs, convection initiates over the Maud Rise–Astrid Ridge complex causing MRPs. The associated pattern of deep mixed layer and low ice concentration propagates slowly westward into the central Weddell Sea. The annual maximum mixed layer depth of each of the six MRP events is greater than 500 m. This allows the core of the WDW to break into the surface layer, which leads to sea ice melting or prevents further sea ice formation.

To quantify the mean spatial extent of the simulated MRPs, and to contrast them to conditions when there are no MRPs, Figure 12 shows the spatial distribution of the maximum mixed layer depth and sea ice concentration during September of the MRP-N and MRP-I years' composites. The typical pattern of MRPs consists of very low ice concentration (Fig. 12b) coinciding with a deep mixed layer around Maud Rise and Astrid Ridge (Fig. 12d). On the other hand, the MRP-N years' composite (Fig 12a,c) shows mostly high sea ice concentration and low mixed layer depth, a distinct crescent of lower mixed layer depth and somewhat lower sea ice concentration encircling the northern flank of Maud Rise, and a similar but wider pattern over Astrid Ridge (note the different color scales for sea ice concentration in MRP-I versus MRP-N years). Relative to the surroundings, the reduction in sea ice concentration amounts to ~5%, and that of the mixed layer depth to at least 100 m in the crescent. The location of the crescent coincides with the strongest gradient in the bathymetry of Maud Rise. The mixed layer pattern and values are strikingly similar to what has been reported by de Steur et al. (2007) from measurements (their Fig.2b), and the reduced sea-ice concentration pattern is remarkably similar to the so-called ice 'halo' that is commonly observed through satellite retrievals (Lindsay et al. 2008). The whole region east of Maud Rise and over Astrid Ridge is also characterized by a shallower mixed layer depth, which overlaps with a somewhat lower sea-ice concentration pattern with respect to the surrounding area.

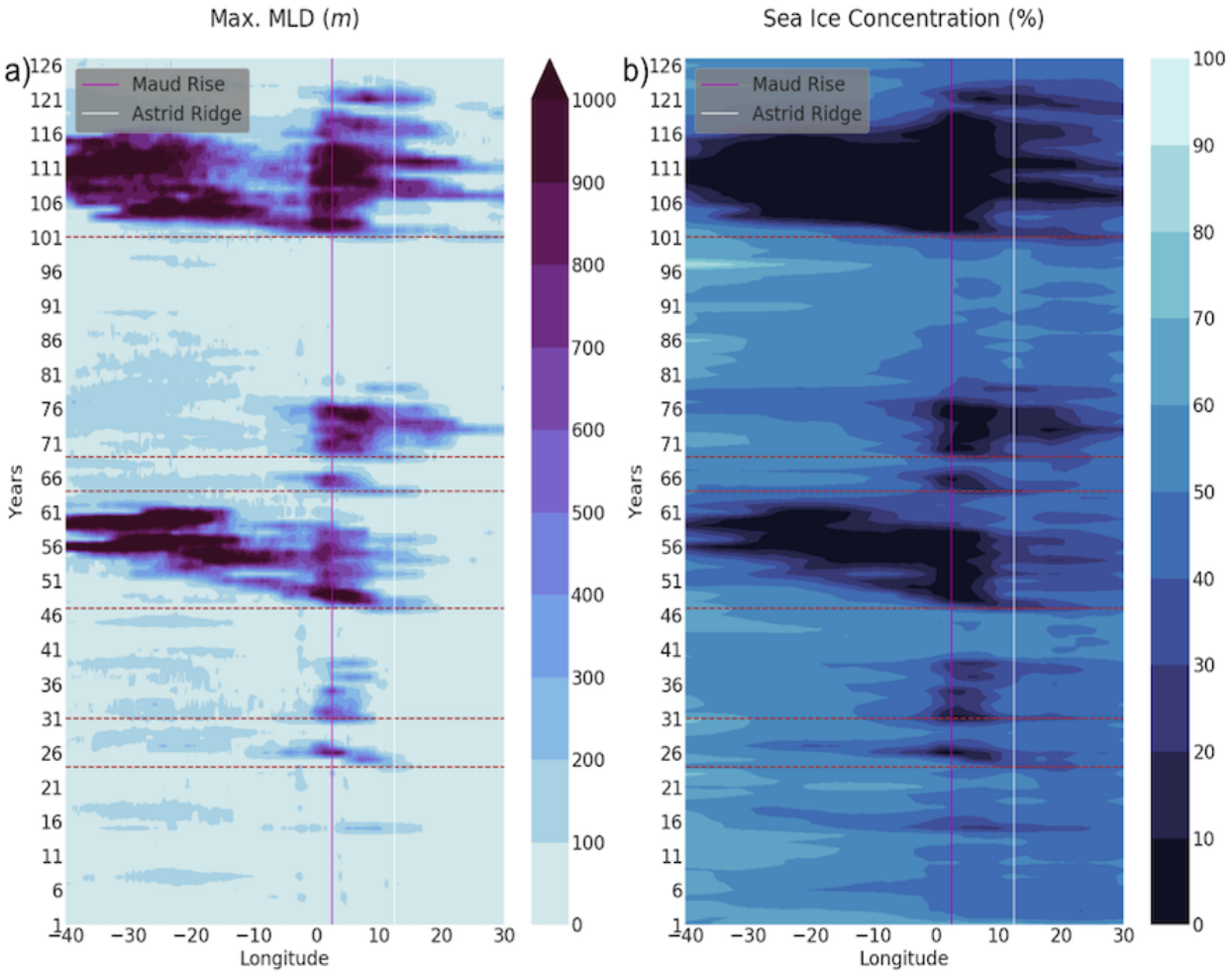

Figure 11: Hovmöller diagram spanning the full simulation of the JASO mean (a) maximum mixed layer depth and (b) sea ice concentration averaged over the region 64°S:68°S. The pink and white lines indicate the central peak of Maud Rise and Astrid Ridge, respectively. The horizontal red dashed lines indicate the six MRP-I years.

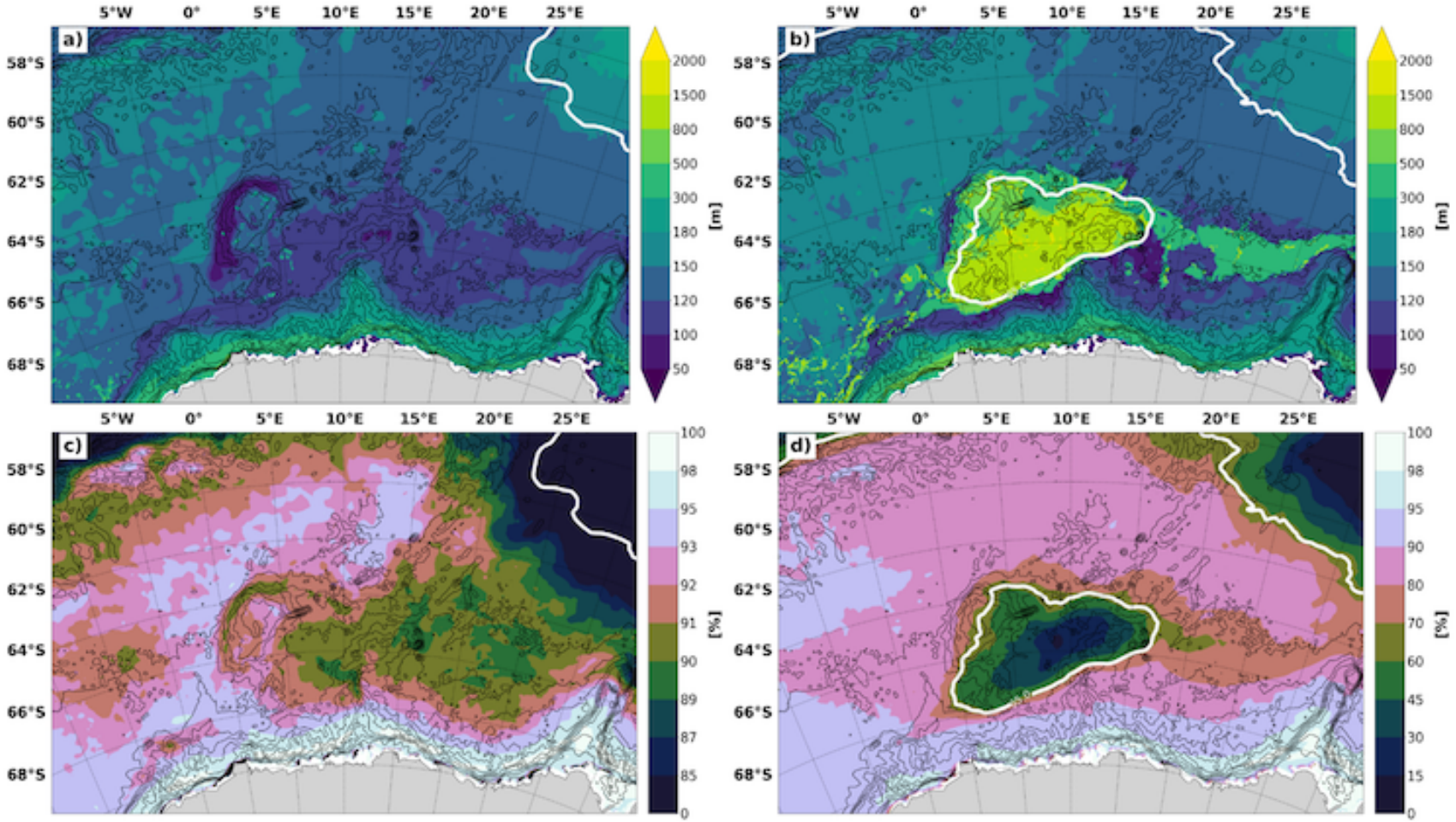

Figure 12: September averages of (a,b) maximum mixed layer depth and (c,d) sea-ice concentration, for (a,c) the MRP-N composite and (b,d) the MRP-I composite. Note the nonlinear colorbar levels and the different ice concentration scales. Black contours indicate bathymetry while the white contour marks the 65% ice concentration level.

To further contrast MRP-N to MRP-I conditions, and eventually study MRP preconditioning, it is useful to compare the typical hydrographic properties in MRP-N years (Fig.13) with those in MRP-I years (Fig. 14). Both figures illustrate the September mean spatial distribution of potential temperature, salinity, and potential density (at surface pressure) at 5 m and at 300 m depth. We choose these two depths to contrast the spatial distribution of the cold surface mixed layer (ASW) with the warm subsurface layer (WDW). The simulated patterns and values of these variables are again strikingly similar to what has been observed around this region (de Steur, Holland, Muench, and Mcphee 2007). In the MRP-I composite, the surface properties around Maud Rise and Astrid Ridge (Fig, 14a,c,e) are distinctly warmer, saltier, and denser than in the corresponding MRP-N composite (Fig. 13a,c,e). Higher density, in particular, indicates considerable convective potential energy release (Stössel and Kim 2001). A striking feature is the highest density emerging on the northeast flank of the Astrid Ridge peak (Fig 14e), which is also the region east of Maud Rise where most MRPs are initiated (Fig. 11b). At depth (300 m; Fig. 14b,d,f), the water over the Maud Rise – Astrid Ridge complex is colder, fresher, and denser compared to the immediate surrounding. In fact, this surrounding is characterized by a crescent of anomalously warm and salty water that reflects the infiltration of WDW seemingly propagating along the northern flank of the Maud Rise – Astrid Ridge complex.

3.2 Local topographic effects of Maud Rise and Astrid Ridge on preconditioning: role of the Taylor cap

We next investigate possible local mechanisms that precondition the Maud Rise region for deep convection and MRP formation. The most striking feature in Fig. 13b,d,f is the halo of high temperature and high salinity at depth around the Maud Rise – Astrid Ridge complex, which is similar to but more pronounced than what is seen in MRP-I years (Fig. 14b,d,f).

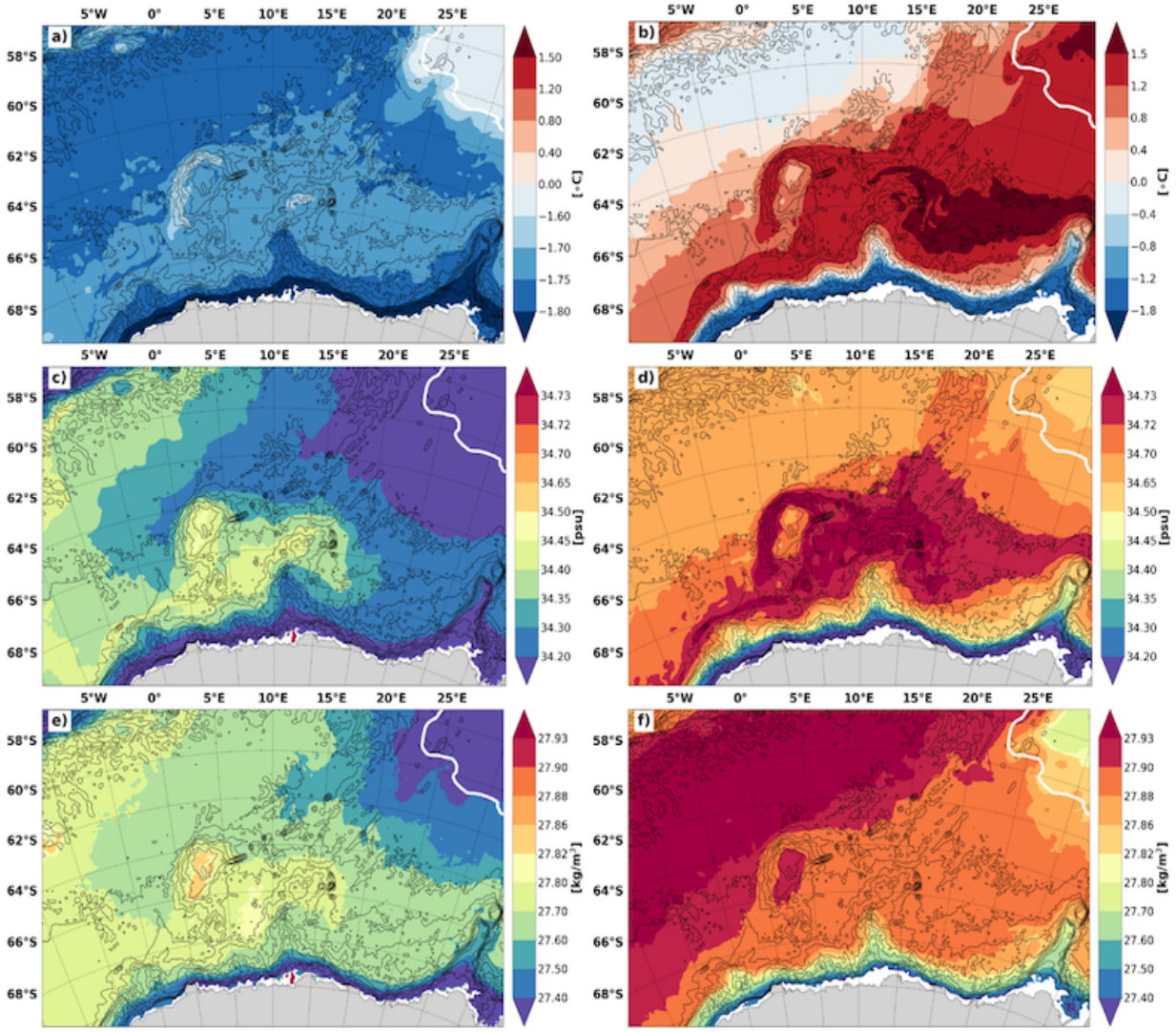

Figure 13: September averages of (a,b) potential temperature, (c,d), salinity, and (e,f) potential density (minus 1000; potential density computed with respect to the surface), for the MRP-N composite at (a,c,e) 5 m and (b,d,f) 300 m depth. Note the different colorbar levels for panels (a) and (b), and the nonlinear colorbar levels for salinity and potential density. The white contour marks the 65% ice concentration level.

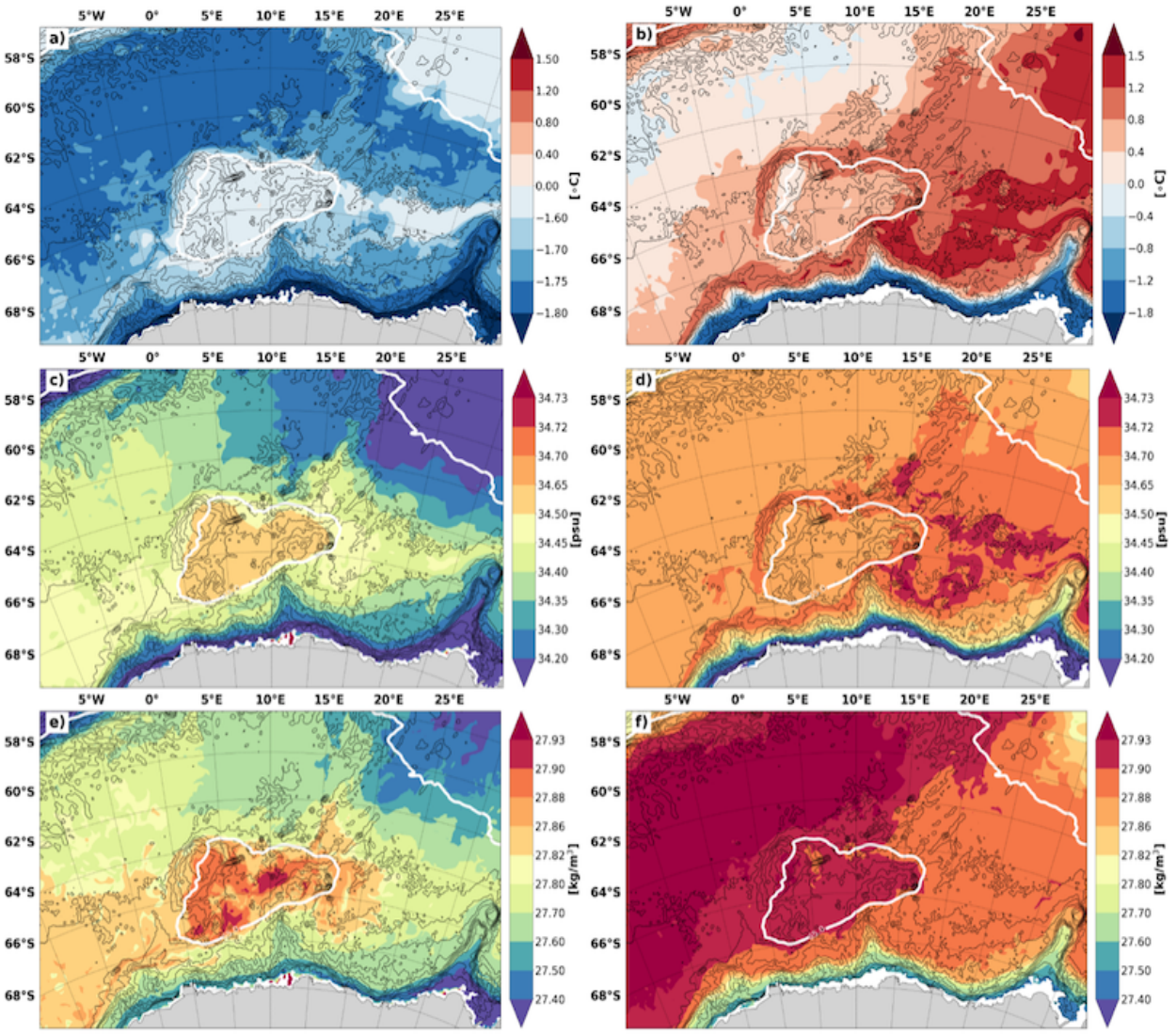

Figure 14: Same as Fig. 13, but for the MRP-I composite.

Even at the surface, the MRP-N composite shows the presence of a crescent shaped region of higher temperature along the northwestern flank of Maud Rise (with a similar but smaller crescent near the peak of Astrid Ridge), a clearly higher salinity pattern over Maud Rise – Astrid Ridge, and a corresponding pattern of denser water (Fig. 13a,c,e). These features point to the presence of a Taylor cap, with the strongest indication for such over Maud Rise. The stronger cap is supported theoretically by the fact that Maud Rise features a significantly larger 'scaled bump height' than Astrid Ridge, in agreement with Meredith et al. 2015 (their Fig. 10). The flow field of the Weddell

Gyre makes it impinge on Maud Rise and Astrid Ridge from the east. This is indicated by the path of warm and salty WDW at 300 m depth. The Taylor cap prevents the impinging flow from going over the seamount even at the surface. As a result, the impinging flow must go around the obstacle, in this case Maud Rise, and to some extent, Astrid Ridge. This causes the subsurface WDW to entrain into the surface layer along the steep bathymetric slopes, creating the slightly elevated temperature signal at the surface. The water mass over Maud Rise having a distinctly different temperature and salinity signature than the surrounding waters points to the presence of a body of water that remains fairly isolated over the seamount, i.e. a persistent Taylor cap, even in MRP-N years. The Taylor cap is thus a crucial preconditioning for MRPs to form at that location, as pointed out in earlier studies (see chapter 1).

The Taylor cap over Maud Rise can accordingly be distinguished by anomalously cold and fresh water relative to its immediate surroundings at depth, i.e. a water mass that is isolated from the impinging WDW. The evolution of this feature in time and space over the entire period of the E3SMv0-HR simulation is illustrated in Fig. 15, which presents the Hovmöller diagram of the temperature and salinity field averaged over the 250-1000 m depth range (i.e., below the pycnocline) and over the latitudinal band 64°S-68°S. The Taylor cap over Maud Rise can readily be identified by the relatively colder and fresher subsurface water over the seamount with respect to its immediate surrounding (WDW). Such feature is always present: even during the MRP-N years 91-101, when the subsurface water over MR is warmer and saltier than in other years, it is still colder and fresher than the surrounding WDW. It is also apparent that a weaker Taylor cap tends to linger over Astrid Ridge, although not as persistently as over Maud Rise. Finally, Fig. 15 shows that low temperature and low salinity episodes are also present east of Astrid Ridge,

propagating westward, getting enhanced over the peak of Astrid Ridge, and even more so over Maud Rise.

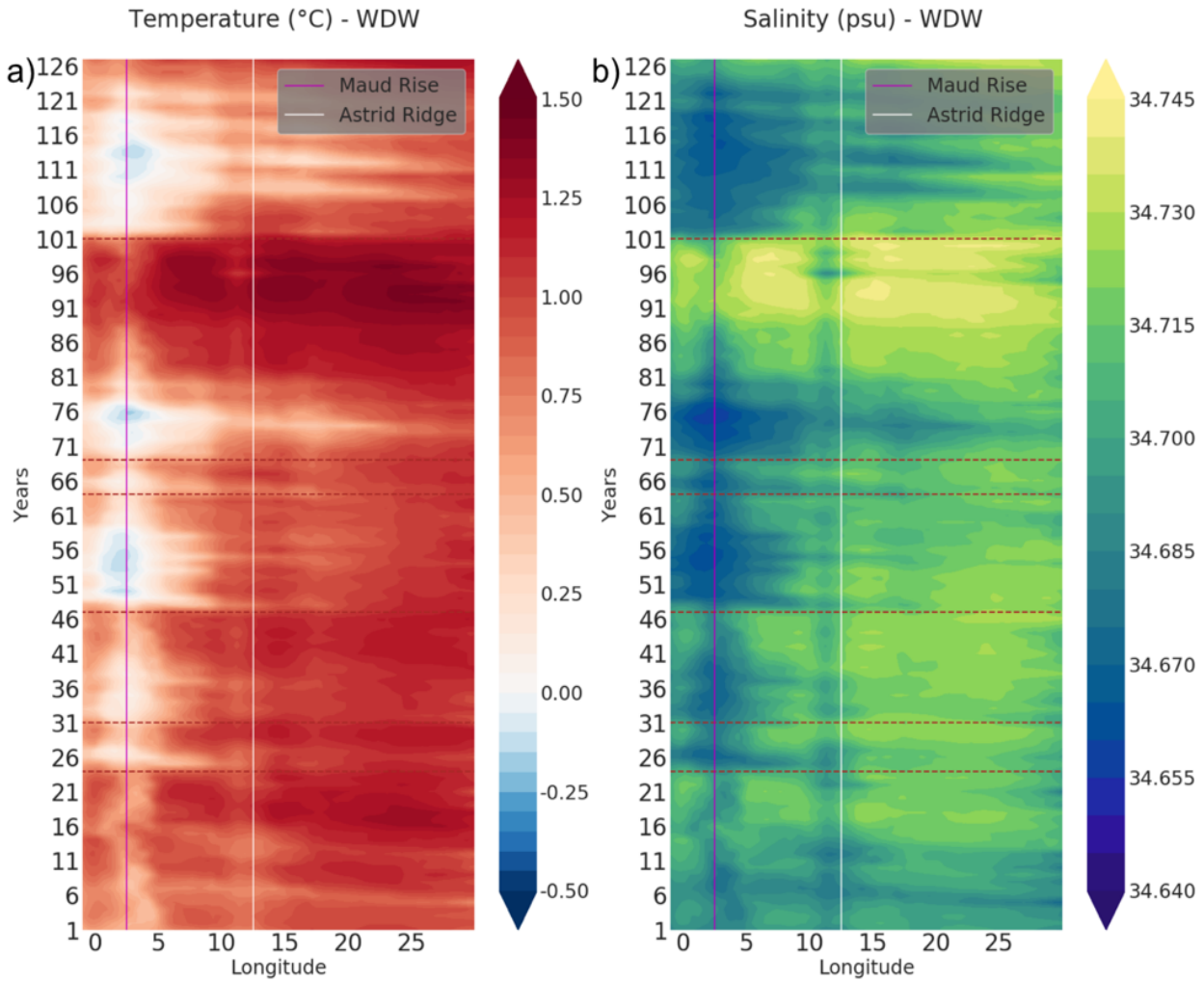

Figure 15: Hovmöller diagram of 1-year running averaged (a) temperature and (b) salinity, spatially averaged over 250-1000 m depth and over the region 64°S-68°S. The pink and white lines indicate the central peak of Maud Rise and Astrid Ridge, respectively. The horizontal red dashed lines indicate the MRP-I years.

It is important to describe the flow field around Maud Rise, which is illustrated in Fig. 16 in terms of vorticity of the sea ice drift (Fig. 16a), and a meridional section across the peak of Maud Rise (which is protruding into the bottom part of the section) of zonal currents overlapped by contours of isopycnals (Fig. 16b). Both panels reflect conditions for September of the MRP-I

years' composite. The strong positive vorticity (red) along the northwestern flank of Maud Rise highlights anticyclonic flow that emerges as the impinging flow goes around the seamount. The currents that create this vorticity pattern are clearly visible at the north side of the section (Fig. 16b), with blue shading meaning westward currents and red shading indicating eastward currents. Both currents are seemingly a baroclinic feature as indicated by the opposite sloping isopycnals north of the seamount. The crescent of positive ice vorticity emerges also in MRP-N years (not shown).

Over the peak of Maud Rise, the sea ice vorticity is negative (blue shaded region in Fig. 16a), indicating weak cyclonic flow. The presence of this cyclonic circulation is contrary to many theoretical studies that look at slow flows impinging on a seamount, using idealized model configurations (Chapman and Haidvogel 1992; Alverson and Owens 1996). These studies show that first the squashing and then the stretching of the water column resulting from the flow interacting with a seamount, causes first anticyclonic and then cyclonic vorticity. Alverson and Owens (1996) show that if the impinging flow is strong enough, then the cyclonic anomaly is advected away and the anticyclonic anomaly remains over the seamount. Our results, indicating an inner circulation of opposite sign over Maud Rise, are more consistent with a theoretical study conducted using laboratory experiments (Mory, Stern, and Griffiths 1987), in which a baroclinic cyclonic eddy is generated over a Taylor column. There is also evidence of a cyclonic inner flow in observations. For example, a weak cyclonic flow over Maud Rise has been reported by Gordon and Huber (1990; their section 6.1), and, while not explicitly mentioned, sampled at hydrographic stations over Maud Rise (de Steur et al. 2007, their Fig. 4; Bersch et al. 1992). Furthermore, our simulated ice vorticity structure (Fig. 16a) is remarkably similar to the results reported in Lindsay et al. (2008; their Fig. 2) based on satellite data analyzed for a year with no MRPs. The pattern of

large positive ice vorticity along the northern flank of Maud Rise emerges in concert with the similarly shaped halo of lower sea-ice concentration shown in Fig. 12c, a feature that has also been reported by Lindsay et al. (2008) and discussed in Holland (2001).

To further investigate preconditioning mechanisms for MRPs, we consider the different hydrographic properties around Maud Rise between MRP-N and MRP-I years in May, which is the last month still unaffected by convection during an MRP-I year. Fig. 17 shows the temperature and salinity profiles for the two composites along the same section as in Fig. 16b. MRP-I years show a more prominent Taylor cap over Maud Rise than in MRP-N years. This is indicated by a more pronounced doming of the isopycnals over the seamount, which forces the warm and salty WDW to flow more tightly around the seamount, and by a more homogenous temperature and salinity distribution below 150 m over Maud Rise. The density distribution described above is consistent with observational studies. For example, de Steur et al. (2007) report doming of the isopycnal σ_0=27.82 between their stations 15 and 17, directly over Maud Rise (their Fig. 3a).

Above 150 m, there is a sharp thermo- and halocline marking the transition to substantially colder and fresher water in the upper ocean. This is true for both MRP-N and MRP-I years, but the MRP-I composite indicates a lower upper ocean stratification (Fig. 17b,d) compared to the MRP-N composite (Fig. 17a,c). In other words, there is a clear indication that, while an MRP has not been triggered yet at this stage (May), the upper 100 m is already saltier (and the subsurface somewhat fresher) in the early stage of MRP-I years compared to MRP-N years. The importance of the upper ocean stratification in triggering MRPs will be further discussed in section 3.1.4.

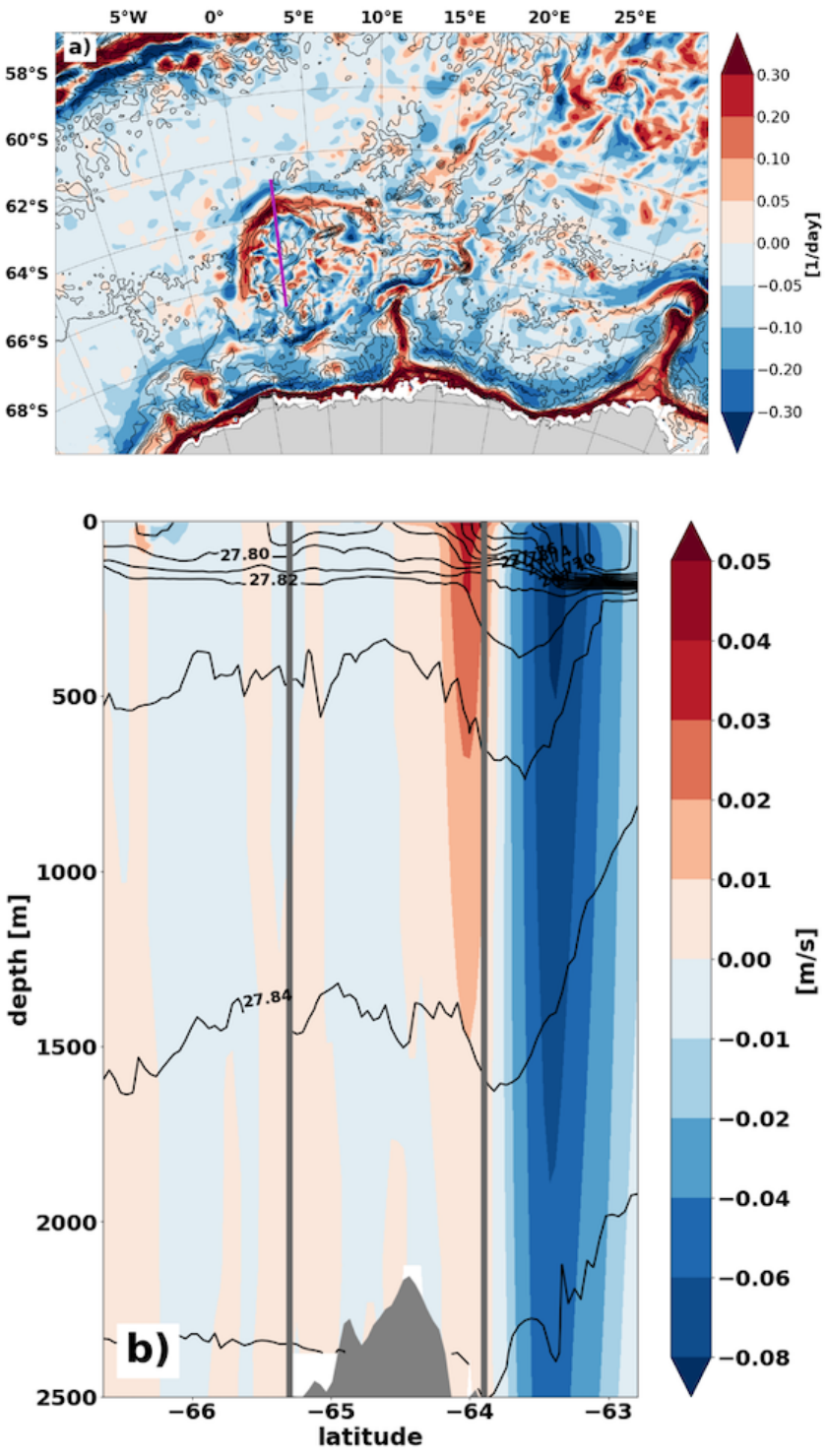

Figure 16: September mean (a) sea-ice vorticity and (b) meridional cross section at 2.3°E (Maud Rise) of zonal velocity for the MRP-I composite. In a), the pink line indicates the position of the cross section plotted in b). In b), potential density contours are in black, while the two grey vertical lines indicate the Maud Rise extent (peak at 64.5°S).

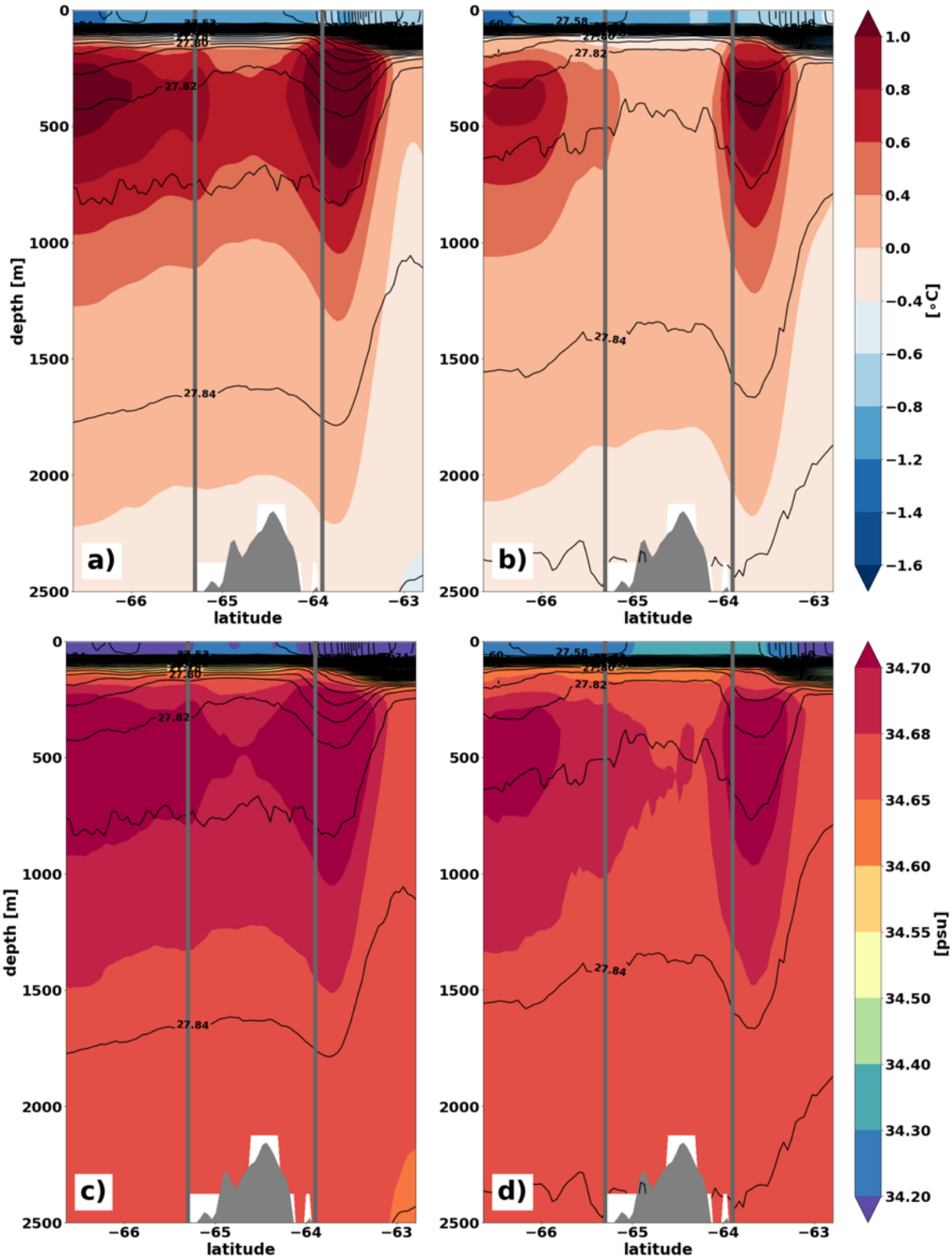

Figure 17: Meridional cross section at 2.3°E of (a,b) potential temperature and (c,d) salinity during the month of May for (a,c) the MRP-N composite and (b,d) the MRP-I composite. Potential density contours are indicated in black. Note the nonlinear colorbar levels.

To summarize, we propose the following local preconditioning mechanism over the Maud Rise – Astrid Ridge complex: the existence of a persistent Taylor cap maintains low stratification over the seamount, making it a preferred location for deep convection if the cap becomes intense enough to interact with the mixed layer above it (see Alverson and Owens, 1996 for the role of stratification in effecting the Taylor cap strength). During MRP-N years, the Taylor cap remains well below the mixed layer (Fig. 17a,c), only causing a reduction in sea-ice concentration or the so-called ice 'halo' at its rim (Fig. 12a). By the fall of MRP-I years, the Taylor cap is strong enough to penetrate the mixed layer, leading to deep convection. In the next two sections, we explore large scale as well as local effects that can trigger convection over the preconditioned region.

3.3 Large scale effects on Maud Rise convection: role of the Weddell gyre strength

A strengthening or a southward shift of the southern hemisphere westerlies creates a stronger negative wind stress curl over the Weddell Sea. This strengthens the cyclonic Weddell gyre and causes WDW to upwell in its center due to Ekman pumping. The associated doming of isopycnals can in turn trigger WSPs. While this is the way WSPs emerge in low-resolution models (e.g., Hirabara et al., 2012; Martin et al., 2013; Cheon et al., 2014), WSPs are in reality and in the E3SMv0-HR simulation preceded by MRPs.

To investigate the possible role of the wind stress in initiating MRPs, we first show the full time series of the wind stress curl anomaly (Fig. 18). Periods when MRPs, WSPs, and embayments occur are indicated by different color shading. Anomalously negative wind stress curl is needed to cause a spin-up of the Weddell gyre and an increased uptake of WDW by the gyre. The following results can be summarized from Fig. 18: i) years when no polynyas are present are characterized by generally positive wind stress curl anomaly. This is especially clear during the MRP-N years; ii) large WSPs and embayments (blue and purple shading) are instead typically

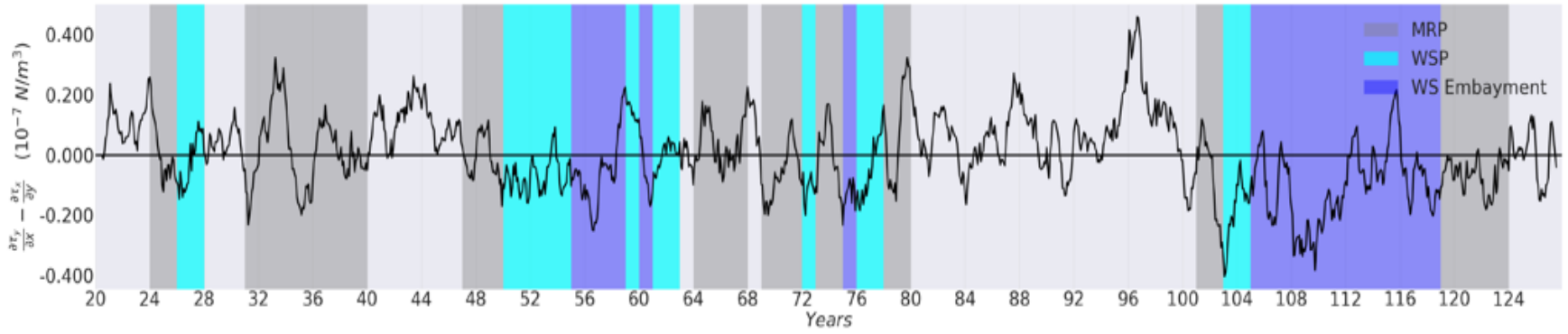

Figure 18: Time series of the wind stress curl anomaly over the Weddell Sea (anomalies are computed with respect to a climatological monthly mean over years 20-127). The shading represents years with the different types of open ocean polynyas.

characterized by negative wind stress curl anomaly. The longer the anomaly stays negative the higher the likelihood that WSPs turn into embayments (compare first WSP in year 26 with the transition WSP to embayments in years 49-59 and 102-112); iii) in all MRP cases (dark grey shading) except for the first one (year 24), the wind stress curl anomaly changes from a positive to a negative state during the MRP-P year or during the first part of the MRP-I year, suggesting that the intensification of the gyre plays a role in the MRP formation. Nevertheless, a negative wind stress curl anomaly is not a sufficient factor in triggering MRPs (and possibly WSPs as well), as there are two negative anomaly events during the MRP-N years and yet no open ocean polynya is formed in those periods.

The spin up of the Weddell gyre can also be quantified by the barotropic stream function of ocean currents in the Weddell Sea. In most of the MRP-I years there is a slight increase in the barotropic stream function values over Maud Rise, Astrid Ridge and most of the Weddell Sea that would indicate a spin-up of the Weddell gyre during the MRP-I years when compared to the MRP-P years (not shown). However, there are also MRP-I years when this relationship does not hold. We therefore conclude that while the spin-up of the gyre may be necessary to create a WSP, it is not a necessary prerequisite for MRPs to occur. We will investigate the relationship between the intensification of the gyre and the formation of WSPs and embayments more closely in a subsequent paper.

3.4 Role of surface salinity in triggering MRPs

Fig.19 shows Hovmöller diagrams of monthly temperature, salinity, and potential density anomalies averaged over the upper 100 m and over the latitudinal band 64°S-68°S. The time-axis (ordinate) is discontinuous in order to zoom in and focus on the transition from an MRP-P year to a MRP-I year separately for all 6 MRP-I cases individually. Also, the longitudinal extent of deep

convection is indicated by a black box in all panels. As can be readily seen, the anomaly patterns of the 6 cases differ considerably. Nevertheless, the following common features can be identified: i) the longitudinal extent of the MRPs themselves and their initiation are indicated by an abrupt switch to warm temperature anomalies in winter of the respective MRP-I year (black box in Fig. 19a). This is caused by convection (see also Fig. 11a), which entrains WDW into the upper ocean. The temperature anomaly pattern largely coincides with the salinity and density anomaly pattern (Fig. 19b,c). Note how density follows mostly the evolution of salinity; ii) there is a clear westward propagation of high salinity anomalies starting early in the MRP-P years in all 6 MRP cases (black arrows in Fig. 19b). This propagation is initiated well east of Astrid Ridge.

Another feature emerging from Fig. 19 is that, except for the MRP triggered in year 31, all MRPs start forming east of Maud Rise. The reason for this seems to be the interaction of the flow with Astrid Ridge. The westward advection of high upper ocean salinity over Astrid Ridge weakens the upper ocean stratification by increasing the surface density (Fig. 19c). Furthermore, convection can be triggered by making the upper 100 m denser than the subsurface layer especially if the high salinity anomalies are advected over Taylor caps. As indicated by all 6 MRPs, we can make the case that the high salinity anomalies trigger MRPs when they advect over the Taylor cap region around Maud Rise and Astrid Ridge.

If high surface salinity anomalies can trigger MRPs, then the null hypothesis, i.e., that MRP-N years do not coincide with high surface salinity anomalies, should also be verified. Fig. 20 is identical to Fig. 20, except that it presents the upper water mass anomalies spanning the entire period of the E3SMv0-HR simulation. This readily shows that all MRP-N years feature exclusively zero or negative salinity anomalies upstream of Maud Rise and Astrid Ridge. Negative salinity anomalies at the surface enhance stratification thus hindering convection and MRP formation.

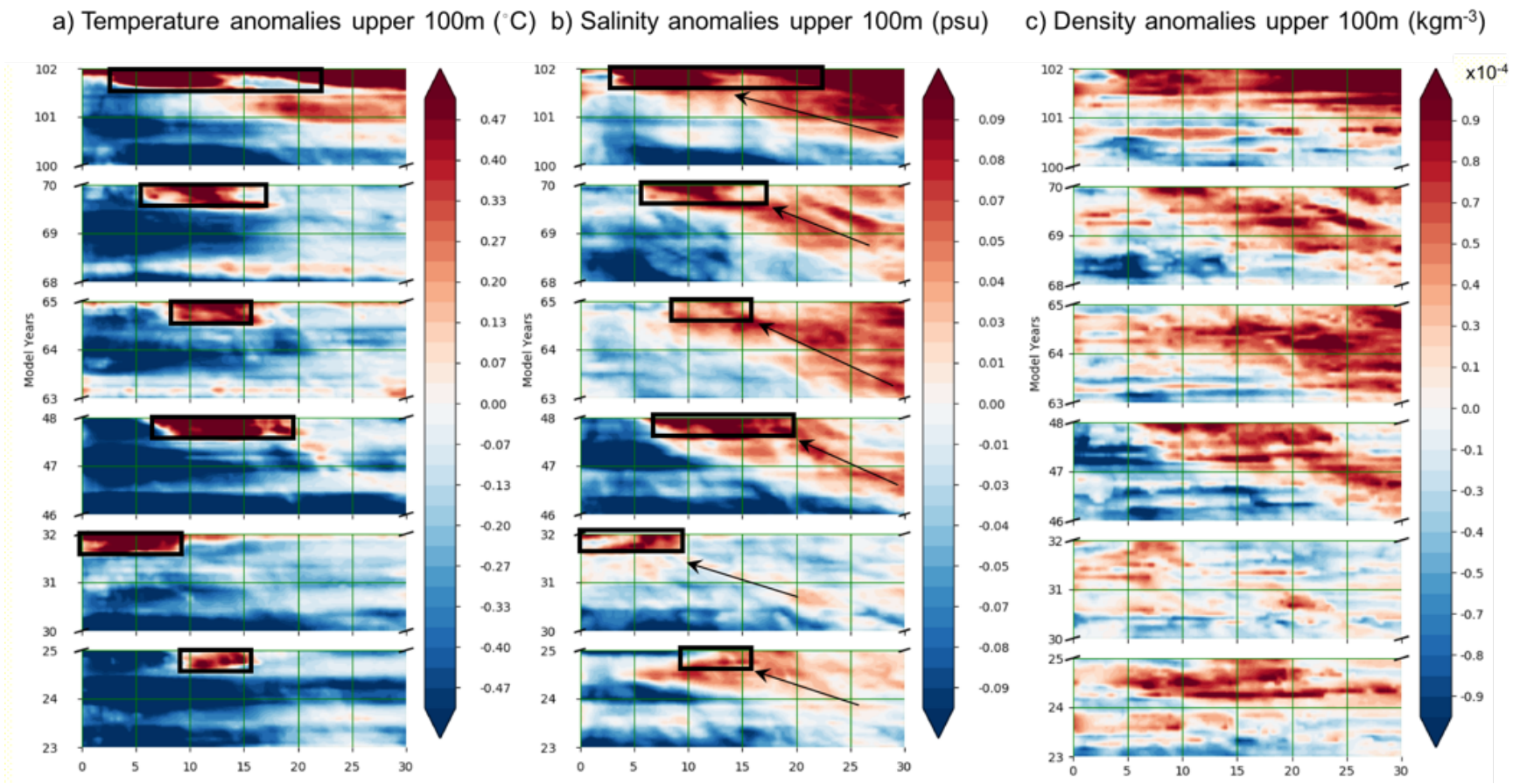

Figure 19: Hovmöller diagrams of (a) potential temperature, (b) salinity, and (c) potential density anomalies averaged over the upper 100 m of the water column and over the region 64°S-68°S. The black contoured boxes indicate the location of convection in association with the individual MRPs, and the arrows in b) show the propagation of the salinity anomalies from east of Astrid Ridge to the Maud Rise-Astrid Ridge complex. The anomalies are computed relative to the mean monthly climatology over years 20-127.

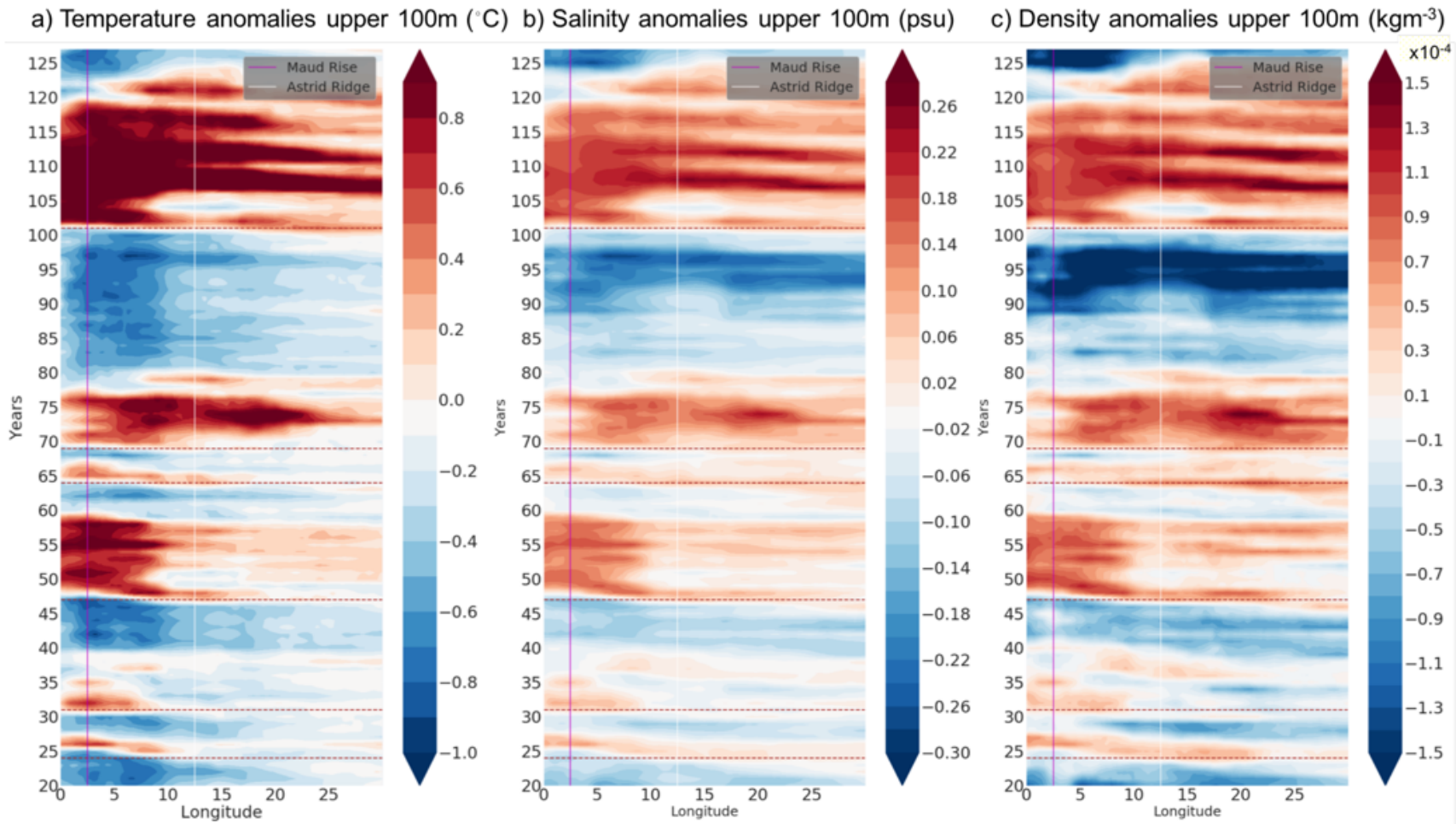

Figure 20: Similar to Fig. 19, but for the full length of the E3SMv0-HR simulation. The pink and white lines indicate the central peak of Maud Rise and Astrid Ridge, respectively. The horizontal red dashed lines indicate the MRP-I years.

3.5 Effect of MRPs on deep water masses

The WDW is the only source of subsurface heat in the Weddell Sea for the region around Maud Rise. The heat content of the WDW is also an important factor for long lasting polynyas (Martin, Park, and Latif 2013; Cheon et al. 2015). The only pathway for the WDW to enter the Maud Rise region is through the eastern limb of the Weddell gyre where the gyre separates from the ACC (Foster and Carmack 1976; Schröder and Fahrbach 1999).

During the discussion of Figs. 15 and 19, we described the effects of convection around Maud Rise on WDW and upper ocean water mass properties. To relate this to the heat reservoir at depth, we next examine the evolution of the water mass properties over time and depth in the region around Maud Rise (64°S-68°S;0°E-20°E) throughout the simulation in terms of temperature and salinity anomalies (Fig. 21). In the years, preceding MRP-I years, we find a pronounced positive temperature anomaly at depth (between 150 and 1500 m; Fig. 21), indicating anomalously warm water. The core of the warm anomaly is located at 300-600 m depth, which corresponds to the WDW core. Once an MRP is triggered, starting in the austral winter of the MRP-I year, we see an abrupt decline in the WDW temperature. This indicates deep convection and mixing of the cold ASW with the warm subsurface WDW, creating a positive temperature anomaly in the upper 150 m and a negative temperature anomaly underneath. During subsequent MRP years, the negative temperature anomaly spreads gradually down to 3000 m, apparently affecting deep and bottom water (WSDW, WSBW) properties. Cooling of the WDW layer has a significant impact on the Southern Ocean as previously reported in observational studies (e.g., Gordon, 1978; Gordon, 1981).

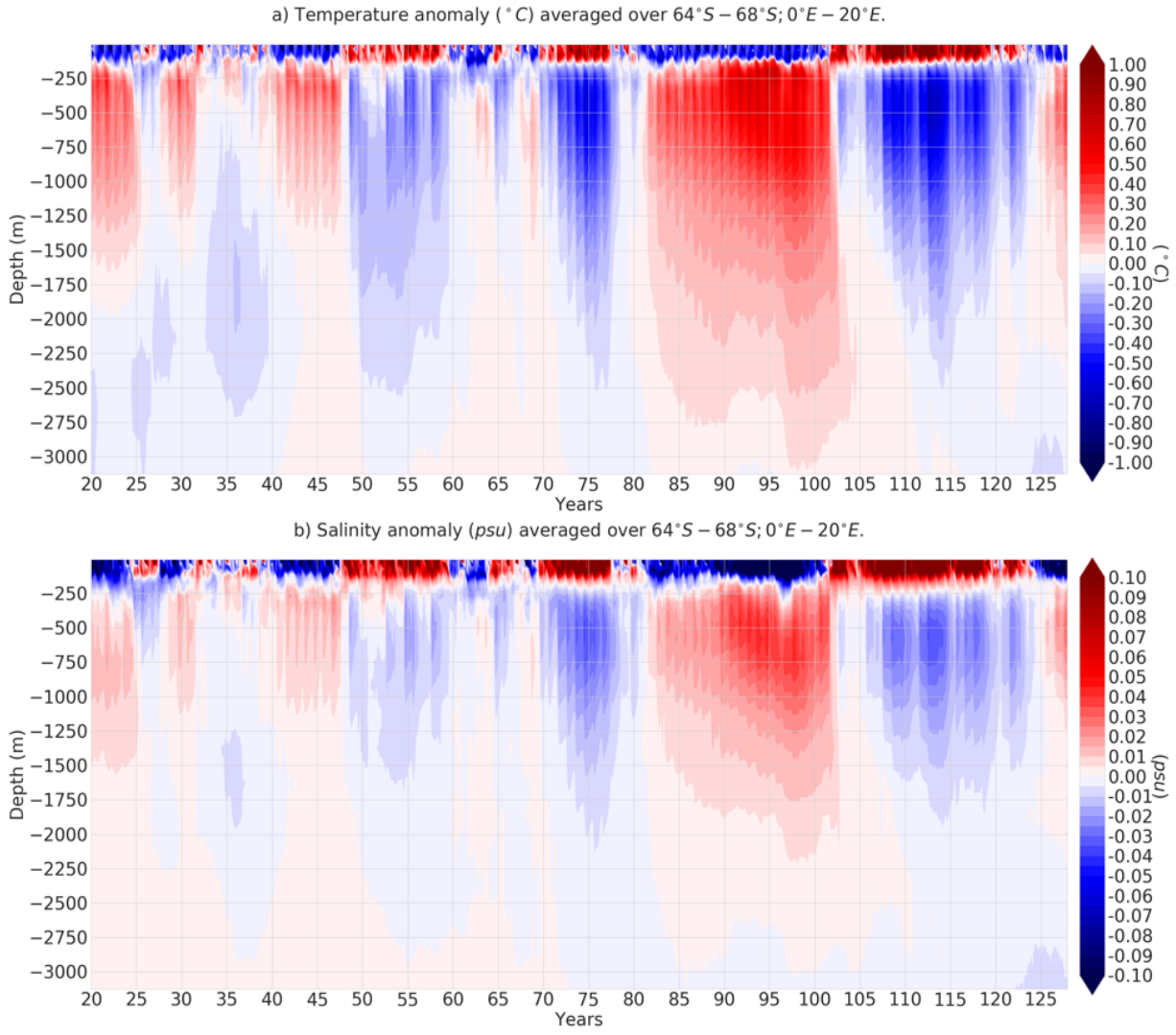

Figure 21: Time series of (a) potential temperature anomaly and (b) salinity anomaly profiles averaged over the area 64°S -68°S; 0°E - 20°E, for the full simulation period. The anomalies are computed relative to the mean monthly climatology over years 20-127.

3.6 Summary and conclusions

Observations in the 1970s, previous modeling studies, and our E3SMv0-HR simulation indicate that MRPs act as a precursor to WSPs (Gordon 1978; Martinson, Killworth, and Gordon 1981; Holland 2001; Dufour et al. 2017). The development of WSPs in the E3SMv0-HR simulation will be the subject of the next chapter. Here we focused on the preconditioning and

formation of MRPs. These are governed by bathymetric effects, and thus highly dependent on model resolution. Our study can be viewed as being complementary to the recent study by Dufour et al. (2017) who focused on the formation of WSPs in a high-resolution ESM simulation. Our key findings are summarized as follows.

a) The upper 100 m salinity structure near Maud Rise and Astrid Ridge is an important factor for triggering MRPs. All of the simulated MRPs are preceded by high upper ocean salinity anomalies upstream of the Maud Rise – Astrid Ridge complex. These anomalies start propagating about 1-2 years prior to an MRP event, in some cases from the eastern limb of the Weddell gyre (30°E), in other cases from the region east of Astrid Ridge (20-25°E). Since the flow in the vicinity of Maud Rise is governed by a semi-permanent Taylor cap, the salinity anomalies propagate along the northern flank of Maud Rise rather than over it. The northern flank is characterized by a crescent of large positive relative vorticity of ocean currents and sea ice drift, slightly lower sea-ice concentration, a shallow mixed layer, warmer and saltier water at depth (WDW), and slightly warmer water at the surface, all relative to its surrounding. The presence of the Taylor cap over the Maud Rise – Astrid Ridge complex preconditions the region with low stratification which, when combined with high salinity anomalies in the upper layer, triggers convection. Once convection has set in, a positive feedback ensues, bringing a reservoir of warmer and saltier WDW to the surface, which, upon cooling, enhances convection, eventually destabilizing the whole region over and around Maud Rise and Astrid Ridge to the point that an MRP emerges. In this process, the first sign of destabilization and polynya formation appears mostly over the peak of Astrid Ridge, if not east of Astrid Ridge.

b) High model resolution is essential for bottom topography to become steep and high enough to produce a realistically tall Taylor cap, and for resolving the detailed circulation around Maud

Rise and Astrid Ridge. Fig. 9 illustrates the difference between the state-of-the-art measured GEBCO bathymetry and that used in E3SMv0-HR and E3SMv0-LR. It can be readily seen that the high-resolution bathymetry matches the measured one substantially better than the one used for the low-resolution model. The crest of Maud Rise in the E3SMv0-LR bathymetry is at most 2200 m below the surface while that of E3SMv0-HR reaches 1600 m, which corresponds almost with the Maud Rise peak in the GEBCO bathymetry. The standard 1° E3SMv0-LR simulation does not produce any open ocean polynya during its entire duration (200 years). Favorable conditions for Taylor columns to emerge and interact with the surface depend on the steepness and height of a seamount above the sea floor, and on the ambient stratification (Chapman and Haidvogel 1992). In the Southern Ocean, Maud Rise has the largest potential for Taylor columns to occur (Meredith et al. 2015). An underrepresented steepness and height of Maud Rise in the model bathymetry prevents the formation of sufficiently strong Taylor columns to form. (a) and (b) together explain the necessary conditions for MRPs to form, and the MRP formation process itself, all on the basis of detailed physical processes that evolved in the fully coupled E3SMv0-HR simulation.

c) The simulated halo of a shallow mixed layer, warm and salty WDW, as well as low sea-ice concentration during MRP-N years closely matches results based on oceanographic measurements and satellite remote sensing (de Steur, Holland, Muench, and Mcphee 2007). The presence of the halo of lower ice concentration is associated with a shoaling of the thermocline that allows for sufficient entrainment of WDW to the upper ocean to prevent a 100% sea-ice coverage as found in the surrounding waters. This feature is seen frequently during non-polynya years in satellite observations. The halo is also proof of a permanent Taylor

cap over Maud Rise, and that this Taylor cap is simply stronger during polynya years (the strength of the Taylor cap is determined by its proximity to the surface mixed layer).

d) The intensification of the Weddell gyre seems to play a minor role for the transition from MRP-P to MRP-I years, but seems more relevant for the maintenance of WSPs and large ice-free embayments in association with a sustained negative wind stress curl anomaly, a subject to be scrutinized in a follow-up study.

e) The heat content of WDW plays an important role in sustaining polynyas. Prior to MRP years, we see an accumulation of WDW heat and salt content around Maud Rise. On the other hand, MRPs reoccurring over a number of consecutive years can impact deep water formation.

A Hovmöller diagram similar to that of Fig. 20, but for the JASO averaged surface freshwater flux anomalies (Fig. 22) shows that in all MRP-I cases, the Maud Rise region transitions from relatively dry to relatively wet atmospheric conditions when going from MRP-P to MRP-I. Comparing these results with Fig.20a, however, reveals a direct correspondence between freshwater flux and upper-ocean salinity and temperature, indicating that the freshwater flux anomalies are mainly caused by warm surface temperature anomalies. Additional comparison with Fig.11b indicates that these are mainly caused by low ice concentration anomalies in association with the MRPs. In our simulation, precipitation anomalies are thus not a cause for MRPs, but rather a result of them, as also found in Weijer *et al.*, 2017. A question that arises is what causes the high salinity anomalies (Fig. 19b) in a), either locally or east of the Maud Rise – Astrid Ridge complex before they are advected westward. This will be investigated more deeply in the following chapter on WSPs.

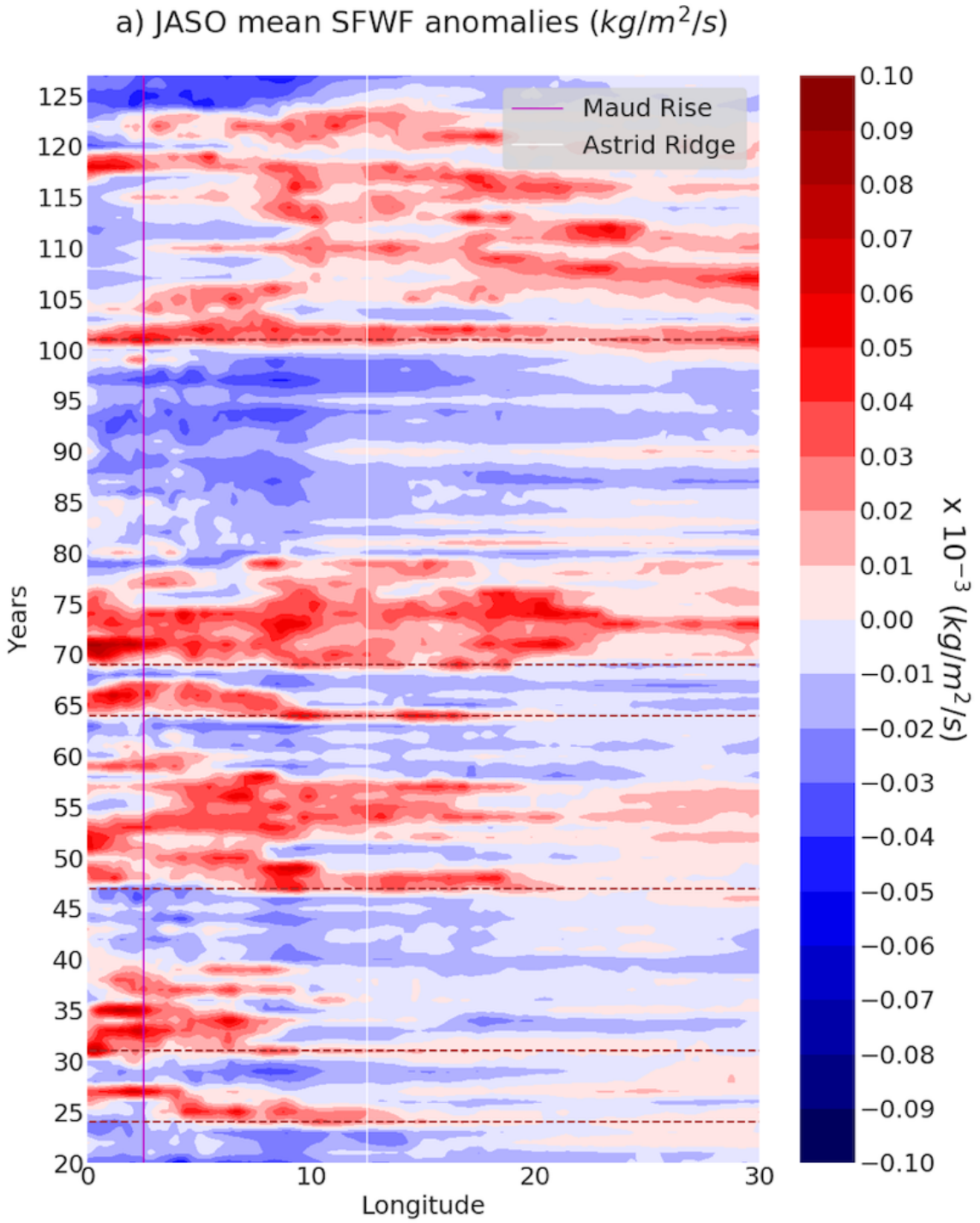

Figure 22: Similar to Fig. 20, but for the JASO mean surface freshwater flux anomalies. The anomalies are computed relative to the mean monthly climatology over years 20-127. The pink and white lines indicate the central peak of Maud Rise and Astrid Ridge, respectively. The horizontal red dashed lines indicate the MRP-I years.

Although we have not considered eddy effects in this paper, it is likely that the ability of a model to produce eddies is important for MRPs to form. Part of the flow impinging on Maud Rise circulates anticyclonically around its northern flank, as expected from conservation of potential vorticity. During this process, cyclonic and anticyclonic eddies are generated (Holland 2001). Some of these mesoscale eddies flow downstream while most of them linger near the seamount, in particular along its eastern flank. There is a weak cyclonic inner circulation over Maud Rise that is intensified along its northern flank, which has also been reported by observations (Gordon and Huber 1990). Anomalous currents in the region where the Weddell gyre separates from the ACC could also play a role in MRP formation, because of the large mesoscale eddies that are usually present in this region and of the possible impact that these eddies may have on horizontal heat and salinity transport towards Maud Rise (Orsi, Whitworth, and Nowlin 1995). A preliminary inspection of the Sea Surface Height anomaly during the months of May and June for two specific MRP-I and MRP-N years (not shown) indicates that there is not a clear distinction between MRP-I and MRP-N years in terms of eddy generation and propagation towards Maud Rise and Astrid Ridge. Therefore, more systematic and quantitative studies are necessary to investigate the possible impact of eddies on MRP formation, which are beyond the scope of this dissertation.

The 130-year long E3SMv0-HR simulation analyzed here reveals 40 years with open ocean polynyas in the greater Weddell Sea. According to Gordon (2014), deep convection in the Weddell Sea was more active in the past and has weakened due to increased freshwater input in the upper ocean related to recent climate change, leading to increased stratification. The study of de Lavergne et al. (2014) addresses the importance of ESMs being capable of producing open-ocean polynyas under pre-industrial conditions. They analyzed a series of CMIP5 ESMs, all of which are low-resolution models. They stressed that there are two classes of CMIP5 models: convecting and non-

convecting ones. Low-resolution CESM (and with that E3SMv0-LR) are of the latter type. They concluded that convecting ESMs are capable of simulating the transition from a convective to a non-convective state with increasing greenhouse gases, while non-convecting ESMs are not. Our study and that of Dufour et al. (2017) demonstrate that high-resolution ESM simulations with pre-industrial CO_2 concentration levels are able to reproduce WSPs. The fact that CESM and thus E3SMv0 becomes a convecting ESM upon switching from low- to high-resolution suggests that E3SMv0-HR will most likely also be able to realistically simulate the transition to a non-convective state with anthropogenic forcing. The crucial difference to the convecting low-resolution ESM simulations is that in E3SMv0-HR convection emerges for the right physical reason, namely as a result of sufficiently resolved bathymetry that leads to the intermittent occurrence of MRPs, which in turn is a necessary condition for WSPs to form. In the following chapter, we will study the mechanisms behind the westward expansion of MRPs into WSPs, and the possible impact of WSPs on AABW formation.

4. ON THE GENERATION AND IMPACT OF WEDDELL SEA POLYNYAS IN A HIGH-RESOLUTION EARTH SYSTEM MODEL

4.1 Comparison of simulated and observed Weddell Sea Polynya effects

The simulated vertical profiles of temperature and salinity before and after the WSPs are shown in Fig. 23 and compared with the 1970s observed profiles from *Gordon*, 1982. The model results were averaged over the hydrographic stations where the observations were made. Years 46 and 48 in Fig. 23 represent conditions prior to the WSP and year 51 is the first WSP year followed by several consecutive WSPs. The deep convective events associated with the WSP lead to a reduction of temperature and salinity below 200 m up to 3000 m depth (Fig. 23c, d), suggesting deep water ventilation in the Weddell Sea. The differences of the simulated temperature and salinity profiles between pre- and post-WSP conditions are strikingly similar to those of the observations made in 1973 (pre-WSP) and 1977 (post-WSP) (Fig. 23a, b), both in magnitude and depth. The drastic loss of heat in the core of WDW and down to ~3000 m affects the volume and characteristics of the deep and bottom water masses in this region. Therefore, these WSPs can drastically increase the contribution of surface waters to the formation of bottom waters in the Weddell Sea and in the past have been estimated to be comparable to those by coastal polynyas (Gordon 1982). Thus, it is equally important to understand the impact of a lack of WSPs on the properties and volume of water masses in the deep Weddell Sea in the last 40 years.

To our knowledge, to date no modeling study has simulated a WSP that grows regularly out of deep convection over the Maud Rise seamount, i.e. an MRP, and covers an area similar to

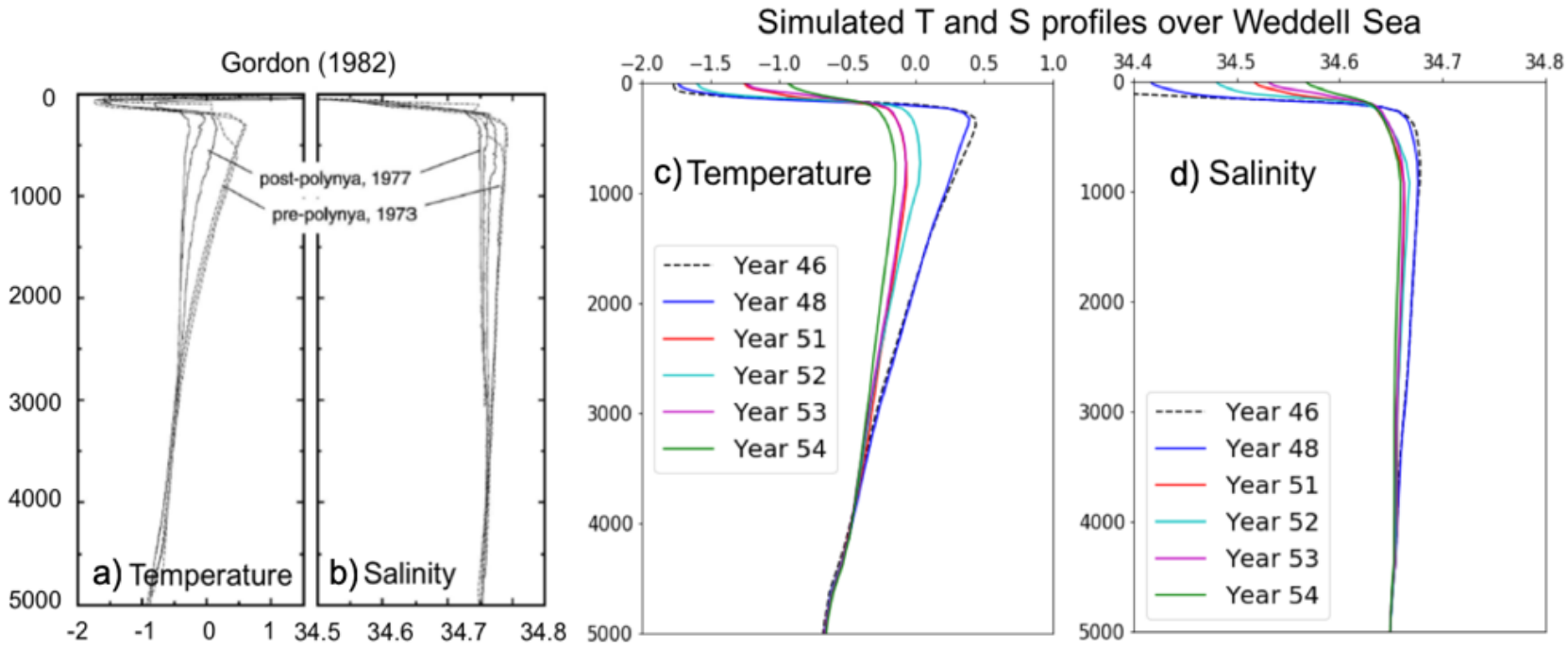

Figure 23: Profiles of observed potential temperature (a) and salinity (b) (from Gordon 1982). Profiles of annual mean temperature (c) and salinity (d) of model simulation: year 46 with no polynya and years in the 50's with strong WSPs. The temperature and salinity fields are averaged over the region that match the areas of the different stations where the observations come from (Hydrographic stations: Glacier in 1973 and Islas Orcadas in 1977, refer to Gordon (1982)).

those observed in the 1970s (Martinson et al. 1981, their Fig.1). The intermittently emerging WSPs in E3SMv0-HR are always preceded by MRPs, while not all MRPs lead to WSPs. The westward expansion of a MRP into a WSP occurs in the model at a rate of ~7° per year, which is consistent with the satellite passive microwave retrievals of the 1970s (Zwally et al. 1983). WSPs emerging in our preindustrial E3SMv0-HR simulation as well as in the preindustrial GFDL-ESM simulation (Dufour et al. 2017) supports the conclusions that WSPs were more common during preindustrial conditions (de Lavergne et al. 2014). The WSP observed in the 1970's was found to contribute significantly to the dense water formation in the Weddell Sea (Martinson, Killworth, and Gordon 1981). The cessation of WSP formation during the last 40 years indicates that they no longer contribute to AABW formation in the way that they may have done in the past (Gordon 2014).

4.2 Role of intensifying southern hemisphere westerlies on the structure of the Weddell Gyre

Numerous studies indicated that a spin-up of the Weddell Gyre can cause WSPs (Martinson, Killworth, and Gordon 1981; Gordon and Huber 1990; Cheon et al. 2015) and trigger deep convection. In theory, the cyclonic Weddell Gyre can be enhanced by a strongly negative wind stress curl, causing a doming of isopycnals in the central Weddell Sea thereby increasing the probability of WSP formation. We find that to be also the case in our E3SMv0-HR simulation, as illustrated in Fig. 24. There is a direct relationship between anomalously negative wind stress curl and a weakening of the pycnocline strength in the Weddell Sea with a lag of ~ 4 years. The doming of the isopycnals over the Weddell Sea is indicated by the low values in both the pycnocline and halocline strength that follow the negative wind stress curl anomalies. The time series of the pycnocline strength being almost identical to that of the halocline strength suggests that the variability in the pycnocline strength is almost solely due to that of the halocline strength. During the WSP/EMB events (see purple/grey shaded region in Fig. 24) we

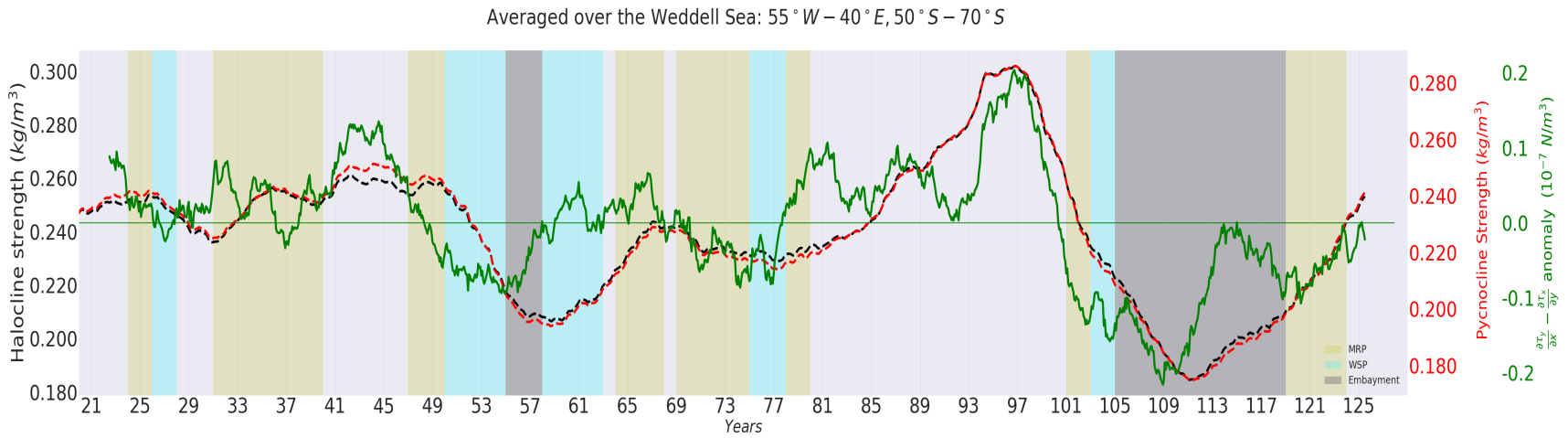

Figure 24: Time series of halocline strength (left axis labels), as well as pycnocline strength and wind stress curl anomaly (right axis labels). The pycnocline strength ($\Delta\sigma_\theta$) and its salinity component ((($\partial\sigma_\theta$)/(∂S)) ΔS) or halocline strength were computed as the difference between 100-200m and 0-100m (de Lavergne et al., 2014). Values were computed and averaged over the Weddell Sea (55°W-40°E;50°S-70°S) and smoothed with a 5-year centered running average. The shading in the time series represents the type of OOP seen during the austral winter of the respective year (yellow: MRP; blue: WSP; gray: EMB). The wind stress curl anomalies are computed relative to the mean monthly climatology over years 20-127.

find that the wind stress curl anomaly is predominantly negative. The opposite is also true, i.e., the wind stress curl anomaly is positive in the no-polynya years. We should mention that although the wind stress curl is sometimes positive during MRP events, it applies to the entire Weddell Sea region and does not necessarily reflect the conditions over Maud Rise, such as the local stratification which may depend on several other factors (Kurtakoti et al. 2018). Our main focus here is the wind stress curl during the gradual transition from no polynyas to the onset of WSPs via MRPs (Fig. 24).

4.2.1 Structure of the eastern Weddell Gyre

While investigating the formation mechanisms of MRPs, we showed that the westward advection of anomalously high surface salinities over the Maud Rise-Astrid Ridge complex combined with Taylor column dynamics triggered a convective mode that resulted in MRPs (Kurtakoti et al. 2018). Anomalous salt introduced in the upper ocean upstream of the Maud Rise-Astrid Ridge complex is not explained by the freshwater flux due to precipitation minus evaporation or sea ice melting minus freezing over the region. It is thus important to consider the role of the eastern Weddell gyre, as the high surface salinity anomalies appear to emerge in the vicinity of the southern limb of the gyre's eastern cell.

Throughout the simulation, the wind stress curl anomalies suggest a spin up of the Weddell Gyre prior to the WSPs. To visualize the impact of the spin up of the central and eastern cell of the Weddell gyre, we compare meridional cross sections of September averages of salinity and density contours at 0°E (Fig. 25) and 35°E (Fig. 26) of no-polynya years composite and pre-WSP years composite (four independent WSP cases). Comparing Fig. 25 a and b, the density contours in the upper 200 m can be seen outcropping in the pre-WSP years, in contrast to what we find in the no-polynya years. This suggests weak stratification in the upper 200m as a result of higher

salinity over the region 65°S - 67°S in the central Weddell Sea. The upper 200 m of the water column between 64°S - 68°S is saltier in Fig.25b, which is indicative of a stronger doming of the isopycnals. In contrast, the upper ocean is much more stratified during the no-polynya years.

To determine if there is a presence of higher salinity in the surface ocean upstream of the Maud Rise-Astrid Ridge complex during the pre-WSP years, we compare the meridional cross section at 35°E (Fig. 26 a,b) of the pre-WSP years' composite with that of the no-polynya years' composite. There is a sharp doming of the upper ocean isopycnals (density contour 27.89 raised to 350 m in pre-WSP years from 500 m in no-polynya years) and an increase in the upper ocean salinity during the pre-WSP years. High salinity anomalies east of the Maud Rise-Astrid Ridge complex play an important role in triggering all simulated MRPs (Kurtakoti et al. 2018). The time evolution of the upper-ocean temperature and salinity averaged over the region 64°S-68°S (Fig. 27) demonstrates a westward advection of anomalously warm and salty waters from east of the Maud Rise-Astrid Ridge complex to the MRP region, and in some years all the way to the central Weddell Sea (25W). Anomalously salty water coinciding with anomalously warm water indicates that WDW is entrained into the upper layer upstream of the Maud Rise-Astrid Ridge complex, a process that will be discussed later.

4.2.2 Role of WDW heat content accumulation

It has been established that a necessary condition for long-lasting, consecutive winter WSPs to occur is the heat reservoir at depth, or the heat content of WDW (Martinson, Killworth, and Gordon 1981; Martin, Park, and Latif 2013; Cheon et al. 2015; Dufour et al. 2017). Once having become part of the (deep) mixed layer, the heat content of WDW prevents the WSP from closing by hindering sea ice formation. Thus, the occurrence of a WSP drastically reduces the WDW heat content. The depletion of WDW heat content can readily be seen especially during the distinct

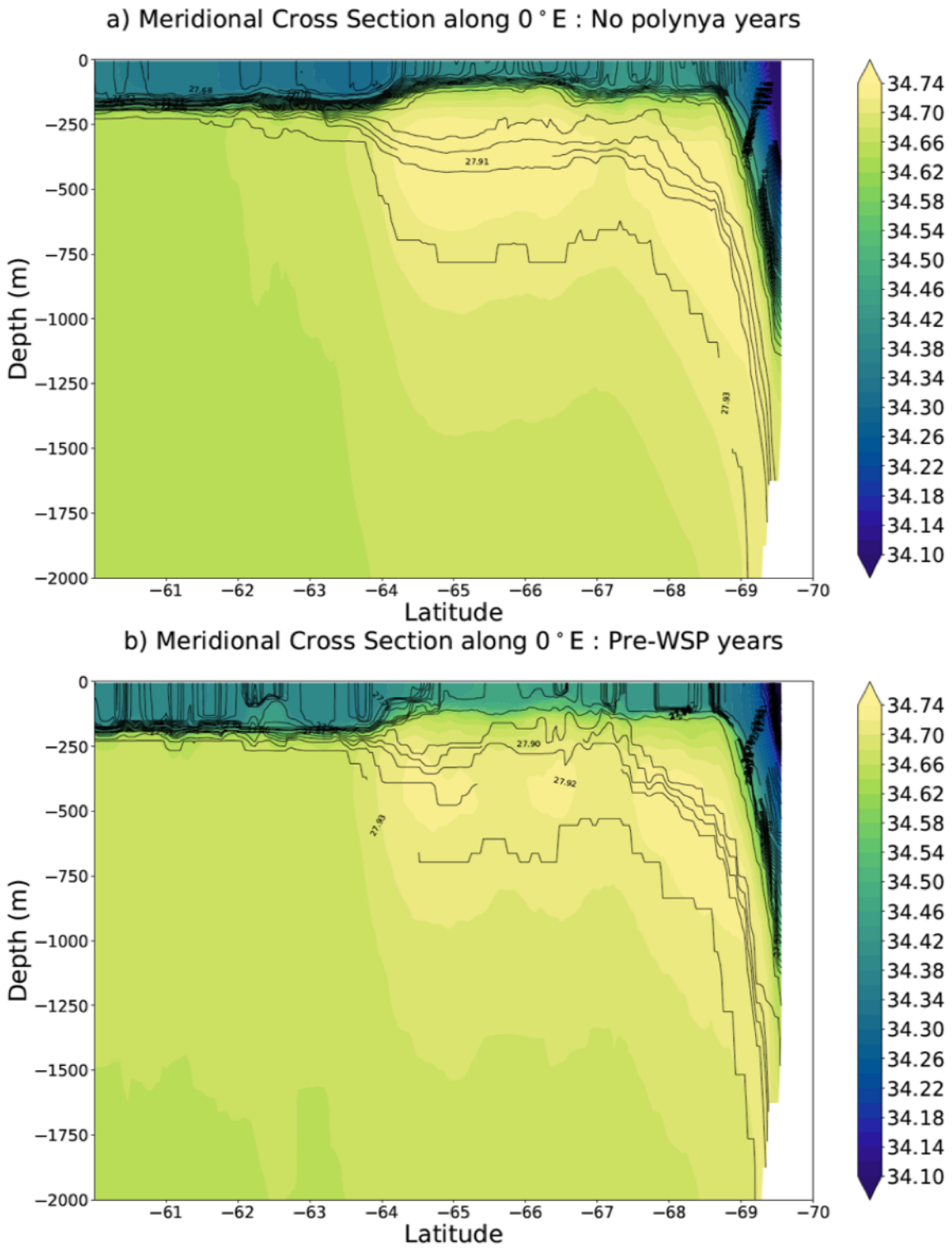

Figure 25: September salinity in the central Weddell Sea along 0°E during the a) no-polynya years 41-45; 82-96 and b) pre-polynya years 23,45,68,100 composites in E3SMv0-HR.

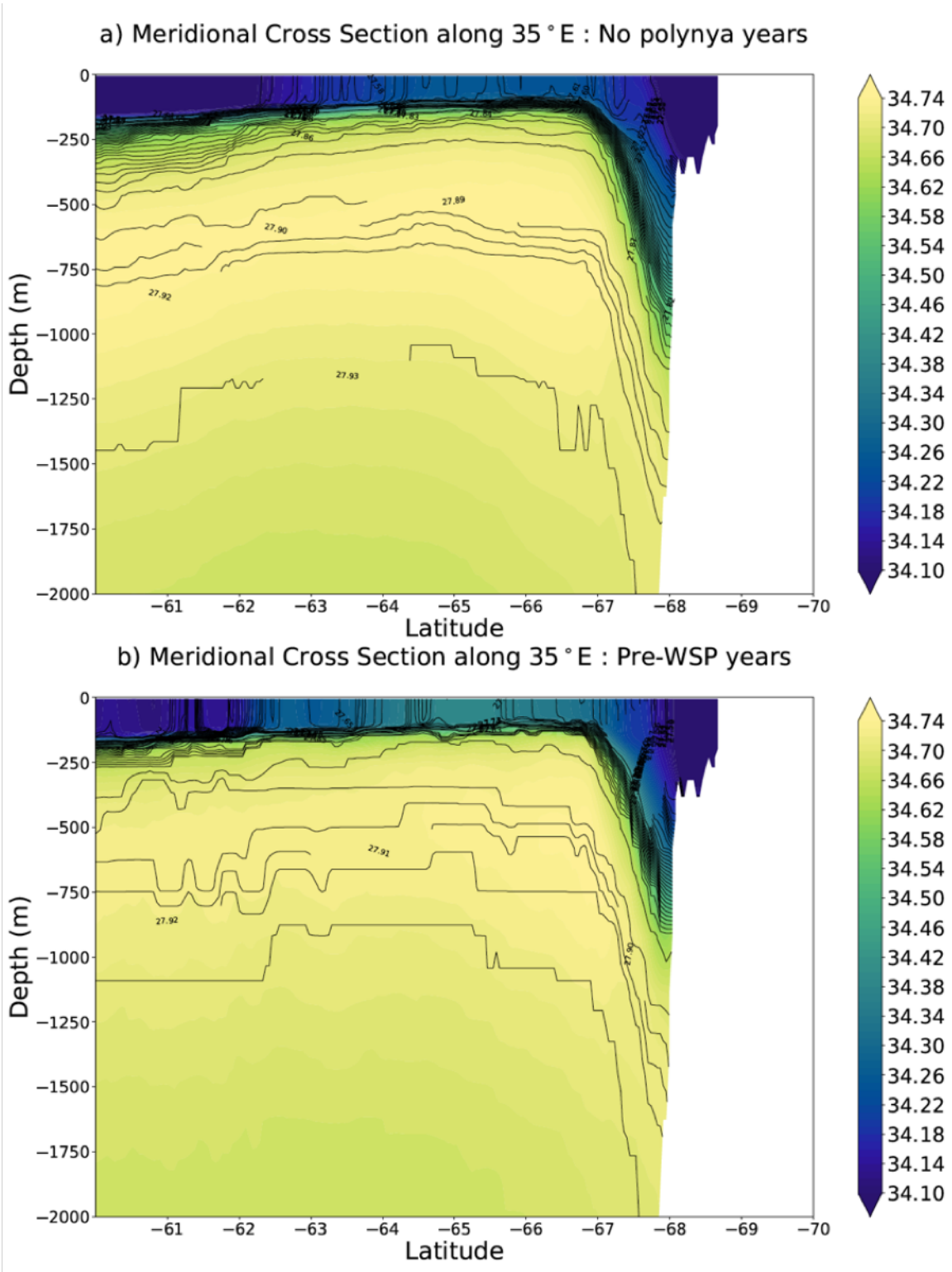

Figure 26: Same as Fig.25, but in eastern Weddell Sea along 35°E.

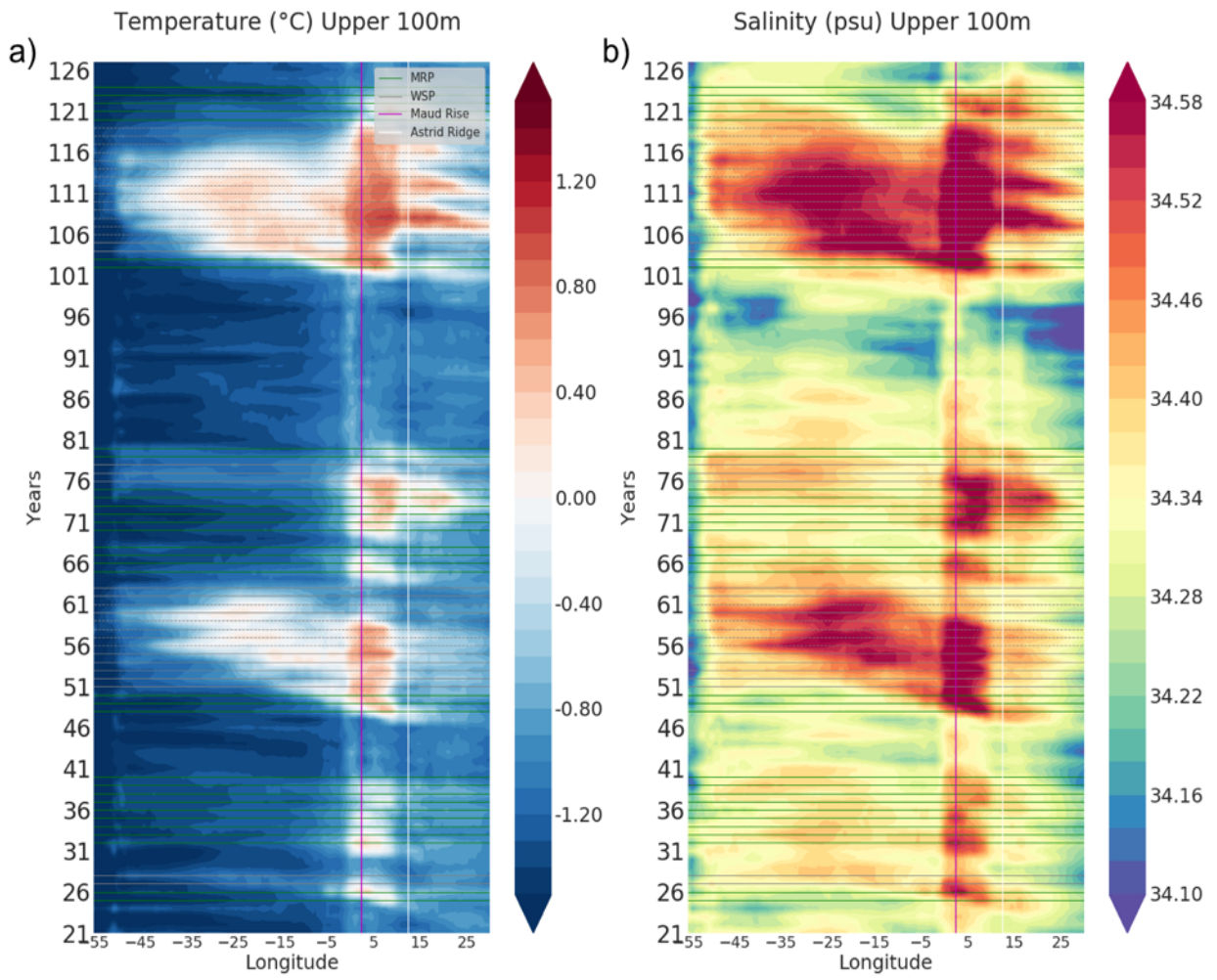

Figure 27: Monthly (a) potential temperature, (b) salinity of the upper 100 m in the Weddell Sea averaged over the region 64°S-68°S for the years 21-127 in E3SMv0-HR.

MRP+WSP years in the simulation (Fig. 28). The temperature averaged over the WDW layer (200-750m) shows the cooling during WSPs to be regionally more than 1°C. Deep convection during the WSPs also affects the salinity of WDW by introducing surface fresh water into the deeper layers and saltier WDW to the surface, thus reducing WDW salinity during the WSP events. A prolonged period of recovery of WDW heat and salt content is thus an important preconditioning for WSP formation. Such period emerges in particular in the years prior to the WSP of year 102 (Fig. 28).

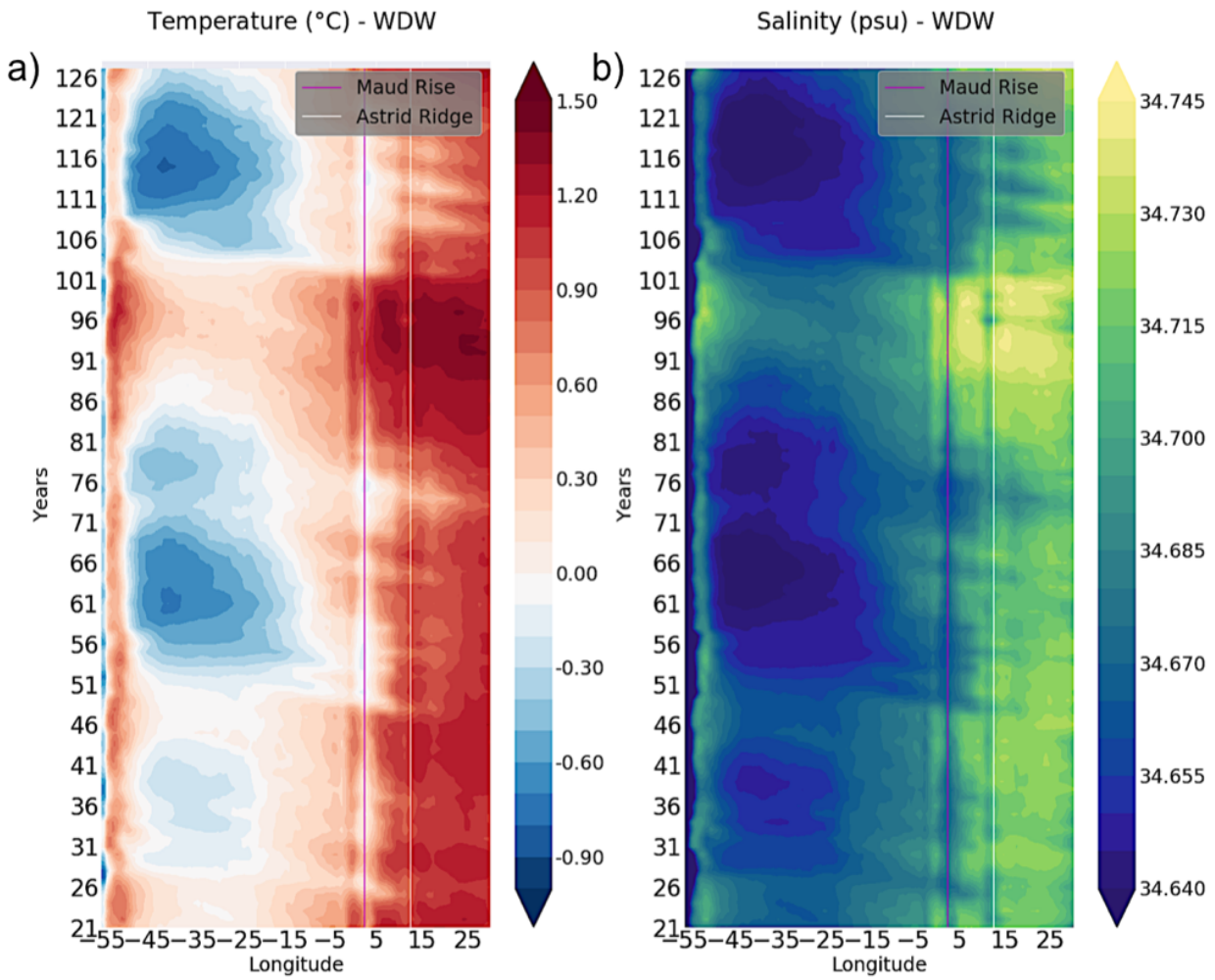

Figure 28: Monthly (a) potential temperature, (b) salinity of the WDW i.e., depth:200-750m in the Weddell Sea averaged over the region 64°S-68°S for the years 21-127 in E3SMv0-HR.

Besides an increase of WDW heat content in the central Weddell Sea, heat is also building up over and east of the Maud Rise-Astrid Ridge complex. The time span when the subsurface heat builds up coincides with positive wind stress curl anomalies in the Weddell Sea, indicating that these anomalies cause a spin down of the Weddell gyre which leads to sinking of the isopycnals in its center and thus a more stable stratification that is needed for a the build-up of a deep heat reservoir (Dufour et al. 2017).

4.2.3 Role of precipitation in conjunction with southward shift of the westerlies

The simulated precipitation and wind stress curl are inversely related as shown in Fig. 29a, where an increase in monthly negative wind stress curl is seen coinciding with an increase in monthly precipitation in the Weddell Sea. The increase in precipitation is caused by the OOPs. Furthermore, more negative wind stress curl mostly overlaps with the periods when WSPs and EMBs emerge, which suggests that dry atmospheric conditions cannot be the trigger. Rather, the time series of the zonal distribution of precipitation reflects the impact of the WSPs on precipitation (Fig. 30). The largest precipitation values (saturated blue areas in the Hovmöller diagram) over Maud Rise and the Weddell Sea are seen during years with winter convection and only over the zonal extent of the polynyas. This can also be seen when comparing with Fig.11b. Thus, it can be concluded that the increase in precipitation is associated with rising motion of moist and relatively warm air over polynyas, as found in Weijer et al. (2017), reflecting a direct response to the heat loss in association with the ventilation of WDW in OOPs. It can also be inferred from Fig. 30 that WSPs do not form when and where dry atmospheric conditions prevail, as e.g. in the western Weddell Sea. In conclusion, in the simulation, the spin up of the gyre has a stronger impact on the initiation of winter convection and WSP formation than dry atmospheric conditions. Anomalously high precipitation is a response to WSPs which occur during periods of strong negative wind stress curl that are affiliated with an intensification and/or southward shift of the southern hemisphere westerlies.

The meridional shift of the southern hemisphere westerlies is often quantified by the SAM index (black shaded graph in Fig.29b). This has been calculated following the definition of Gong and Wang 1999 as the difference between the zonal-mean SLP at 40°S and at 65°S. The positive phase of SAM is affiliated with southward shifted and/or intensified westerlies over the entire

Southern Ocean, and vice versa (Gong and Wang 1999; Thompson, Wallace, and Hegerl 1999; G. J. Marshall 2003; Hall and Visbeck 2002). This, however, does not necessarily reflect the regional conditions over the Weddell Sea. We would thus not expect to see a perfect correlation between the variation of the SAM index and that of the wind stress curl over the Weddell Sea. The SAM index calculated from observations (G. J. Marshall 2003)(G. J. Marshall 2003) reflects this. However, according to Gordon (2014), a positive phase of the SAM index is associated with a southward shift of the storm track which leads to a negative (cyclonic) wind stress curl anomaly as well as more precipitation over the Weddell Sea. These two variables have opposing effects on the stratification of the Weddell Sea: on the one hand, a cyclonic wind stress curl leads to a spin up of the cyclonic Weddell gyre, thereby weakening the stratification in its center due to a more pronounced doming of isopycnals; on the other hand, an increase in precipitation will lower the surface density and thereby strengthen the stratification. Some studies suggest that the opposite phase consists of a northward expansion of dry polar air masses over the Weddell Sea, creating conditions that are conducive for OOP formation (Gordon 2014). Such conditions prevail during periods when the SAM index is negative, which coincides with the core of the precipitation-rich westerlies being located further north than on average. At the same time, however, the associated positive (or less cyclonic) wind stress curl anomalies would lead to a spin-down of the Weddell gyre that deepens the isopycnals in its center. In this context, one must acknowledge the simultaneous occurrence of two competing effects of which one tends to hinder and the other tends to support winter convection.

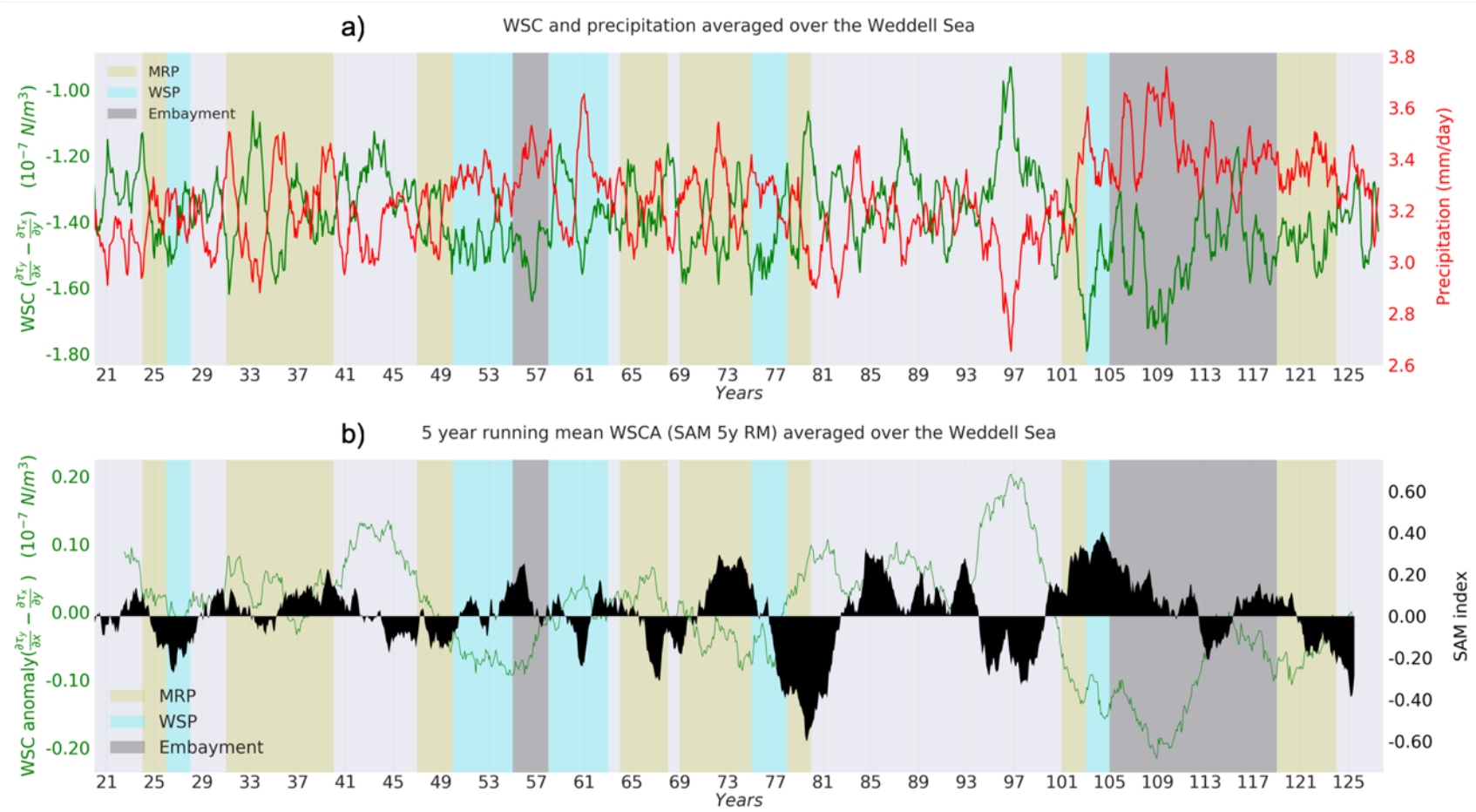

Figure 29: a) Time series of monthly wind stress curl (WSC), and total precipitation over the Weddell Sea and b) time series of 5-year running mean of monthly wind stress curl along with the SAM index.

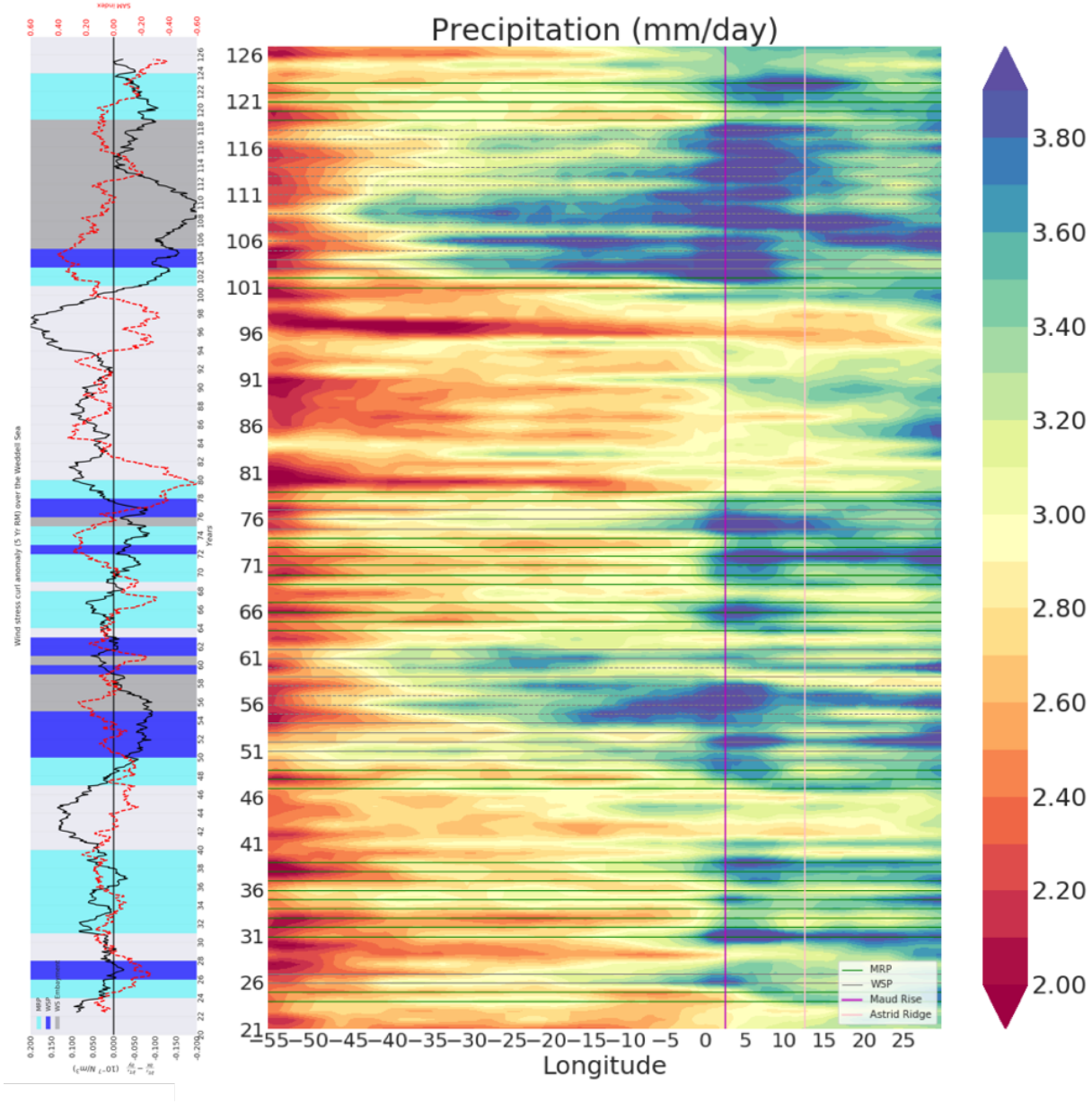

Figure 30: Hovmöller diagrams of (right) monthly precipitation averaged over the region 64°S-68°S and (left) a time series plot of wind stress curl anomalies (black line) and the SAM index (dashed red line). The wind stress curl values were computed and averaged over the Weddell Sea (55°W-40°E;50°S-70°S) and smoothed with a 5-year centered running average.

4.3 Role of modified upper ocean stratification by MRPs in triggering WSPs

Once MRPs are triggered, convection erodes the pycnocline and deepens the mixed layer. This introduces WDW into the upper ocean which gives rise to anomalously high upper-ocean temperature and salinity. This reinforcement of upper-ocean anomalies due to convection can readily be seen in Fig. 27 between the region of Maud Rise (red line) and Astrid Ridge (white line). Furthermore, Fig.27 reveals that anomalously strong MRPs (associated with anomalously warmer and saltier upper-ocean conditions) are necessary for upper-ocean warm and salty anomalies to continue propagating westward to the central Weddell Sea where they eventually contribute to the formation of WSPs. This happens in simulation years 47-61 and 101-118.

However, it is not clear why some MRPs develop into WSPs (e.g. over the period of years 47 to 62; "MRP+WSP" years), while other MRPs do not (e.g. those that prevailed during years 31 to 39; "MRP-only" years). The stratification in this region being marginally stable (Martinson, Killworth, and Gordon 1981), the entrainment of salt into the winter mixed layer can easily turn conditions from a stable mode to a convective mode (Gordon and Huber 1990; Kurtakoti et al. 2018). The MRPs during the MRP+WSP years bring up more heat and salt into the surface layer when compared to the MRP-only years. We can illustrate this by comparing the salinity averaged over Maud Rise during one case of "MRP-only" years (Fig. 31a) with one case of "MRP+WSP" years (Fig. 31b). The salinity in the upper 200 m is clearly much larger in the "MRP+WSP" years (upper panel of Fig.31b) than that in the "MRP-only" years (upper panel of Fig.31a). In this sense, we define the MRPs preceding the MRP+WSP years as 'strong'. The increase in the surface salinity allows the surface to destabilize downstream, thus creating a WSP in the following winters. It is important to note that the onset of strong convection over Maud Rise in year 48 (Fig. 31b) continues during the subsequent WSP years (from year 50 onwards). Thus, while these high

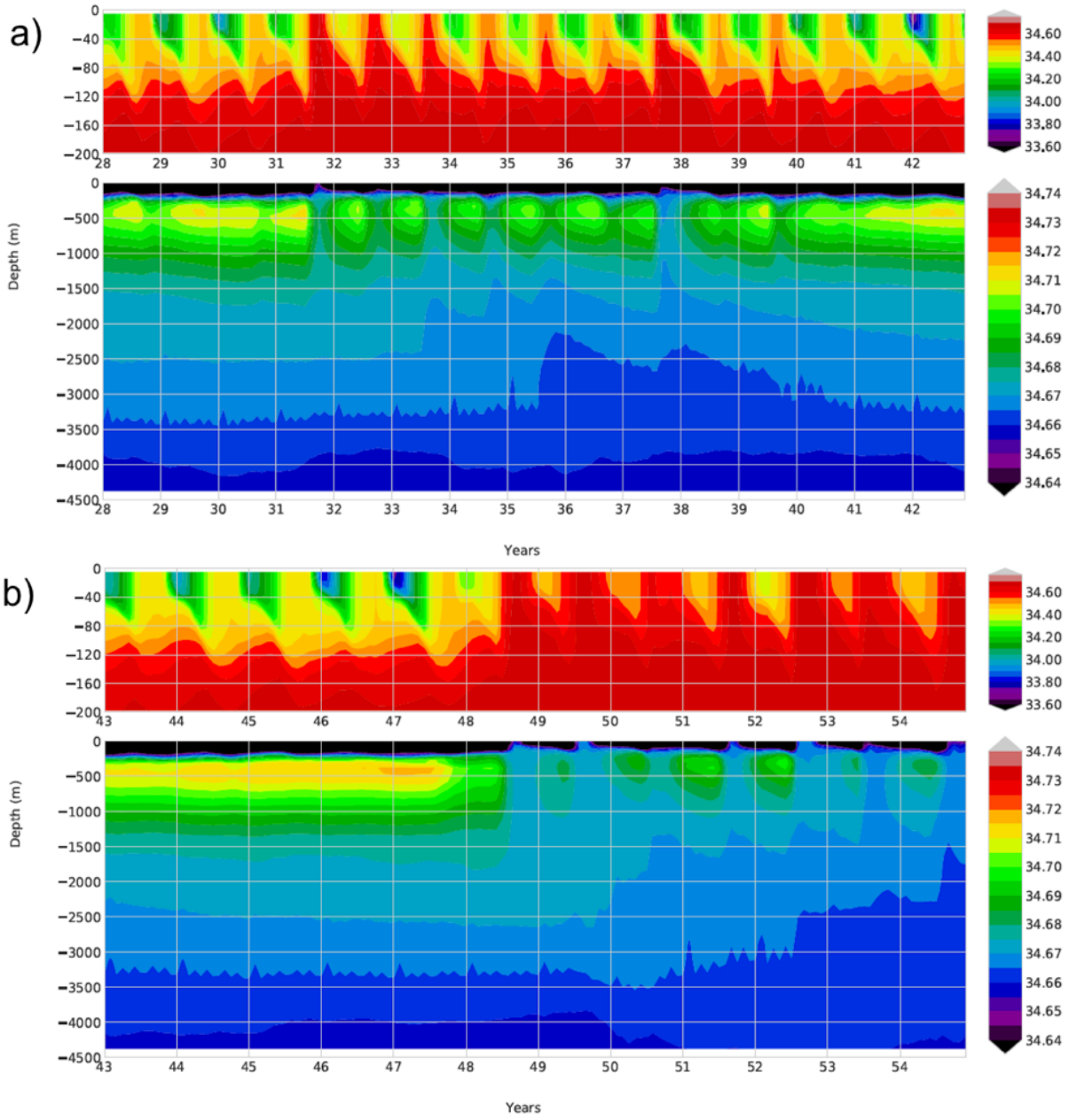

Figure 31: Time series of salinity depth profiles averaged over Maud Rise seamount during the (a) MRP years 31-39 (b) MRP+WSP years 47-54. Note that we use a different colorbar range for upper 200m and full depth.

surface salinity waters flow downstream, the convection over Maud Rise stays active and continues to introduce large salinity anomalies into the upper 100 m, which in turn get advected downstream with the southern limb of the Weddell gyre. Once the switch is made from stable to convective mode, the underlying WDW plays the dominant role in keeping the polynya open by supplying the heat needed to prevent sea ice formation. Comparing the winter mixed layer depth of MRPs in the "MRP+WSP" years with that of MRPs in the "MRP-only" years, one can confirm that only very strong MRPs provide high enough upper-ocean salinity anomalies (Figs. 32, 33), which then gives rise to WSPs. The size of the polynya is illustrated by the anomalously large MLD indicating deep convection. The MRPs in the "MRP-only" years (Fig. 32) are much smaller in area than the MRPs that precede the WSP in the "MRP+WSP" years (Fig. 33). This also holds for the other MRP+WSP periods of the simulation (see appendix).

We thus propose the following mechanism: when a strong MRP is triggered over Maud Rise, the ensuing deep convection erodes the weak stratification over Maud Rise and brings up WDW into the winter mixed layer which then flows downstream into the central Weddell Sea. Since the stratification in the Weddell Sea is more stable than that over Maud Rise (due to the Taylor cap dynamics over Maud Rise; see Chapter 3), one way to trigger the convective mode in the Weddell Sea is by introducing salinity anomalies into the winter mixed layer that are high enough to destabilize the stratification in the Weddell Sea. The high salinity anomalies during the MRPs of MRP+WSP years are large enough to trigger convection downstream, thus allowing for the switch from a stable mode to a convective mode in the Weddell Sea, hence leading to the formation of a full-scale WSP.

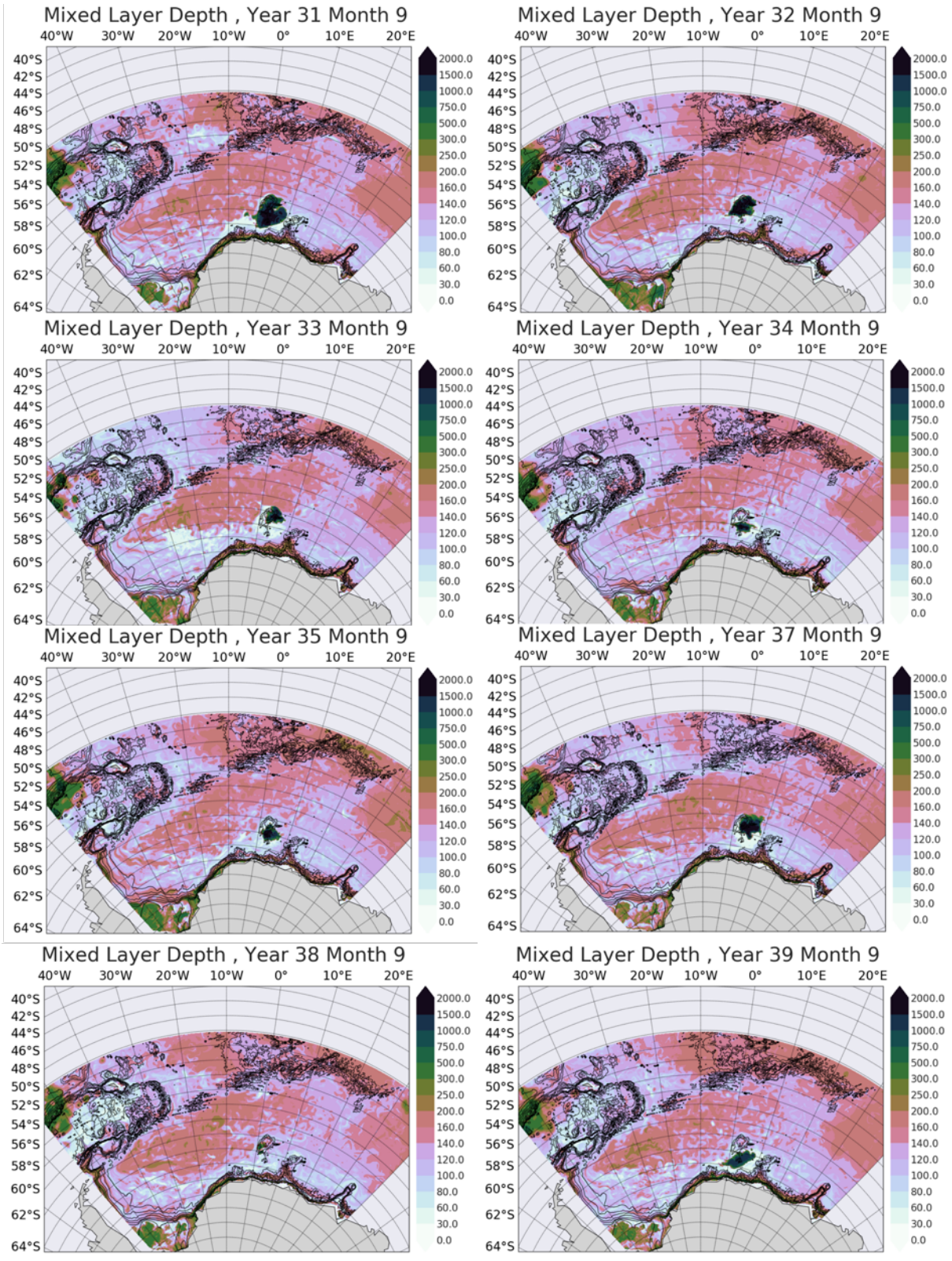

Figure 32: September mixed layer depth during the MRP-only years 31-39 with the bathymetric contours in black.

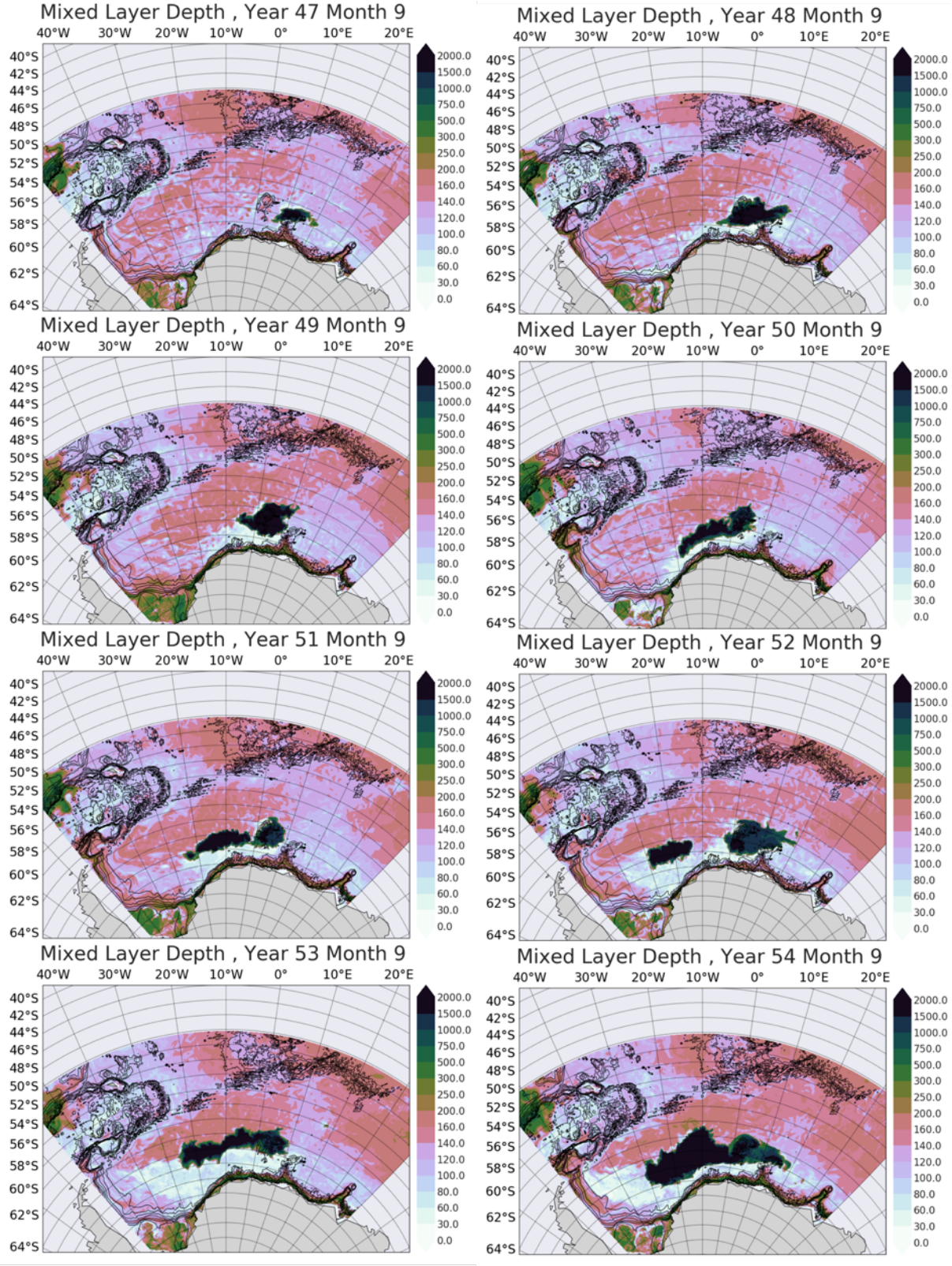

Figure 33: Same as Fig.32, but for MRP+WSP years 47-54.

4.3.1 Evolution of convection using salinity as a tracer

The convection triggered over the Maud Rise – Astrid Ridge complex can be further scrutinized by analyzing high temporal frequency data which was stored for a short period of the E3SMv0-HR simulation, in order to study short term features that cannot be properly identified in the monthly data. In particular, daily data was stored during years 35-37, during which MRPs occurred in year 35 and 37. The onset of deep convection can be followed by studying the individual terms in the advection-diffusion equation [1], for any tracer θ, were K_H is the horizontal diffusivity and K_V is the vertical diffusivity. The dominant terms in the tracer equation for salinity were computed over an area of 10 km by 10 km (corresponding to ~10x10 grid cells) for the upper 1500 m, in a region where deep convection appears first, and subsequently leads to a mature MRP. The stratification in the box goes from being stably stratified to fully convecting in a matter of days (not shown).

$$\underbrace{\frac{\partial \theta}{\partial t}}_{rate} = -\left(\underbrace{u\frac{\partial \theta}{\partial x} + v\frac{\partial \theta}{\partial y}}_{horizontal\ advection} \right) - \underbrace{w\frac{\partial \theta}{\partial z}}_{vertical\ advection}$$

$$+ \left(\underbrace{\frac{\partial}{\partial x}\left(K_H \frac{\partial \theta}{\partial x}\right) + \frac{\partial}{\partial y}\left(K_H \frac{\partial \theta}{\partial y}\right)}_{horizontal\ mixing} \right) + \underbrace{\frac{\partial}{\partial z}\left(K_V \frac{\partial \theta}{\partial z}\right)}_{vertical\ mixing} + \underbrace{F}_{forcing} \qquad Eq[1]$$

The regional baroclinic Rossby deformation radius ranges from 4 to 17 km (Foster and Middleton 1979; Chelton, Deszoeke, and Schlax 1998). While the resolution of the model is insufficient to resolve convective plumes (O~0.5-1km), it can resolve convecting chimneys which have been observed in the ocean and can span tens of kilometers in width (J. Marshall and Schott 1999). A convective chimney is a region where density is nearly homogeneous with depth.

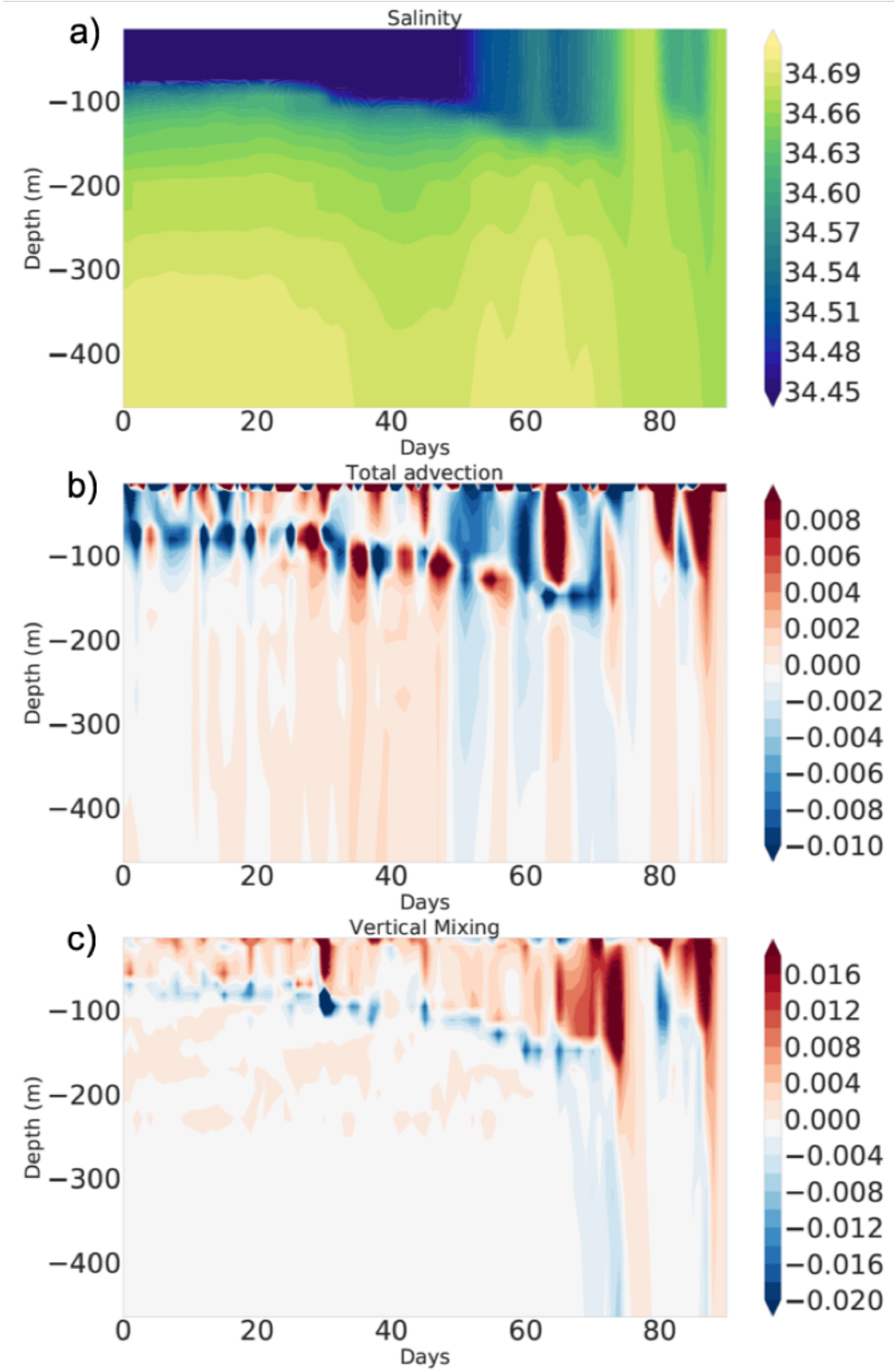

Figure 34: Timeseries of a) salinity, b) total advection and c) vertical mixing (diffusion) over Maud Rise in a square box of 10 by 10km just before, and after convection begins in year 37 June-August.

A Hovmöller time series of the dominant terms in the tracer equation that contribute to the total rate of change of salinity (total advection and vertical mixing terms for salt in Eq [1] without the negative sign) along with salinity over the same area is shown in Fig.34 and is focused around the time when the MRP is triggered in year 37. The change in salinity (Fig.34a) is analyzed by tracking total (horizontal plus vertical) advection (Fig.34b) and vertical mixing (Fig.34c) over the same region. Fig.34a indicates that salinity in the upper 100m layer begins to increase noticeably between day 50 and 60. Negative values in total advection at the same time indicate convergence, which in turn indicates salinity being added to this layer. There is a strong divergence in that layer right after day 60 indicated by positive values in the total advection which has the effect of freshening. Lower salinity in the upper layer suggests restratification. After restratification (day 70), this is followed by a large increase in upper ocean salinity which is preceded by strong vertical mixing (Fig. 34c) that suggests convection. Convection continues till day 80 when divergence within the box acts to restratify the water column by removing anomalously salty water from the box thus spreading it out. This process seems to repeat itself around day 85.

4.4 Summary and Conclusions

In this chapter, we have explained the widening of MRPs into the Weddell Sea and the role of the large scale circulation in preconditioning the region for WSPs in the E3SMv0-HR simulation. The preconditioning and formation mechanisms of WSPs and MRPs, while related, are distinctly different and it can be ascribed to differences in the topography between central Weddell Sea and Maud Rise-Astrid Ridge complex. Our main conclusions are outlined in the following:

a) The vertical structure of the central and the eastern Weddell Gyre in the simulation compares well with observations. Capturing the double cell structure of the gyre is critical

as it determines the preconditioning and formation mechanisms of both MRPs and WSPs. MRPs occur in the eastern Weddell Gyre and the vertical structure of the eastern cell plays a key role in explaining the presence of advecting salinity anomalies that trigger MRPs. WSPs occur in the central Weddell Sea and thus its water mass structure prior to polynya formation is key to explaining the weakening of the ambient stratification by the large scale circulation.

b) The large scale circulation in the Weddell Sea plays an important role in priming the Weddell Sea for OOPs. The spin up of the double cell Weddell Gyre leads to a doming of isopycnals which weakens the ambient stratification in both the central as well as the eastern Weddell cell, although more so in the former. This effect amplifies the entrainment of WDW into the upper ocean along the eastern end of the eastern cell, producing salinity anomalies that then advect into the Maud Rise - Astrid Ridge complex. These anomalies combined with Taylor cap effects trigger MRPs as shown in Chapter 3.

c) The occurrences of the WSPs in E3SMv0-HR are closely tied to the strengthening of the Weddell Gyre which in turn are tied to strong negative wind stress curl anomalies in the Weddell Sea, as last seen in 1974-76. E3SMv0-HR is a preindustrial simulation and thus it does not address consequences of a warming and freshening surface ocean and the role of precipitation in inhibiting OOPs as in the present-day Weddell Sea. In E3SMv0-HR, the stratifying effect of precipitation during the spin up of the Weddell Gyre does not overtake the effect of doming of the isopycnals that weaken the stratification. We only see anomalous precipitation as a consequence of heat released into the atmosphere due to OOPs in the Weddell Sea.

d) In E3SMv0-HR, the years of absence of OOPs in the Weddell Sea overlap with years in which there is a spin-down of the Weddell Gyre. The stratifying effect of a weak Weddell gyre promotes the accumulation of WDW, thereby increasing the heat and salt content in the subsurface ocean. These periods of subsurface heat reservoir recovery are a necessary condition sustaining OOPs once convection has been triggered, be it an MRP or a WSP.

e) The size of the MRPs combined with the availability of subsurface heat appears to dictate whether MRPs will expand westward into the central Weddell Sea during subsequent years. Comparing the size of MRP area in MRP-only years with that of MRP+WSP years, a clear pattern emerges. The size of the MRP dictates the scale of open ocean convection which in turn determines the amount of salt brought to the surface layer, which is subsequently advected downstream to the central Weddell Sea region. The stratification over the Maud Rise - Astrid Ridge complex is weaker than in the central Weddell Sea due to the presence of Taylor column dynamics (see Chapter 3). Thus, large upper ocean salinity anomalies are needed to trigger convection over the central Weddell Sea, which in turn are provided by anomalously large MRPs.

5. POTENTIAL EFFECTS OF AABW ANOMALIES DUE TO WSPs ON THE STRENGTH OF THE AMOC

5.1 Introduction

The Weddell Gyre is an important part of the global climate pathway due to its influence on the formation of dense water masses and long-term sequestration of atmospheric heat, and carbon (Marinov et al. 2006). This region is the most important source of AABW (Orsi, Nowlin JR, and Whitworth 1993) produced by coastal (Morales Maqueda 2004) as well as open-ocean polynyas (Martinson, Killworth, and Gordon 1981). The long-term sequestration of atmospheric heat and carbon (Hoppema 2004) in the Weddell Sea happens through deep ocean convection (de Lavergne et al. 2014) and subsequent dense water formation. Deep ocean convection occurs along the continental slope of Antarctica as well as in the offshore Weddell Basin in austral winter (Morales Maqueda 2004; Z. Zhang et al. 2015).

To understand if there is a relationship between the size and impact of OOPs at different depths, we analyzed the spatial ocean heat content (OHC) anomalies of water masses in the Weddell Sea at three depths, namely a) Upper 200m (ASW) b) 200-1500m (WDW) and c) 1500m-bottom (below WDW). In the case of OOPs in the Weddell Sea, the impact on bottom water masses depends on their size. The OOPs in the MRP-only years affect the OHC anomalies of the ASW and WDW, but they do not have a significant effect at deeper depths. The WSPs do have a significant impact on the OHC of the entire water column including below 4000m which affects AABW properties. Analyzing every MRP event in the MRP-only years, we conclude that relatively small MRPs do not significantly affect AABW properties. We have further analyzed the

salinity anomalies at the same depths. Both temperature and salinity show a clear impact of WSPs on bottom water formation.

The method of formation of AABW determines its characteristics (Carmack 1990; Coles et al. 1996; Legg et al. 2009). Open ocean convection in the Weddell Sea adds a distinct flavor to the bottom waters being produced through this process. Observations of AABW properties since the WSPs during 1974-76 indicate that deep convection makes the bottom water more "minty", i.e., cold and fresh, and that the lack of large WSPs ever since has made it more spicy, i.e., warm and salty (Coles et al. 1996; Purkey and Johnson 2010). The processes affecting AABW production affect the global overturning circulation, and with that the heat and carbon uptake by the oceans (Sabine Christopher et al. 2004; Watanabe et al. 2013; Thomas, Waugh, and Gnanadesikan 2018).

The understanding of the formation processes of AABW has evolved over the past few decades as observational capabilities have expanded in the Southern Ocean. However, there are still large uncertainties about the formation rate and source regions of AABW and its natural variability due to anthropogenic causes. Extensive observational studies carried out in the Southern Ocean and Weddell Sea have made it possible for us to understand the different formation methods of AABW and the dominant source region of AABW as well as their impact on the global ocean (Orsi, Johnson, and Bullister 1999; Orsi, Smethie, and Bullister 2002; van Sebille et al. 2013; Ferreira and Kerr 2017). In the Weddell Sea, one of the formation processes of AABW includes a mixture of High Salinity Shelf Water (HSSW) (formed on the continental shelf via coastal polynyas (Grumbine 1991)) and modified WDW (a mixture of ASW and WDW) forming the densest version of AABW. As this water mass flows down the continental slope, it can further mix with WDW, creating a lighter version of AABW, also called WSDW (Carmack and Foster 1975;

Foster and Carmack 1976; Carmack 1990). Another variety of AABW involves the mixture of Ice Shelf Water (ISW) (which is HSSW mixed with water from the base of the ice shelves (Nicholls, Østerhus, and Makinson 2009)) with WDW/ modified WDW (Foldvik, Gammelsrød, and Tørresen 1985). Thus, OOPs in the Weddell Sea can modulate AABW characteristics by modifying any of the parent water masses.

The Weddell Sea has not had a winter-long OOP since the late 1970s. There are several theories that explain why there is a dramatic reduction in OOPs in the Weddell Sea. The present-day poleward shifted southern hemisphere westerlies due to anthropogenic CO_2 emissions and ozone depletion (Oke and England 2004; Russell et al. 2006; Fyfe et al. 2007) results in a positive trend of the SAM index (Thompson and Solomon, 2002). Intensifying winds over the high-latitude Southern Ocean due to this shift leads to a spin up of the Weddell gyre (Cheon et al. 2014) which would typically cause a doming of isopycnals that is traditionally one of the mechanisms leading up to a WSP [*Hirabara et al.*, 2012; *Cheon et al.*, 2015b; see Chapter 4]. However, the southward shift of the westerlies also leads to an increase in precipitation over the Weddell Sea, thus freshening the surface ocean and flattening the isopycnals at the surface (Gordon 2014). The associated increase in Ekman divergence increases the interaction of the subsurface heat reservoir in the Weddell Gyre with the ice shelves thereby increasing glacial melt, which contributes to surface freshening (Rignot et al. 2013). The total sum of the anthropogenic effects have resulted in warming and freshening of the Southern Ocean (Swart et al. 2018), and the absence of WSPs since the late 1970s appears to be one of its consequences (de Lavergne et al. 2014). However, due to the dominant role of Taylor cap dynamics over tall seamounts, the Weddell Sea is preconditioned for the smaller MRPs to occur, as has last been observed in year 2017 (Fig.1b) (Kurtakoti et al. 2018).

Several modeling studies show that the switch from periods of deep convection in the Weddell Sea (WSPs) and periods of recovery when there are no OOPs, gives rise to AABW anomalies (below 4000 m depth). These anomalies propagate along the deep western boundary into the Argentine Basin and appear to have a significant impact on ocean circulation (Stössel and Kim 2001; Hirabara et al. 2012; Martin, Park, and Latif 2013; Cabré, Marinov, and Gnanadesikan 2017; Zanowski and Hallberg 2017). Observations since the WSP in the late 1970s also suggest that AABW is warming and its volume is shrinking (Coles et al. 1996; Hogg and Zenk 1997; Zenk and Morozov 2007; Zenk and Visbeck 2013; Johnson, McTaggart, and Wanninkhof 2014). Changes in temperature and salinity of AABW have competing effects on density. These AABW anomalies radiate away from the source region in the Weddell Sea into the South Atlantic basin on relatively short timescales in the form of Kelvin and Rossby waves (Kawase 1987; Hallberg and Rhines 1996), propagating northward along the deep western boundary (Hirabara et al. 2012; Purkey and Johnson 2010; Zanowski and Hallberg 2017).

Typically, changes in the strength of the AMOC are attributed to changes in surface buoyancy fluxes in the North Atlantic, with associated impact on NADW formation (Yeager and Danabasoglu 2014). The AMOC is a significant part of the ocean overturning circulation and thus the global climate system, and is responsible for transporting heat northwards in the Atlantic. The formation of the deep water masses NADW and AABW are major components of the AMOC. While a slowdown of the AMOC is predicted by most climate models, it has not yet been observed. Paleo modeling studies indicate that a reduction in the strength of the AMOC in the past is due to enhanced freshwater input in the high latitude North Atlantic region (Chang et al. 2008; Ritz et al. 2013). Similarly, enhanced surface freshwater fluxes can also nowadays be provided by meltwater

from the Greenland ice sheet and precipitation (Latif et al. 2004; Send, Lankhorst, and Kanzow 2011; Smeed et al. 2014; Rahmstorf et al. 2015).

Several studies indicate that it is possible to influence the strength of the AMOC via changes in the Southern Hemisphere. This is because the AMOC and the global overturning circulation are connected by the Southern Ocean. Modeling studies have shown that the Agulhas leakage is correlated with the AMOC on multidecadal timescales (Biastoch et al. 2015). There is also indication that AABW inflow (i.e., northward transport) can modulate the NADW outflow (i.e., southward transport) across 30°S (Stössel and Kim 2001; Swingedouw et al. 2009; Martin, Park, and Latif 2015). The AABW inflow is in turn affected by large OOPs in the Weddell Sea. Stössel and Kim (2001) showed that AABW outflow is negatively correlated with NADW inflow with a lead of ~2 years. Several studies have shown that AABW anomalies radiate away from the Weddell Sea via topographic Rossby and baroclinic Kelvin waves (Kawase 1987; Hallberg and Rhines 1996; Hirabara, Ishizaki, and Ishikawa 2007) that act on a timescale of several years to decades. The AABW anomalies also spread through advection that acts on decadal to longer timescales (Zanowski and Hallberg 2017).

Modeling studies show that the retreat of AABW in the South Atlantic causes the upper cell of the AMOC to strengthen by 5-10% (Patara and Böning 2014) and also infer that the lack of OOPs in the Weddell Sea since the late 1970s must already contributing to a strengthening of the AMOC. A reduction in AABW formation and its northward transport leads to augment the meridional density gradient in the deep ocean, thus intensifying the NADW outflow (southward transport) and thus strengthening the AMOC [*Swingedouw et al.*, 2009; *Martin et al.*, 2014]. These theories illustrating the impact of AABW outflow on the AMOC are incomplete and thus not fully understood.

5.2 Outlook on propagation of AABW anomalies along deep western boundary (DWB)

In order to understand how WSPs influence the abyssal ocean properties in the Weddell basin, we show the abyssal ocean (below 4000 m) salinity anomalies during the WSP events (during the MRP+WSP years: 101-124, which begin with an MRP year 101) shown in Figs. 35-36. The cold temperature anomalies propagate exactly as the fresh salinity anomalies and are not shown. Figs 35-36 show the salinity anomalies below 4000m spreading along the DWB after the onset of WSP event in year 102 in E3SMv0-HR (see Chapters 2 through 4, and Kurtakoti et al., 2018). Prior to the onset of the WSP, there is a recovery of the subsurface heat and salt reservoir. During the years 102-124 (Fig. 35), large WSPs occur every winter. There is a freshening of 0.05psu (Fig. 35) and cooling of more than 1°C (not shown) below 4000 m during these 22 years. The salinity anomalies propagate along the DWB (along the Scotia Ridge through the South Sandwich trench) into the Argentine Basin. Here they induce a gradual freshening and cooling that is seemingly being reinforced a decade later at the DWB at 30°S where it could potentially affect the outflow of NADW and thus the strength of the AMOC. Looking at the variability of the AMOC strength at 26°N (Fig.36), however there is no clear evidence of a correlation with the variability of open-ocean convection in the Weddell Sea or WSP formation even though the AMOC reveals interdecadal variability after year 50 that could potentially be related to strong WSB/EMB events. The anomalies propagate from near Maud Rise and go as far as 10°S by the end of 20 years from the first WSP in the sequence. Further analysis is needed to quantify the potential relationship between the spreading of AABW anomalies and the strength of the AMOC in this HR ESM simulation, in particular to clarify whether a strong correlation between the two, as suggested in earlier modeling studies, is not just an artifact of low model resolution.

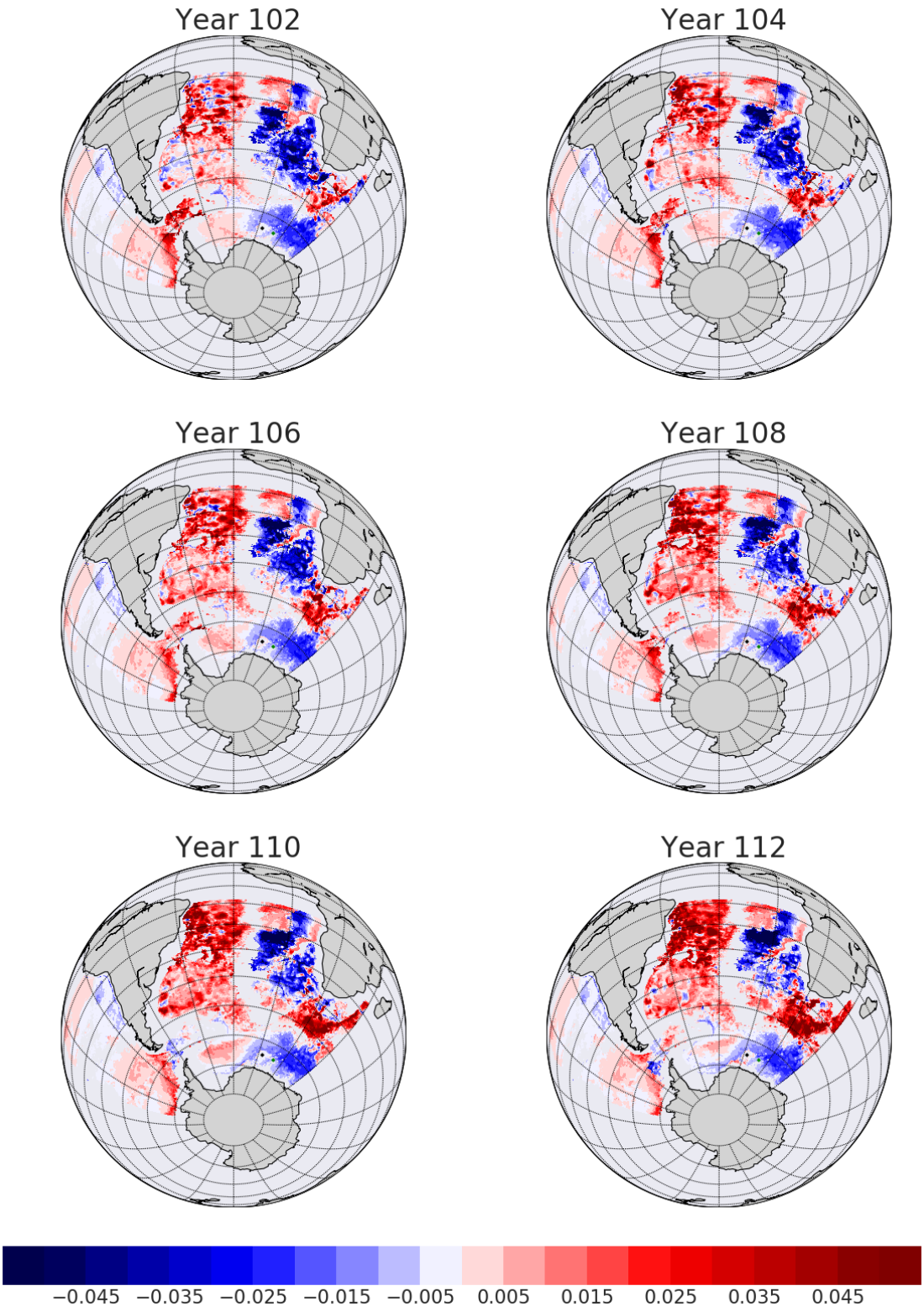

Figure 35: Salinity anomalies (January) below 4000m after the onset of WSPs in year 102. The peak of Maud Rise seamount is indicated with a black dot and the center of Astrid Ridge is indicated with a green dot.

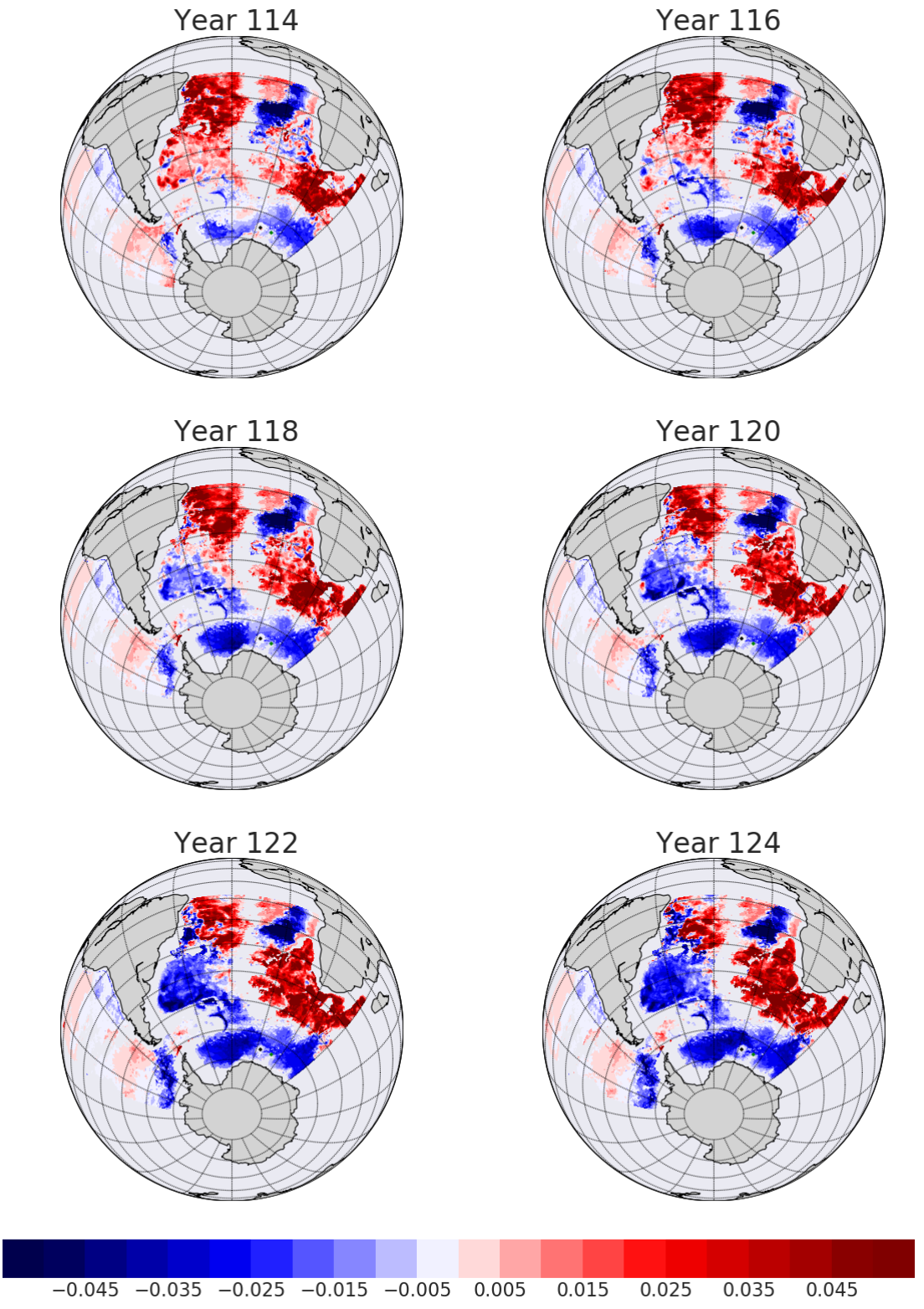

Figure 35: Continued.

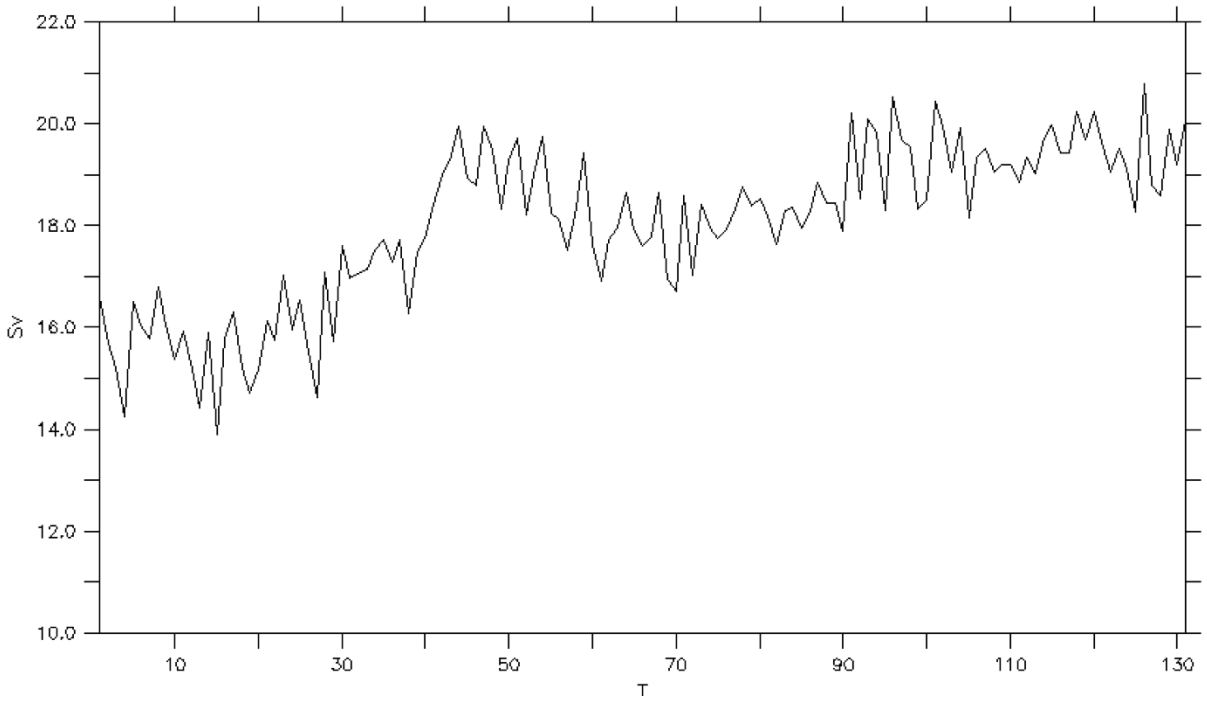

Figure 36: Timeseries of AMOC strength at 26.5°N for the full E3SMv0-HR simulation.

5.3 Outlook on propagation of WSDW and WSBW anomalies

It is important to understand the source of AABW variability, which cannot be properly done without analyzing the anomalies in its different source water masses. The temperature (not shown) and salinity (Fig. 37) anomalies between 2000-4000m are presented to study the impact of the WSP events on water masses below WDW during the WSP events (during the MRP+WSP years: 101-124). The fresh and cold anomalies at 2000-4000m depth spread into the South Atlantic to 40°S as well as into the Pacific Ocean basin via the Drake Passage. The WSP events reduce the average temperature by 2°C and salinity by 0.16psu between 2000-4000m in the central Weddell Sea.

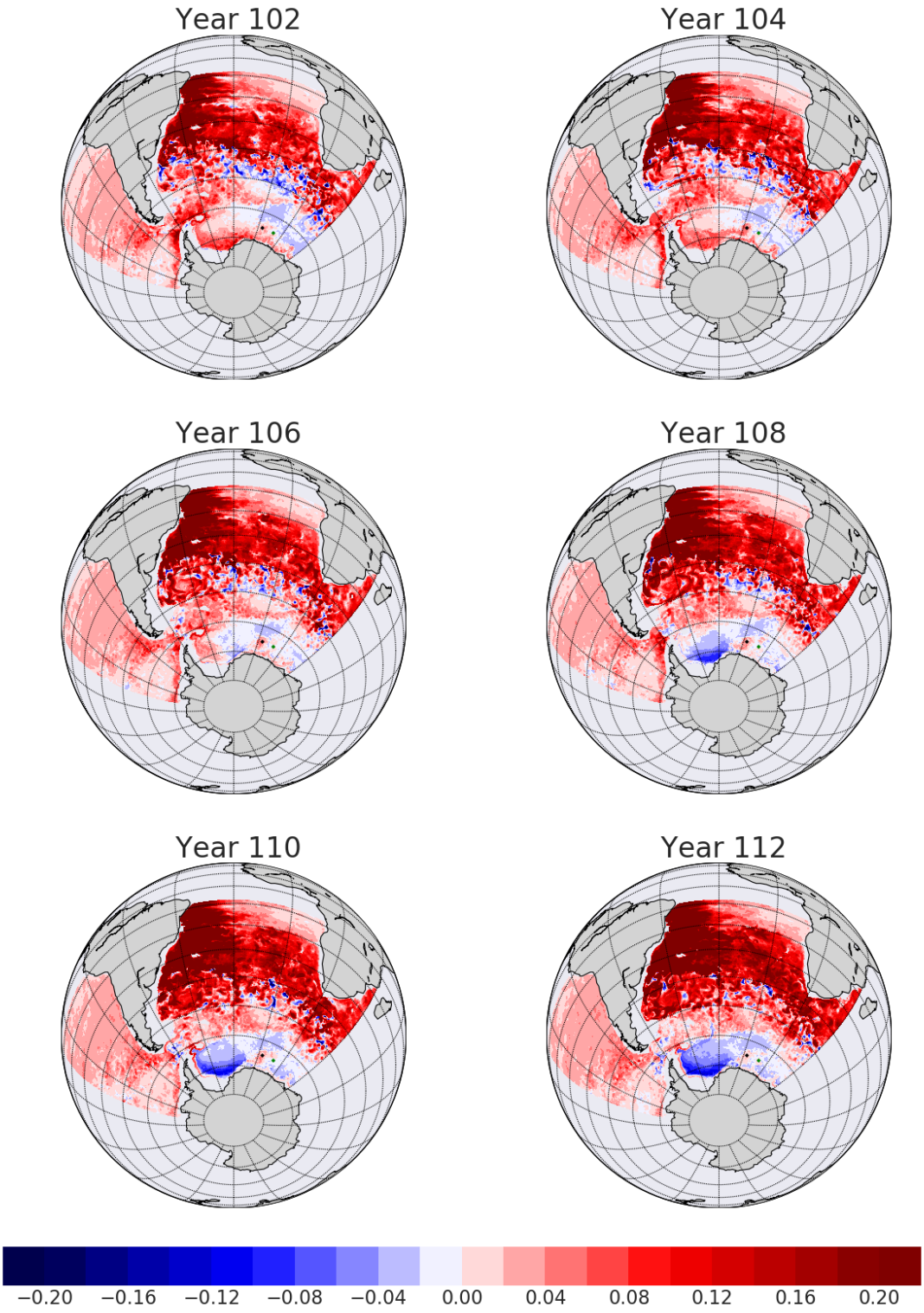

Figure 37: Same as Fig.35, but for layer between 2000 - 4000 m.

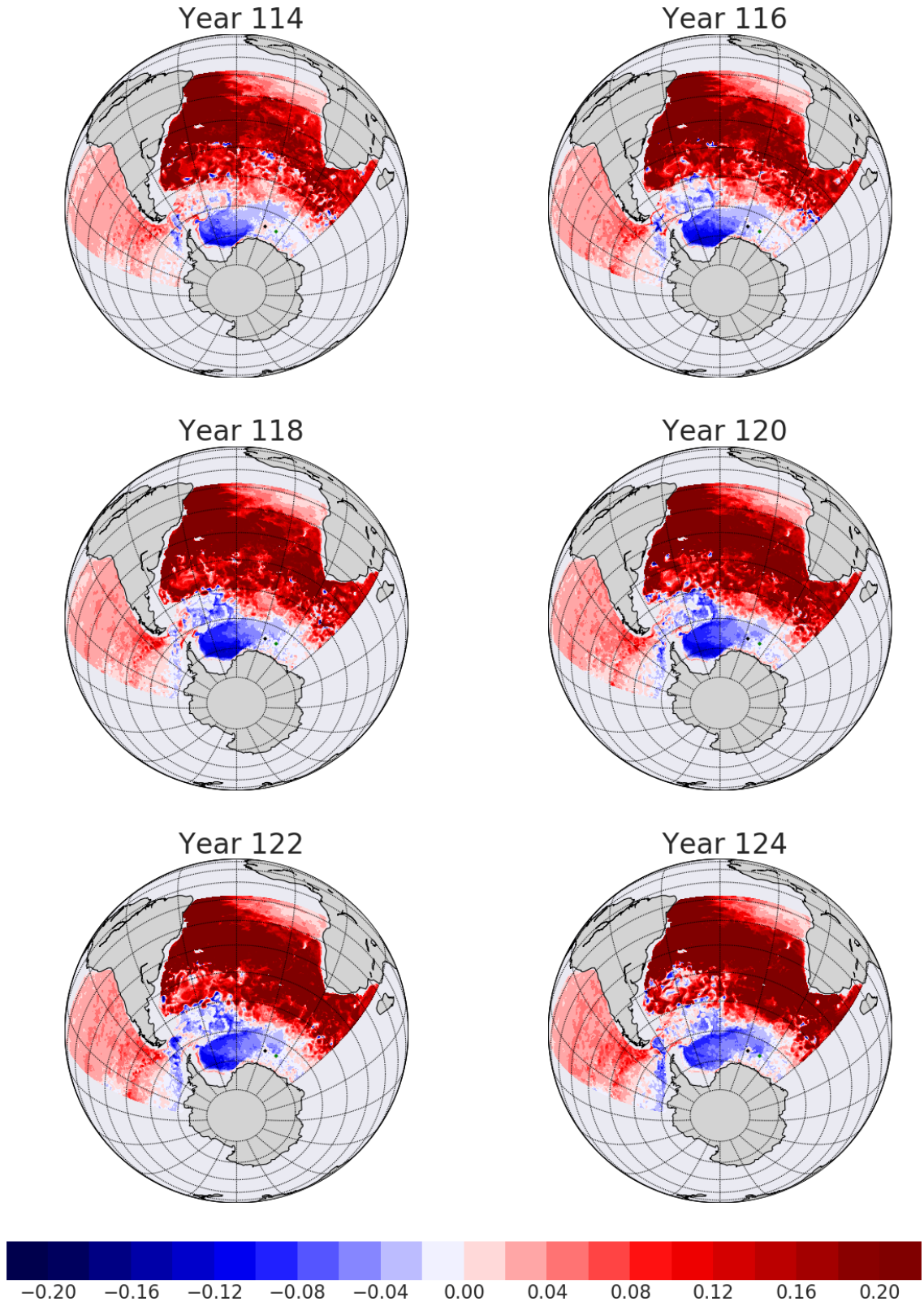

Figure 37: Continued.

Model resolution and in particular the resolution of the ocean bathymetry are important for both coastal polynyas and OOPs in the Weddell Sea (Dufour et al. 2017; Kurtakoti et al. 2018). The formation of OOPs in the Weddell Sea through realistic processes require the model to produce Taylor cap effects over the Maud Rise - Astrid Ridge complex, which needs bathymetric features to be represented in great detail. The propagation of AABW anomalies arising from the WSPs that propagate along the DWB (via Rossby and Kelvin waves) and the associated heaving of the interface between AABW and NADW also require an accurate representation of bathymetry. These preliminary findings based on a HR ESM simulation support our initial hypothesis that the apparently strong impact of AABW anomalies on the outflow of NADW, and thus the AMOC strength, found in earlier studies may just be an artifact of low model resolution.

6. SUMMARY AND OUTLOOK

6.1 Summary

In the early 1970's, satellite observations unveiled the presence of a large OOP within the Antarctic ice pack in the Weddell Sea (Gordon et al., 1988). OOPs in the Southern Ocean are large ice-free areas within the winter ice pack that are associated with deep convection and thus potentially contribute to the formation of AABW. The OOP of the 1970's was observed for three consecutive winters and was thus assumed to be a normal event at first. But since then it hasn't been observed with the same scale. This sudden cessation of OOPs in the Southern Ocean has been attributed to anthropogenic climate change (de Lavergne et al., 2014). These convective events play a fundamental role in the global ocean circulation and the impacts of their cessation are not fully understood. This dissertation has evaluated the preconditioning and formation mechanisms of these convective events and their potential impacts on the abyssal ocean using a high-resolution simulation (E3SMv0-HR) in which persistent winter OOPs were simulated in the Weddell Sea (WSP) and over the Maud Rise seamount (MRP).

In Chapter 3, I analyzed the processes responsible for the preconditioning and formation of MRPs in the E3SMv0-HR simulation, where, in that part of the study, I focused on the impact of a Taylor cap that formed as a result of high-resolution representation of bathymetry of Maud Rise, which was decisive for preconditioning the region for deep convection. The general model hydrographic conditions over the Maud Rise-Astrid Ridge region are comparable to observations. E3SMv0-HR simulates the anticyclonic flow north of Maud Rise, the doming of the isopycnals over the seamount, the halo of low sea ice concentration and a baroclinic cyclonic circulation over the Taylor cap. The MRPs are ultimately triggered by enhanced upper ocean salinity that is

advected into the region. These processes are illustrated in a schematic in Fig. 38 (a,b). These anomalies are seen prior to every MRP-I event throughout the E3SMv0-HR simulation. The upper ocean salinity is enhanced as a result of entrainment of WDW at the eastern limb of the eastern Weddell Gyre upon experiencing strongly negative wind stress curl. The heat released from the WDW during deep convection keeps the surface ice free and plays a key role in long lasting MRPs. The accurate representation of the bathymetry over the Maud Rise- Astrid Ridge complex plays a key role in its ability to develop a Taylor cap which is dependent on the ratio of the seamount height to its width which in turn is dependent on the horizontal resolution of the model. The WSPs in the simulation are comparable to the WSPs in the late 1970s in size and begin over Maud Rise before spreading into the Weddell Sea.

In Chapter 4, I studied the formation mechanism of Weddell Sea Polynyas in E3SMv0-HR (Fig. 38 c,d). The simulated WSPs grow realistically out of MRPs, similarly to the observed WSP events of 1974-1976. The formation of MRPs requires high model resolution to simulate the detailed flow around Maud Rise seamount, while a realistic formation process of WSPs requires the ability of a model to produce MRPs. Deep convection over Maud Rise being triggered by the advection of near-surface waters with anomalously high salinity is confirmed by the balance of terms in the advection-diffusion equation over a short winter period using daily output data of the simulation. Furthermore, WSP formation is shown to not occur without a prolonged build-up of a heat reservoir at depth. The prerequisite for such is a strong stratification and a thick cold and fresh surface layer, which usually prevails when the core of the southern hemisphere westerlies is at an anomalously northern position. If in a subsequent period the westerlies shift southward, the negative wind stress curl over the Weddell gyre strengthens, and leads to a spin up of foremost the eastern portion of the double-cell structure of the gyre. The spin up also leads to a stronger inflow

of WDW into the Weddell Gyre as indicated by the large increase in WDW temperature and salinity upstream of the Maud Rise- Astrid Ridge complex. Thus, the spin up of the Weddell Gyre appears to be a necessary condition for WSP formation in E3SMv0-HR. The ultimate trigger is the formation of pronounced MRPs, which bring warm and salty WDW to the surface. If the associated surface salinity anomalies are high enough, their westward propagation with the background flow of the Weddell gyre eventually triggers the formation of a WSP. These WSP formation mechanisms are illustrated in a schematic in Fig. 38 (c,d).

In Chapter 5, I discussed the spreading of AABW anomalies due to WSPs and its possible impact on the AMOC strength. The northward propagation of cold and fresh AABW anomalies after major WSP events are clearly discernible in the simulation. They reach subtropical latitudes within about 10 years, suggesting that the propagation mechanism is internal boundary waves rather than advection. These waves propagate on timescales much shorter than advective timescales. The effect of the Southern Ocean open ocean convection on the abyssal ocean is not fully understood primarily because these events have not been observed since the late 1970s and thus can only be studied in ocean models in which the response tends to vary. In E3SMv0-HR, the cooling and freshening signal in the abyssal ocean tends to 1) propagate as a fast deep western boundary current into the Atlantic Basin and 2) leak into the Pacific and Indian Basin. *Martin et al.*, 2015 using a low-resolution climate model, showed that such anomalies have a direct impact on the AMOC strength on centennial timescale. In E3SMv0-HR, we find that WSPs impact AABW anomalies but these do not seem to affect the AMOC strength. We also acknowledge that the simulation is not long enough to show effects that occur on centennial time scales.

6.2 Implications and Outlook

In this dissertation, I have studied open ocean convection in the Weddell Sea using a state-of-the-art high-resolution climate simulation, an enormous multi-institutional effort which allowed me to study the effects of several small scale processes in preconditioning the Weddell Sea to produce realistic MRPs, WSPs and study the how it affects both the atmosphere and the abyssal ocean. The effect of WSPs on the local atmospheric circulation (Weijer et al. 2017) and the abyssal ocean have recently been investigated in eddy resolving climate models (Dufour et al. 2017). Previously, their impacts were also studied in eddy permitting and low-resolution models (Stössel and Kim 2001; Martin, Park, and Latif 2015; Swingedouw et al. 2009; Patara and Böning 2014; Zanowski and Hallberg 2017). Observational studies have also documented the effect of WSPs on the abyssal ocean and also shown the effect of their dramatic reduction since the late 1970s (van Sebille et al. 2013; Ferreira and Kerr 2017; Purkey and Johnson 2010; Johnson and Purkey 2012; Purkey and Johnson 2013).

Observational studies suggest that AABW volume is warming and shrinking (Hogg and Zenk 1997; Johnson, McTaggart, and Wanninkhof 2014). There are some questions that are not yet answered: 1) When its volume shrinks along the DWB, is it being replaced by NADW, which itself is warmer? 2) Is there a reduction in the volume of AABW in the Weddell Sea, or is it a result of the interface between NADW and well-known colder type of AABW moving deeper. *Meredith et al.*, 2011 use observations from the Weddell Sea to suggest that the observed warming and reduction of the well-known colder type of AABW volume does not necessarily mean that the contribution of AABW volume in the Weddell Sea to the global oceans has reduced.

In this dissertation, I also explore the role of strengthening Southern Hemisphere westerlies in the Weddell Sea on open ocean convection in a pre-industrial simulation. Throughout the

E3SMv0-HR, intensification of the westerlies in the Weddell Sea are an important precursor to WSPs. This was also a well-accepted explanation for the onset of WSPs in the late 1970s (Hirabara et al. 2012; Cheon et al. 2015). Present day conditions suggest that the surface freshening and warming of the Southern Ocean has prevented the occurrence of WSP despite strengthening Southern Hemisphere westerlies (Gordon 2014; de Lavergne et al. 2014). This dissertation reveals a possible consequence of anthropogenic effects on open ocean convection in the Southern Ocean. The pre-industrial E3SMv0-HR simulation also features a reasonable representation of near-boundary convection along the continental margins in the Weddell Sea. Improved representation of open ocean convection in E3SMv0-HR are also a result of higher model resolution and are in line with the conclusions of *Stössel et al.*, 2015.

The resolution of the model is considered an important factor to consider while trying to study the impact of changing Southern Hemisphere westerlies on AMOC via surface Ekman transport (Gent 2015). This is not the same as estimating the impact of anomalies in the formation of AABW on AMOC in E3SMv0-HR even though the WSPs are all preceded by intensifying Westerlies. *Gent*, 2015 primarily addresses the "Drake Passage effect" which is the idea that NADW outflow is modulated by the winds across the Drake Passage. *Toggweiler and Samuels*, 1995 using a low-resolution model showed that intensifying winds in the latitude band of the Drake Passage leads to an increase in the northward Ekman transport thus increasing the NADW outflow. However this effect is consistently absent in eddy resolving models (Gent 2015). I draw parallels between the "Drake Passage effect on AMOC" and the "impact of AABW anomalies on AMOC on decadal timescales" due to the change in conclusions caused by an increase in model resolution. AMOC estimated at 26.5°N in the E3SMv0-HR simulation does not show a readily discernible relationship between WSPs and AMOC. However, we cannot comment on the impact of WSPs on

the strength of AMOC on centennial timescales. High-resolution climate modeling presents us with an opportunity to revisit old conclusions in a new light and to estimate the importance of resolving eddies in the Southern Ocean.

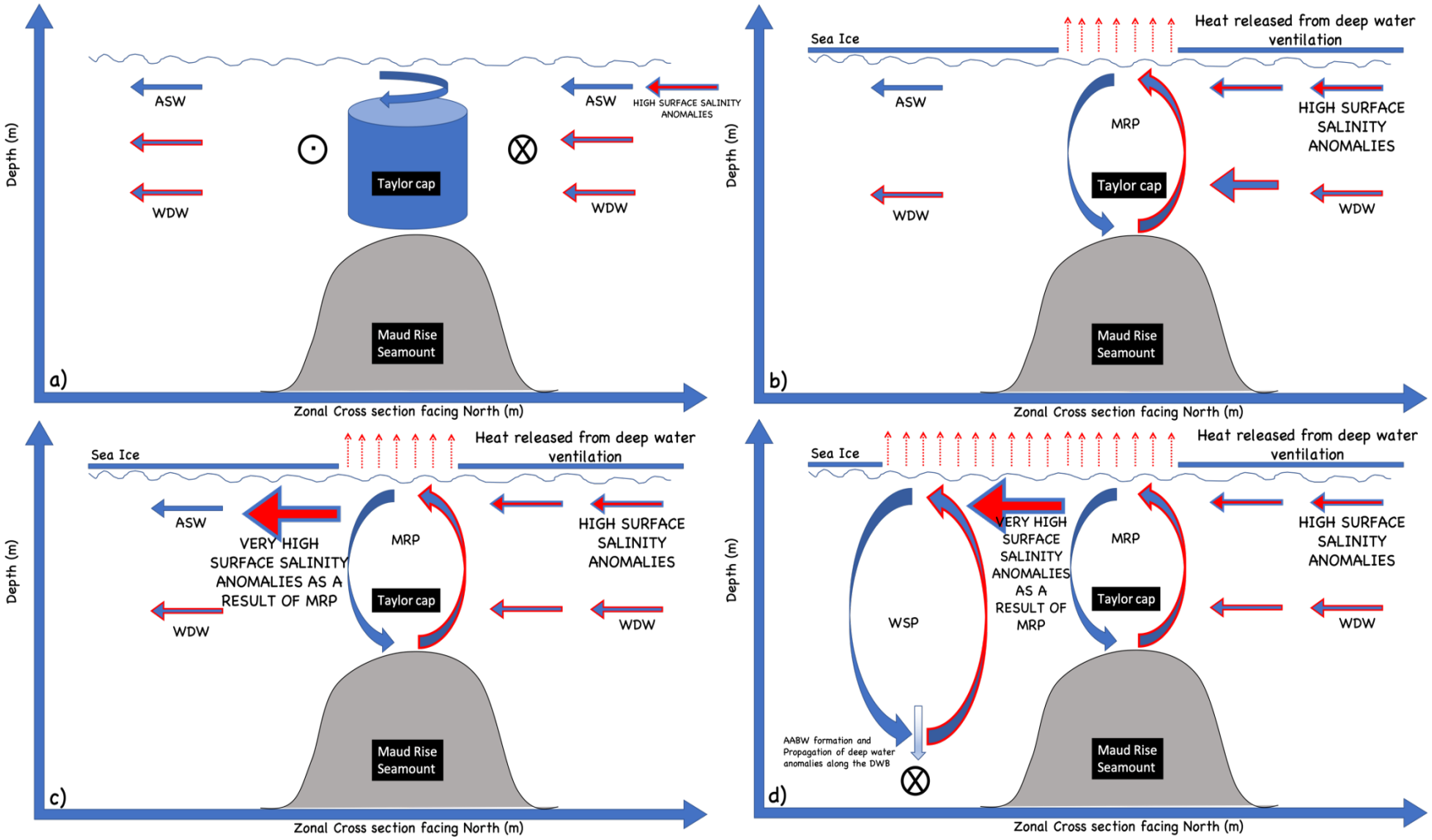

Figure 38: A schematic summarizing the processes necessary for the formation of MRP (top panels) and WSP (bottom panels).

REFERENCES

Alverson, Keith, and Brechner Owens. 1996. "Topographic Pre-Conditioning of Open-Ocean Deep Convection." *Journal of Physical Oceanography* 26 (10): 2196–2213. https://doi.org/10.1175/1520-0485(1996)026<2196:TPOOOD>2.0.CO;2.

Beckmann, Aike, Ralph Timmermann, Adriene F. Pereira, and Christian Mohn. 2001. "The Effect of Flow at Maud Rise on the Sea-Ice Cover - Numerical Experiments." *Ocean Dynamics* 52 (1): 11–25. https://doi.org/10.1007/s10236-001-8173-5.

Bergh, Hugh W. 1987. "Underlying Fracture Zone Nature of Astrid Ridge off Antarctica's Queen Maud Land." *Journal of Geophysical Research* 92 (B1): 475. https://doi.org/10.1029/JB092iB01p00475.

Bersch, Manfred, Gerd A. Becker, Helmut Frey, and Klaus P. Koltermann. 1992. "Topographic Effects of the Maud Rise on the Stratification and Circulation of the Weddell Gyre." *Deep Sea Research Part A, Oceanographic Research Papers* 39 (2): 303–31. https://doi.org/10.1016/0198-0149(92)90111-6.

Biastoch, Arne, Jonathan V. Durgadoo, Adele K. Morrison, Erik Van Sebille, Wilbert Weijer, and Stephen M. Griffies. 2015. "Atlantic Multi-Decadal Oscillation Covaries with Agulhas Leakage." *Nature Communications* 6: 1–7. https://doi.org/10.1038/ncomms10082.

Cabré, Anna, Irina Marinov, and Anand Gnanadesikan. 2017. "Global Atmospheric Teleconnections and Multidecadal Climate Oscillations Driven by Southern Ocean Convection." *Journal of Climate* 30 (20): 8107–26. https://doi.org/10.1175/JCLI-D-16-0741.1.

Carmack, Eddy C. 1990. “Large-Scale Physical Oceanography of Polar Oceans.” *Polar Oceanography (Part A)*, 171–222.

Carmack, Eddy C., and Theodore D. Foster. 1975. “On the Flow of Water out of the Weddell Sea.” *Deep Sea Research and Oceanographic Abstracts* 22 (11): 711–24. https://doi.org/10.1016/0011-7471(75)90077-7.

Carmack, Eddy C. 1986. “Circulation and Mixing in Ice-Covered Waters.” In *The Geophysics of Sea Ice*, edited by Norbert Untersteiner, 641–712. Boston, MA: Springer US. https://doi.org/10.1007/978-1-4899-5352-0_11.

Carsey, F. D. 1980. “Microwave Observation of the Weddell Polynya.” *Monthly Weather Review*. https://doi.org/10.1175/1520-0493(1980)108<2032:MOOTWP>2.0.CO;2.

Chang, Ping, Rong Zhang, Wilco Hazeleger, Caihong Wen, Xiuquan Wan, Link Ji, Reindert J. Haarsma, Wim-Paul Breugem, and Howard Seidel. 2008. “Oceanic Link between Abrupt Changes in the North Atlantic Ocean and the African Monsoon.” *Nature Geoscience* 1 (7): 444–48. https://doi.org/10.1038/ngeo218.

Chapman, David C., and Dale B. Haidvogel. 1992. “Formation of Taylor Caps over a Tall Isolated Seamount in a Stratified Ocean.” *Geophysical & Astrophysical Fluid Dynamics* 64 (1–4): 31–65. https://doi.org/10.1080/03091929208228084.

Chelton, Dudley B, Roland A Deszoeke, and Micheal G Schlax. 1998. “Geographical Variability of the First Baroclinic Rossby Radius of Deformation.” *Journal of Physical Oceanography* 28 (3): 433–60. https://doi.org/10.1175/1520-0485(1998)028<0433:GVOTFB>2.0.CO;2.

Cheon, Woo Geun, Sang-ki Lee, Arnold L Gordon, Yanyun Liu, Chang-bong Cho, and Jong Jin Park. 2015. “Replicating the 1970s’ Weddell Polynya Using a Coupled Ocean-Sea Ice Model with Reanalysis Surface Flux Fields.” *Geophysical Research Letters* 42 (13): 5411–18.

https://doi.org/10.1002/2015GL064364.

Cheon, Woo Geun, Young-Gyu Park, J. R. Toggweiler, and Sang-Ki Lee. 2014. "The Relationship of Weddell Polynya and Open-Ocean Deep Convection to the Southern Hemisphere Westerlies." *Journal of Physical Oceanography* 44 (2): 694–713. https://doi.org/10.1175/JPO-D-13-0112.1.

Coles, Victoria J, Michael S Mccartney, Donald B Olson, and M Smethie. 1996. "Changes in Antarctic Bottom Water Properties in the Western Rise." *Journal of Geophysical Research* 101: 8957–70. http://dx.doi.org/10.1029/95JC03721; doi:10.1029/95JC03721.

Cunningham, S.A, S.G Alderson, B.A King, and M.A Brandon. 2004. "Transport and Variability of the Antarctic Circumpolar Current in Drake Passage." *Deep-Sea Research Part II: Topical Studies in Oceanography* 108 (C5): 1–17. https://doi.org/10.1029/2001JC001147.

Deacon, G.R.E. 1963. "The Southern Ocean." *M.N. Hill (Ed.), The Sea, Interscience, New York*, p.281.

Dennis, John M, Jim Edwards, Katherine J Evans, Oksana Guba, Peter H Lauritzen, Arthur A Mirin, Amik St-Cyr, Mark A Taylor, and Patrick H Worley. 2011. "CAM-SE: A Scalable Spectral Element Dynamical Core for the Community Atmosphere Model." *The International Journal of High Performance Computing Applications* 26 (1): 74–89. https://doi.org/10.1177/1094342011428142.

Donohue, K. A., K. L. Tracey, D. R. Watts, M. P. Chidichimo, and T. K. Chereskin. 2016. "Mean Antarctic Circumpolar Current Transport Measured in Drake Passage." *Geophysical Research Letters* 43 (22): 11,760-11,767. https://doi.org/10.1002/2016GL070319.

Dufour, Carolina O., Adele K. Morrison, Stephen M. Griffies, Ivy Frenger, Hannah Zanowski, and Michael Winton. 2017. "Preconditioning of the Weddell Sea Polynya by the Ocean

Mesoscale and Dense Water Overflows." *Journal of Climate*, 7719–37. https://doi.org/10.1175/JCLI-D-16-0586.1.

Fahrbach, E., M. Hoppema, G. Rohardt, O. Boebel, O. Klatt, and A. Wisotzki. 2011. "Warming of Deep and Abyssal Water Masses along the Greenwich Meridian on Decadal Time Scales: The Weddell Gyre as a Heat Buffer." *Deep-Sea Research Part II: Topical Studies in Oceanography* 58 (25–26): 2509–23. https://doi.org/10.1016/j.dsr2.2011.06.007.

Ferreira, Maria Luiza de Carvalho, and Rodrigo Kerr. 2017. "Source Water Distribution and Quantification of North Atlantic Deep Water and Antarctic Bottom Water in the Atlantic Ocean." *Progress in Oceanography* 153: 66–83. https://doi.org/10.1016/j.pocean.2017.04.003.

Foldvik, A., T. Gammelsrød, and T. Tørresen. 1985. "Circulation and Water Masses on the Southern Weddell Sea Shelf." In , 5–20. American Geophysical Union (AGU). https://doi.org/10.1029/AR043p0005.

Foster, Theodore D., and Eddy C. Carmack. 1976. "Frontal Zone Mixing and Antarctic Bottom Water Formation in the Southern Weddell Sea." *Deep Sea Research* 23 (4): 301–17. https://doi.org/10.1016/0011-7471(76)90872-X.

Foster, Theodore D., and Jason H. Middleton. 1979. "Variability in the Bottom Water of the Weddell Sea." *Deep Sea Research Part A, Oceanographic Research Papers* 26 (7): 743–62. https://doi.org/10.1016/0198-0149(79)90011-6.

Fyfe, John C., Oleg a. Saenko, Kirsten Zickfeld, Michael Eby, and Andrew J. Weaver. 2007. "The Role of Poleward-Intensifying Winds on Southern Ocean Warming." *Journal of Climate* 20 (21): 5391–5400. https://doi.org/10.1175/2007JCLI1764.1.

Gent, Peter R. 2015. "Effects of Southern Hemisphere Wind Changes on the Meridional

Overturning Circulation in Ocean Models." *Annual Review of Marine Science* 8 (1): 79–94. https://doi.org/10.1146/annurev-marine-122414-033929.

Gong, Daoyi, and Shaowu Wang. 1999. "Definition of Antarctic Oscillation Index." *Geophysical Research Letters* 26 (4): 459–62. https://doi.org/10.1029/1999GL900003.

Gordon, Arnold L. 1978. "Deep Antarctic Convection West of Maud Rise." *Journal of Physical Oceanography*. https://doi.org/10.1175/1520-0485(1978)008<0600:DACWOM>2.0.CO;2.

Gordon, Arnold L., and Bruce A. Huber. 1990. "Southern Ocean Winter Mixed Layer." *Journal of Geophysical Research* 95 (C7): 11655. https://doi.org/10.1029/JC095iC07p11655.

Gordon, Arnold L., Martin Visbeck, and Josefino C. Comiso. 2007. "A Possible Link between the Weddell Polynya and the Southern Annular Mode." *Journal of Climate* 20 (11): 2558–71. https://doi.org/10.1175/JCLI4046.1.

Gordon, Arnold L. 1982. "Weddell Deep Water: Source and Variability." *Journal of Marine Research* 16 (5): 199–217.

———. 2014. "Southern Ocean Polynya." *Nature Climate Change* 4 (April): 249–50.

Grumbine, Robert W. 1991. "A Model of the Formation of High-Salinity Shelf Water on Polar Continental Shelves." *Journal of Geophysical Research* 96 (C12): 22049. https://doi.org/10.1029/91JC00531.

Hall, Alex, and Martin Visbeck. 2002. "Synchronous Variability in the Southern Hemisphere Atmosphere, Sea Ice, and Ocean Resulting from the Annular Mode." *American Meteorological Society* 15: 3043–57. https://doi.org/10.1175/1520-0442(2002)015<3043:SVITSH>2.0.CO;2.

Hallberg, Robert, and Peter Rhines. 1996. "Buoyancy-Driven Circulation in an Ocean Basin with Isopycnals Intersecting the Sloping Boundary." *J. Phys. Oceanogr.*

https://doi.org/10.1175/1520-0485(1996)026<0913:BDCIAO>2.0.CO;2.

Hirabara, Mikitoshi, Hiroshi Ishizaki, and Ichiro Ishikawa. 2007. "Effects of the Westerly Wind Stress over the Southern Ocean on the Meridional Overturning." *Journal of Physical Oceanography* 37 (8): 2114–32. https://doi.org/10.1175/JPO3112.1.

Hirabara, Mikitoshi, Hiroyuki Tsujino, Hideyuki Nakano, and Goro Yamanaka. 2012. "Formation Mechanism of the Weddell Sea Polynya and the Impact on the Global Abyssal Ocean." *Journal of Oceanography* 68 (5): 771–96. https://doi.org/10.1007/s10872-012-0139-3.

Hogg, Nelson G., and Walter Zenk. 1997. "Long-Period Changes in the Bottom Water Flowing through Vema Channel." *Journal of Geophysical Research C: Oceans* 102 (C7): 15639–46. https://doi.org/10.1029/97JC00591.

Hogg, Nelson G. 1973. "On the Stratified Taylor Column." *Journal of Fluid Mechanics* 58 (03): 517–37. https://doi.org/10.1017/S0022112073002302.

Holland, D M. 2001. "Explaining the Weddell Polynya-a Large Ocean Eddy Shed at Maud Rise." *Science* 292 (5522): 1697–1700. https://doi.org/10.1126/science.1059322.

Hoppema, Mario. 2004. "Weddell Sea Is a Globally Significant Contributor to Deep-Sea Sequestration of Natural Carbon Dioxide." *Deep-Sea Research Part I: Oceanographic Research Papers* 51 (9): 1169–77. https://doi.org/10.1016/j.dsr.2004.02.011.

Hunke, Elizabeth C, and William H Lipscomb. 2008. "CICE: The Los Alamos Sea Ice Model User's Manual, Version 4. Los Alamos National Laboratory Tech. Rep." LA-CC-06-0.

Hurrell, James W., M. M. Holland, P. R. Gent, S. Ghan, Jennifer E. Kay, P. J. Kushner, J.-F. Lamarque, et al. 2013. "The Community Earth System Model: A Framework for Collaborative Research." *Bulletin of the American Meteorological Society* 94 (9): 1339–60. https://doi.org/10.1175/bams-d-12-00121.1.

Johnson, Gregory C., Kristene E. McTaggart, and Rik Wanninkhof. 2014. "Antarctic BottomWater Temperature Changes in the Western South Atlantic from 1989 to 2014." *Journal of Geophysical Research, Oceans* 119 (12): 8567–77. https://doi.org/https://doi.org/10.1002/2014JC010367.

Johnson, Gregory C., and Sarah G. Purkey. 2012. "Global Contraction of Antarctic Bottom Water between the 1980s and 2000s*." *Journal of Climate* 25 (17): 5830–44. https://doi.org/10.1175/JCLI-D-11-00612.1.

Kawase, Mitsuhiro. 1987. "Establishment of Deep Ocean Circulation Driven by Deep Water Production." *Journal of Physical Oceanography* 17: 2294–2317. https://doi.org/https://doi.org/10.1175/1520-0485(1987)017<2294:EODOCD>2.0.CO;2.

Kurtakoti, Prajvala, Milena Veneziani, Achim Stössel, and Wilbert Weijer. 2018. "Preconditioning and Formation of Maud Rise Polynyas in a High-Resolution Earth System Model." *Journal of Climate* 31 (23): 9659–78. https://doi.org/10.1175/JCLI-D-18-0392.1.

Large, W G, J C Mcwilliams, and S C Doney. 1994. "Oceanic Vertical Mixing - a Review and a Model with a Nonlocal Boundary-Layer Parameterization." *Reviews of Geophysics* 32 (94): 363–403. https://doi.org/10.1029/94rg01872.

Latif, M., E. Roeckner, M. Botzet, M. Esch, H. Haak, S. Hagemann, J. Jungclaus, et al. 2004. "Reconstructing, Monitoring, and Predicting Multidecadal-Scale Changes in the North Atlantic Thermohaline Circulation with Sea Surface Temperature." *Journal of Climate* 17 (7): 1605–14. https://doi.org/10.1175/1520-0442(2004)017<1605:RMAPMC>2.0.CO;2.

Lavergne, Casimir de, Jaime B. Palter, Eric D. Galbraith, Raffaele Bernardello, and Irina Marinov. 2014. "Cessation of Deep Convection in the Open Southern Ocean under Anthropogenic

Climate Change: Supplementary Information." *Nature Climate Change* 4 (4): 278–82. https://doi.org/10.1038/nclimate2132.

Lawrence, David M, Keith W Oleson, Mark G Flanner, Peter E Thornton, Sean C Swenson, Peter J Lawrence, Xubin Zeng, et al. 2011. "Parameterization Improvements and Functional and Structural Advances in Version 4 of the Community Land Model." *Journal of Advances in Modeling Earth Systems* 3 (1). https://doi.org/10.1029/2011MS00045.

Legg, Sonya, Bruce Briegleb, Yeon Chang, Eric P Chassignet, Gokhan Danabasoglu, Tal Ezer, Arnold L Gordon, et al. 2009. "Improving Oceanic Overflow Representation in Climate Models." *Bulletin of the American Meteorological Society* 90 (5): 657–70. https://doi.org/10.1175/2008BAMS2667.1.

Lindsay, R. W., R. Kwok, L. de Steur, and W. Meier. 2008. "Halo of Ice Deformation Observed over the Maud Rise Seamount." *Geophysical Research Letters* 35 (15): 8–11. https://doi.org/10.1029/2008GL034629.

Marinov, I., A. Gnanadesikan, J. R. Toggweiler, and J. L. Sarmiento. 2006. "The Southern Ocean Biogeochemical Divide." *Nature* 441 (7096): 964–67. https://doi.org/10.1038/nature04883.

Markus, T., C. Kottmeier, and E. Fahrbach. 1998. "Ice Formation in Coastal Polynyas In the Weddell Sea and Their Impact on Oceanic Salinity." *Antarctic Sea Ice: Physical Processes, Interactions and Variability* 74: 273–92. https://doi.org/https://doi.org/10.1029/AR074p0273.

Marshall, Gareth J. 2003. "Trends in the Southern Annular Mode from Observations and Reanalyses." *Journal of Climate* 16 (24): 4134–43. https://doi.org/10.1175/1520-0442(2003)016<4134:TITSAM>2.0.CO;2.

Marshall, J., and Friedrich Schott. 1999. "Open-Ocean Convection ' Theory , and Models

Observations ,." *Reviews of Geophysics* 37 (98): 1–64. https://doi.org/10.1029/98RG02739.

Martin, Torge, Wonsun Park, and Mojib Latif. 2013. "Multi-Centennial Variability Controlled by Southern Ocean Convection in the Kiel Climate Model." *Climate Dynamics* 40: 2005–22. https://doi.org/10.1007/s00382-012-1586-7.

———. 2015. "Southern Ocean Forcing of the North Atlantic at Multi-Centennial Time Scales in the Kiel Climate Model." *Deep-Sea Research Part II: Topical Studies in Oceanography* 114: 39–48. https://doi.org/10.1016/j.dsr2.2014.01.018.

Martinson, Douglas G. 1990. "Evolution of the Southern Ocean Winter Mixed Layer and Sea Ice: Open Ocean Deepwater Formation and Ventilation." *Journal of Geophysical Research* 95 (C7): 11641. https://doi.org/10.1029/JC095iC07p11641.

Martinson, Douglas G., Peter D. Killworth, and Arnold L. Gordon. 1981. "A Convective Model for the Weddell Polynya." *Journal of Physical Oceanography*. https://doi.org/10.1175/1520-0485(1981)011.

Mazloff, Matthew R., Patrick Heimbach, and Carl Wunsch. 2010. "An Eddy-Permitting Southern Ocean State Estimate." *Journal of Physical Oceanography* 40 (5): 880–99. https://doi.org/10.1175/2009JPO4236.1.

McClean, J., D. Bader, M. Maltrud, K. Evans, D. Ivanova, M. Taylor, Q. Tang, M. Veneziani, M. Branstetter, and S. Mahajan. 2019. "High-Resolution Fully-Coupled E3SMv0.1 Present Day Transient Climate Simulations." *To Be Submitted*.

Meredith, Michael P., Arnold L. Gordon, Alberto C. Naveira Garabato, E. Povl Abrahamsen, Bruce A. Huber, Loïc Jullion, and Hugh J. Venables. 2011. "Synchronous Intensification and Warming of Antarctic Bottom Water Outflow from the Weddell Gyre." *Geophysical Research Letters* 38 (3): n/a-n/a. https://doi.org/10.1029/2010gl046265.

Meredith, Michael P., Andrew S. Meijers, Alberto C. Naveira Garabato, Peter J. Brown, Hugh J. Venables, E. Povl Abrahamsen, Loıc Jullion, and Marie-Jose Messias. 2015. "Circulation, Retention, Andmixing of Waters within the Weddell-Scotia Confluence, Southern Ocean: The Role of Stratified Taylor Columns." *Journal of Geophysical Research: Oceans* 120 (1): 547–62. https://doi.org/10.1002/2014JC010462.

Morales Maqueda, M. 2004. "Polynya Dynamics: A Review of Observations and Modeling." *Reviews Of Geophysics* 42 (1): RG1004. https://doi.org/10.1029/2002RG000116.

Mory, M., M. E. Stern, and R. W. Griffiths. 1987. "Coherent Baroclinic Eddies on a Sloping Bottom." *Journal of Fluid Mechanics* 183: 45–62. https://doi.org/10.1017/S0022112087002519.

Muench, R. D., J. H. Morison, L. Padman, D. Martinson, P. Schlosser, B. Huber, and Roland Hohmann. 2001. "Maud Rise Revisited." *Journal of Geophysical Research* 106 (C2): 2423. https://doi.org/10.1029/2000JC000531.

Nicholls, K W, S Østerhus, and K Makinson. 2009. "… over the Continental Shelf of the Southern Weddell Sea, Antarctica: A Review." *Reviews of Geophysics* 47 (RG3003): 1–23. https://doi.org/10.1029/2007RG000250.

Oke, Peter R., and Matthew H. England. 2004. "Oceanic Response to Changes in the Latitude of the Southern Hemisphere Subpolar Westerly Winds." *Journal of Climate* 17 (5): 1040–54. https://doi.org/10.1175/1520-0442(2004)017<1040:ORTCIT>2.0.CO;2.

Orsi, Alejandro H., Gregory C. Johnson, and John L. Bullister. 1999. "Circulation, Mixing, and Production of Antarctic Bottom Water." *Progress in Oceanography* 43: 55–109. https://doi.org/https://doi.org/10.1016/S0079-6611(99)00004-X.

Orsi, Alejandro H., Worth D. Nowlin JR, and Thomas Whitworth. 1993. "On the Circulation and

Stratification of the Weddell Gyre." *Deep Sea Research* 41 (1): 169–203.

Orsi, Alejandro H., William M. Smethie, and John L. Bullister. 2002. "On the Total Input of Antarctic Waters to the Deep Ocean : A Preliminary Estimate from Chlorofluorocarbon Measurements." *Journal of Geophysical Research* 107 (C8): 1–17. https://doi.org/10.1029/2001JC000976.

Orsi, Alejandro H., Thomas Whitworth, and Worth D. Nowlin. 1995. "On the Meridional Extent and Fronts of the Antarctic Circumpolar Current." *Deep-Sea Research Part I* 42 (5): 641–73. https://doi.org/10.1016/0967-0637(95)00021-W.

Ou, Hsien Wang. 1991. "Some Effects of a Seamount on Oceanic Flows." *Journal of Physical Oceanography*.

Patara, Lavinia, and Claus W. Böning. 2014. "Abyssal Ocean Warming around Antarctica Strengthens the Atlantic Overturning Circulation." *Geophysical Research Letters* 41 (11): 3972–78. https://doi.org/10.1002/2014GL059923.

Proudman, J. 1916. "On the Motion of Solids in a Liquid Possessing Vorticity." *Proceedings of the Royal Society of London. Series A: Containing Papers of a Mathematical and Physical Character* 92 (642): 408–24.

Purkey, Sarah G., and Gregory C. Johnson. 2010. "Warming of Global Abyssal and Deep Southern Ocean Waters between the 1990s and 2000s : Contributions to Global Heat and Sea Level Rise Budgets *." *Journal of Climate*, 6336–51. https://doi.org/10.1175/2010JCLI3682.1.

———. 2013. "Antarctic Bottom Water Warming and Freshening: Contributions to Sea Level Rise, Ocean Freshwater Budgets, and Global Heat Gain." *Journal of Climate* 26 (16): 6105–22. https://doi.org/10.1175/JCLI-D-12-00834.1.

Rahmstorf, Stefan, Jason E. Box, Georg Feulner, Michael E. Mann, Alexander Robinson, Scott

Rutherford, and Erik J. Schaffernicht. 2015. “Exceptional Twentieth-Century Slowdown in Atlantic Ocean Overturning Circulation.” *Nature Climate Change* 5 (5): 475–80. https://doi.org/10.1038/nclimate2554.

Rignot, E., Stanley S. Jacobs, J. Mouginot, and B. Scheuchl. 2013. “Ice-Shelf Melting around Antarctica.” *Science* 341 (6143): 266–70. https://doi.org/10.1126/science.1235798.

Ritz, Stefan P., Thomas F. Stocker, Joan O. Grimalt, Laurie Menviel, and Axel Timmermann. 2013. “Estimated Strength of the Atlantic Overturning Circulation during the Last Deglaciation.” *Nature Geoscience* 6 (3): 208–12. https://doi.org/10.1038/ngeo1723.

Russell, Joellen L., Keith W. Dixon, Anand Gnanadesikan, Ronald J. Stouffer, and J. R. Toggweiler. 2006. “The Southern Hemisphere Westerlies in a Warming World: Propping Open the Door to the Deep Ocean.” *Journal of Climate* 19 (24): 6382–90. https://doi.org/10.1175/JCLI3984.1.

Sabine Christopher, L, A Feely Richard, Nicolas Gruber, M Key Robert, Kitack Lee, L Bullister John, Rik Wanninkhof, et al. 2004. “The Oceanic Sink for Anthropogenic CO2.” *Science* 305 (5682): 367–71. https://doi.org/10.1126/science.1097403.

Schröder, Michael, and Eberhard Fahrbach. 1999. “On the Structure and the Transport of the Eastern Weddell Gyre.” *Deep-Sea Research Part II: Topical Studies in Oceanography* 46 (1–2): 501–27. https://doi.org/10.1016/S0967-0645(98)00112-X.

Sebille, Erik van, Stephen R. Rintoul, Matthew H. England, Matthew R. Mazloff, Oleg A. Saenko, and Paul Spence. 2013. “Abyssal Connections of Antarctic Bottom Water in a Southern Ocean State Estimate.” *Geophysical Research Letters* 40 (10): 2177–82. https://doi.org/10.1002/grl.50483.

Send, Uwe, Matthias Lankhorst, and Torsten Kanzow. 2011. “Observation of Decadal Change in

the Atlantic Meridional Overturning Circulation Using 10 Years of Continuous Transport Data." *Geophysical Research Letters* 38 (24): 1–5. https://doi.org/10.1029/2011GL049801.

Small, R Justin, Julio Bacmeister, David Bailey, Allison Baker, Stuart Bishop, Frank Bryan, Julie Caron, et al. 2014. "A New Synoptic Scale Resolving Global Climate Simulation Using the Community Earth System Model." *Journal of Advances in Modeling Earth Systems* 6 (4): 1065–94. https://doi.org/10.1002/2014MS000363.

Smeed, D. A., G. D. McCarthy, S. A. Cunningham, E. Frajka-Williams, D. Rayner, W. E. Johns, C. S. Meinen, et al. 2014. "Observed Decline of the Atlantic Meridional Overturning Circulation 2004-2012." *Ocean Science* 10 (1): 29–38. https://doi.org/10.5194/os-10-29-2014.

Smith, R, P Jones, B Briegleb, Frank Bryan, Danabasoglu, Gokhan, J Dennis, J Dukowicz, et al. 2010. "The Parallel Ocean Program (POP) Reference Manual: Ocean Component of the Community Climate System Model (CCSM)." *Rep. LAUR-01853, 141*, 1–140.

Steur, L. de, D. M. Holland, R. D. Muench, and M. G. McPhee. 2007. "The Warm-Water 'Halo' around Maud Rise: Properties, Dynamics and Impact." *Deep-Sea Research Part I: Oceanographic Research Papers* 54 (6): 871–96. https://doi.org/10.1016/j.dsr.2007.03.009.

Steur, L. de, D. M. Holland, R. D. Muench, and Miles G. Mcphee. 2007. "The Warm-Water 'Halo' around Maud Rise: Properties, Dynamics and Impact." *Deep-Sea Research Part I: Oceanographic Research Papers* 54 (6): 871–96. https://doi.org/10.1016/j.dsr.2007.03.009.

Stössel, Achim, and Seong-Joong Kim. 2001. "Decadal Deep-Water Variability in the Subtropical Atlantic and Convection in the Weddell Sea." *Journal of Geophysical Research* 106 (C10): 22425. https://doi.org/10.1029/2000JC000335.

Stössel, Achim, Dirk Notz, F Alexander Haumann, Helmuth Haak, Johann Jungclaus, and Uwe

Mikolajewicz. 2015. “Controlling High-Latitude Southern Ocean Convection in Climate Models.” *Ocean Modelling* 86: 58–75. https://doi.org/10.1016/j.ocemod.2014.11.008.

Stössel, Achim, Zhaoru Zhang, and Timo Vihma. 2011. “The Effect of Alternative Real-Time Wind Forcing on Southern Ocean Sea Ice Simulations.” *Journal of Geophysical Research: Oceans* 116 (11): 1–19. https://doi.org/10.1029/2011JC007328.

Swart, Neil C., Sarah T. Gille, John C. Fyfe, and Nathan P. Gillett. 2018. “Recent Southern Ocean Warming and Freshening Driven by Greenhouse Gas Emissions and Ozone Depletion.” *Nature Geoscience* 11 (11): 836–41. https://doi.org/10.1038/s41561-018-0226-1.

Swingedouw, Didier, T. Fichefet, H. Goosse, and M. F. Loutre. 2009. “Impact of Transient Freshwater Releases in the Southern Ocean on the AMOC and Climate.” *Climate Dynamics* 33 (2–3): 365–81. https://doi.org/10.1007/s00382-008-0496-1.

Taylor, G.I. 1923. “Experiments on the Motion of Solid Bodies in Rotating Fluids.” *Proceedings of the Royal Society of London A: Mathematical, Physical and Engineering Sciences.* 104 (725): 213–18. https://doi.org/10.1098/rspa.1983.0054.

Thomas, Jordan, Darryn Waugh, and Anand Gnanadesikan. 2018. “Relationship between Ocean Carbon and Heat Multidecadal Variability.” *Journal of Climate* 31 (4): 1467–82. https://doi.org/10.1175/JCLI-D-17-0134.1.

Thompson, David, John Wallace, and Gabriele Hegerl. 1999. “Annular Modes in the Extratropical Circulation. Part II: Trends.” *Journal of Climate*, no. 689: 1018–36. https://doi.org/10.1007/s00420-018-1350-3.

Timmermann, R. 2002. “Simulations of Ice-Ocean Dynamics in the Weddell Sea 2. Interannual Variability 1985–1993.” *Journal of Geophysical Research* 107 (C3): 3025. https://doi.org/10.1029/2000JC000742.

Toggweiler, J. R., and Joellen Russell. 2008. “Ocean Circulation in a Warming Climate.” *Nature* 22 (3): 259–62. https://doi.org/10.1038/nature06590.

Toggweiler, J. R., and B. Samuels. 1995. “Effect of Drake Passage on the Global Thermohaline Circulation.” *Deep-Sea Research Part I* 42 (4): 477–500. https://doi.org/10.1016/0967-0637(95)00012-U.

Watanabe, Masahiro, Youichi Kamae, Masakazu Yoshimori, Akira Oka, Makiko Sato, Masayoshi Ishii, Takashi Mochizuki, and Masahide Kimoto. 2013. “Strengthening of Ocean Heat Uptake Efficiency Associated with the Recent Climate Hiatus.” *Geophysical Research Letters* 40 (12): 3175–79. https://doi.org/10.1002/grl.50541.

Weijer, Wilbert, Milena Veneziani, Achim Stössel, Matthew W. Hecht, Nicole Jeffery, Alexandra Jonko, Travis Hodos, and Hailong Wang. 2017. “Local Atmospheric Response to an Open-Ocean Polynya in a High-Resolution Climate Model.” *Journal of Climate* 30 (5): 1629–41. https://doi.org/10.1175/JCLI-D-16-0120.1.

Yeager, Stephen, and Gokhan Danabasoglu. 2014. “The Origins of Late-Twentieth-Century Variations in the Large-Scale North Atlantic Circulation.” *Journal of Climate* 27 (9): 3222–47. https://doi.org/10.1175/JCLI-D-13-00125.1.

Zanowski, Hannah, and Robert Hallberg. 2017. “Weddell Polynya Transport Mechanisms in the Abyssal Ocean.” *Journal of Physical Oceanography*, JPO-D-17-0091.1. https://doi.org/10.1175/JPO-D-17-0091.1.

Zanowski, Hannah, Robert Hallberg, and Jorge L. Sarmiento. 2015. “Abyssal Ocean Warming and Salinification after Weddell Polynyas in the GFDL CM2G Coupled Climate Model.” *Journal of Physical Oceanography* 45 (11): 2755–72. https://doi.org/10.1175/JPO-D-15-0109.1.

Zenk, Walter, and Eugene Morozov. 2007. “Decadal Warming of the Coldest Antarctic Bottom

Water Flow through the Vema Channel." *Geophysical Research Letters* 34 (14): 2–6. https://doi.org/10.1029/2007GL030340.

Zenk, Walter, and Martin Visbeck. 2013. "Structure and Evolution of the Abyssal Jet in the Vema Channel of the South Atlantic." *Deep-Sea Research Part II: Topical Studies in Oceanography* 85: 244–60. https://doi.org/10.1016/j.dsr2.2012.07.033.

Zhang, Liping, Thomas L. Delworth, William Cooke, and Xiaosong Yang. 2019. "Natural Variability of Southern Ocean Convection as a Driver of Observed Climate Trends." *Nature Climate Change* 9 (1): 59–65. https://doi.org/10.1038/s41558-018-0350-3.

Zhang, Zhaoru, Timo Vihma, Achim Stössel, and Petteri Uotila. 2015. "The Role of Wind Forcing from Operational Analyses for the Model Representation of Antarctic Coastal Sea Ice." *Ocean Modelling* 94: 95–111. https://doi.org/10.1016/j.ocemod.2015.07.019.

Zwally, H. J., J. C. Comiso, C. L. Parkinson, W. J. Campbell, F. D. Carsey, and P. Gloersen. 1983. "Antartic Sea Ice, 1973-1976: Satellite Passive-Microwave Observations."